Escuela Superior de Tecnología y Ciencias Experimentales
Departamento de Física. Física Aplicada

CHARGE TRANSPORT IN ORGANIC SEMICONDUCTORS WITH APPLICATION TO OPTOELECTRONIC DEVICES

José María Montero Martín

Supervised by Juan Bisquert Mascarell

PhD Thesis
Castellón de la Plana, 7 April 2010

Escuela Superior de Tecnología y Ciencias Experimentales
Departamento de Física. Física Aplicada

TRANSPORTE DE CARGA EN SEMICONDUCTORES ORGÁNICOS CON APLICACIÓN A DISPOSITIVOS OPTOELECTRÓNICOS

José María Montero Martín

Dirigida por Juan Bisquert Mascarell

Tesis doctoral
Castellón de la Plana, 07 de abril de 2010

En Juan Bisquert Mascarell, Catedràtic d'Universitat en el Departament de Física de la Universitat Jaume I de Castelló,

CERTIFICA:

Que **En José María Montero Martín**, Licenciado en Física per la Universidad de Salamanca amb posesió del DEA, ha realitzat la següent memòria sota la seua direcció: **"Charge transport in organic semiconductors with application to optoelectronic devices"** i amb la que opta a la consecució del títol de Doctor.

Aquesta investigació s'ha dut a terme en el Grup de Dispositius Fotovoltaics i Optoelectrònics del Departament de Física de la Universitat Jaume I.

I així per a que conste i en compliment de la legislació vigent, signa el present certificat per als efectes oportuns, en Castelló de la Plana, a dimecres, 7 / abril / 2010.

Signat: Professor Juan Bisquert Mascarell

Catedràtic d'Universitat de la Universitat Jaume I

A mi familia: mis padres Jesús y María Teresa, a mi hermano Óscar y Lacramioara.

A la memoria de mi padre.

Agradecimientos

Deseo expresar mis agradecimientos al Grup de Dispositius Fotovoltaics i Optoelectrònics, por integrarme en el Departamento de Física de la Universitat Jaume I de Castellón, y al Ministerio de Educación y Ciencia por su necesaria financiación. Mención especial merece mi director de tesis doctoral, D. Juan Bisquert, Catedrático de Universidad, por su aportación incesante de ideas. Así mismo, quisiera destacar al Profesor Titular, Dr. Germà Garcia-Belmonte por sus conocimientos y enseñanzas a nivel experimental.

Mi gratitud a las diferentes colaboraciones mantenidas durante estos años. Comenzando por el Dr. Henk Bolink, por su provechosa contribución experimental en el Instituto de Ciencias Moleculares de Valencia con la Dr. Eva M. Barea en la preparación de dispositivos. En el campo teórico, agradezco a los Profesores: Dr. Alison W. Walter de la University of Bath (Inglaterra) y al Dr. Beat Ruhstaller de la Zurich University of Applied Sciences (Suiza), sus clarificadoras contribuciones a mi tesis en relación con el modelado de dispositivos orgánicos.

Al resto del grupo trabajo, Dr. Francisco Fabregat-Santiago, Dr. Iván Mora-Seró, Dr. Sixto Giménez, Lourdes Márquez y Pablo Pérez, así mismo, al Dr. Jorge García-Cañadas, Dr. Thomas Moehl, Fabiola Iacono y a Loles Merchán en la administración.

A mi hermano, Dr. Óscar Montero, por sus consejos y discusiones físicas a lo largo de todos estos años, a mis padres, por inculcarme la admiración por descubrir y conocer, y a mis amigos, por brindarme su apoyo y amistad.

Prefacio

Un diodo orgánico electroluminiscente (OLED) consiste en una capa muy fina (unos 100 nm) que tiene una función trabajo muy alta para facilitar la inyección de huecos (el ánodo), y el otro una función de trabajo muy baja para favorecer la inyección de electrones (el cátodo). La inyección se facilita con capas adicionales de transporte, que realizan una función de bloqueo. Los electrones inyectados por el cátodo y los huecos que entran por el ánodo avanzan conducidos por un campo eléctrico hasta la capa emisora, donde forman excitones y recombinan emitiendo luz. Estos dispositivos presentan grandes ventajas tecnológicas en aplicaciones de muestreo de información e iluminación ambiental. Presentan una mayor eficiencia respecto a los sistemas actuales convencionales, contribuyendo así al cada vez más necesario ahorro energético. Sin embargo, presentan limitaciones (estabilidad y degradación, principalmente) y por tanto, se hace necesario un profundo estudio científico de estos dispositivos con la finalidad de mejorar su optimización.

En los estudios realizados se han aportado modelos de inyección en capas orgánicas a través de estados interfaciales, capaces de explicar el fenómeno de capacidades negativas observado en diodos orgánicos de dos portadores a bajas frecuencias. Esta característica no aparece experimentalmente en el transporte de carga en materiales de un único portador. Además, se ha estudiado experimentalmente la inyección y emisión de luz azul en un OLED de polyfluoreno con diferentes cátodos, concluyendo que la corriente estaba gobernada por los huecos mientras que la luz lo hacía por los electrones inyectados. Para dispositivos OLED de un sólo portador se ha encontrado una fórmula explícita de la característica densidad de corriente y potencial (*J*-*V*) con movilidad dependiente del campo eléctrico. Un test para diferenciar la movilidad dependiente del campo y de la densidad en capas orgánicas ha sido dado por medio de una ley universal de escalado. Los espectros de capacidad y los tiempos de tránsito han sido examinados con la inclusión de la movilidad

dependiente del campo eléctrico y comparado con los datos experimentales, verificándose el modelo teórico planteado.

La mayor aportación de la tesis doctoral consiste en la descripción de la movilidad de portadores de carga en materiales orgánicos a través de un modelo de transporte con una densidad exponencial de trampas. Se han utilizado técnicas de espectroscopía de impedancia para explicar la movilidad dependiente del campo eléctrico en términos del múltiple atrapamiento ejercido por los estados energéticamente localizados. Este modelo ha explicado de forma coherente los espectros de capacidad recogidos en medidas experimentales, particularmente su comportamiento a bajas e intermedias frecuencias. Además, este análisis no se encontraba presente en la literatura científica y supone un progreso importante en el conocimiento y caracterización del transporte de carga en materiales orgánicos.

La respuesta de los OLED (con polímero SY) ha sido estudiada en los regímenes estacionario y transitorio. En el comportamiento estacionario, se han descrito las corrientes de fuga a bajos potenciales. Se ha analizado la existencia de mayor corriente circulando por el perímetro que por el área del dispositivo. Respecto al comportamiento transitorio, se ha proporcionado una explicación sobre las colas de luz emitida observadas al cesar la perturbación de potencial escalón: su origen procede de la inyección limitada de electrones en el cátodo.

Los estudios realizados han dado lugar a la producción científica que se encuentra recogida en la lista de publicaciones de la introducción de la tesis.

Para concluir, cabe reseñar que el transporte de carga y, particularmente, la movilidad de portadores en capas orgánicas es un tema todavía hoy sin pleno acuerdo en la comunidad científica. Por consiguiente, el estudio de nuevos modelos de movilidad y transporte siguen siendo una línea de investigación vigente a desarrollar.

Index of Contents

Index of Contents

1

Introduction

1.1. Overview

Organic light-emitting diodes (OLED) are a special type of light-emitting diode (LED) where the emissive layer comprises a thin film of a certain organic semiconductor. The emissive electroluminescent layer can include a polymeric substance that allows the deposition of very suitable organic compounds, for instance, in rows and columns on a flat configuration by using a simple printing method to create a matrix of pixels which can emit different coloured light as in Fig. 1.1.

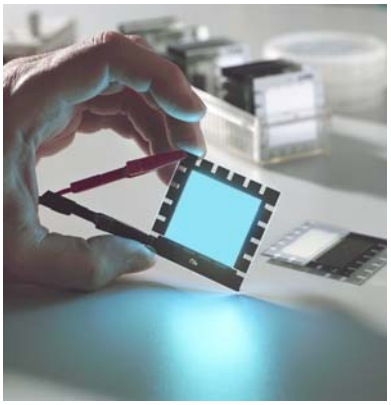

Fig. 1.1 Philips blue OLED

Such systems become of relevant interest for displaying information, e.g., in television screens, computer displays, portable system screens, advertising information and visual signal indicators.[1] The association of OLEDs in active matrices controlled by transistor circuitry results in the so-called AMOLED panel displays. In addition, OLED technology represents a promising light source for general space illumination since white organic light-emitting diodes have recently reached the value of 90 lm W^{-1}, surpassing the benchmark of the fluorescent tube efficiency (60-70 lumens per watt).[2] In western countries, lightning consumption reaches up to 20% of the overall energy usage and the predominant incandescent light bulbs perform only a luminous power efficiency of 14 lm/W.[3] Several countries are seeking to entirely eliminate the

bulbs as a way to control energy consumption and carbon dioxide emissions. In 2007, for example, Australia became the first country to completely ban incandescent bulbs; the phase out is scheduled to be completed by 2012. The European Union agreed to a similar ban in 2008 and the United States has pledged to eliminate most incandescents by 2014.[4]

OLED displays are currently present in commercial applications with relatively small screen (mobiles, mp3…) whereas not in the lightning field. This type of displays offers different advantages in contrast to liquid-crystal displays (LCD) and traditional LED-based displays. One of the great benefits of an OLED display over the LCD is that a backlight is not required (which is basically polarized by filters) to function. This means that they draw far less power and, when powered from a battery, can operate longer on the same charge. It is also known that OLED-based display devices can be more effectively manufactured than LCDs and plasma displays. In addition, OLED displays are lighter and present wider viewing angles, exceptional colour reproduction, outstanding contrast levels and higher brightness. As regards the OLED major advantage over the LED-based displays, large area, low-cost and flexible display applications can be achieved due to the glass substrate and the performing techniques utilized, Fig. 1.2.[5]

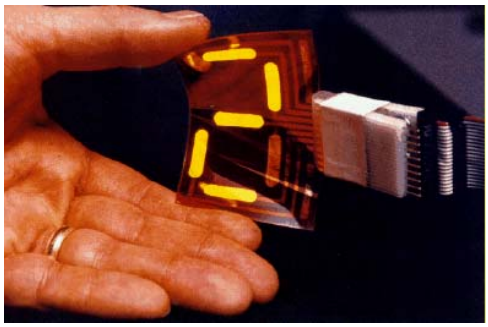

Fig. 1.2 Thin-film flexible seven-segment display based on semiconducting polymers.

Nevertheless, the main problem with OLEDs is that the organic materials are degradable by water and oxygen, which tends to give the devices a short

lifespan. This can be solved, to some extent, by encapsulating the organic compounds in an inert, transparent polymer such as epoxy resin. However, the compounds intrinsically degrade anyway, especially the blue OLEDs that are required for mixing with red and green to generate white light. As a matter of fact, further efforts to optimize device performance are still necessary to definitely improve its reliability and life expectancy.[6] Studies of charge transport become of prominent importance to provide foundations in the understanding of the physical processes occurring within the organic materials.[7] Particularly, the recombination process (responsible of the light output) is gathered in the literature as a Langevin type therefore it is strongly dependent on the charge transport mobility (see chapter 2 sections 6.2 and 6.3).[8] The scientific research carried out on charge transport mobility constitutes a key role for further optimization of light emission in OLEDs.[9,10] Furthermore, the performance of organic electronic devices depends strongly on the quality of the semiconductor used which is greatly affected by the defect states of the material. The formation of defects in organic materials is still not well understood, and consequently, it is difficult to control the defect states in organic devices.[11] In this framework, the impedance spectroscopy (IS) technique emerges as a powerful tool capable to analyze the two relevant physical properties involved in the performance of organic devices: the charge transport mobility and the role of localized-states in the band-gap (traps) in organic layers, both at the same time.[12] The IS method has proven its success on the characterization of novel electronic devices such as dye-sensitized solar cells (DSSCs).[13,14] The present thesis is focused on the application of IS on charge transport in organic layers by a theoretical and computational approach in order to enhance the optimization of OLEDs.

The evolution of organic light-emitting diodes in organic materials has been impressive since the first organic electroluminescence (EL) devices were fabricated by applying a high-voltage alternating current (ac) to crystalline thin films of acridine orange and quinacrine. Bernanose and co-workers carried out

these studies in 1953. During these early experiments, aluminium quinolinol (Alq), one of the most promising compounds in the recent OLED devices, focused the attention of the scientific community.[15] In the 1960s, research moved on to the carrier-injection type of electroluminescence, namely OLED, by using a highly purified condensed aromatic single crystal, especially an anthracene. In particular, Pope et al. experimented on carrier recombination and the emission mechanism, and their physical interpretation is still very useful today. Whereas a highly purified zone-refined anthracene single crystal essentially showed a conductivity of 10-20 S/cm, double injection of holes and electrons, however, were achieved efficiently based on space-charge-limited current (SCLC) with the appropriate charge-carrier-injection electrodes. The presence of both carrier species in the material resulted in a successive carrier recombination, the creation of single and triplet excitons, and radiative decay of them.[16] Thus, the basic EL process has been established since the 1960s.

From the 1970s to the 1980s, in addition to the studies on the EL mechanisms, the focus of research shifted from single crystals to organic thin films. Therefore, in the thin-film devices, two major target areas were addressed for efficient EL: improving the charge carrier injection though the electrodes, in particular, electron injection, and forming electron-only thin films. This basic research was extremely useful to provide a foundation for the development of EL thin-film devices. In 1977, Shirakawa and coworkers reported high conductivity in oxidized and iodine-doped polyacetylene.[17]

Next, in the 1980s, the organic multilayer structures, which are another key technology of present high-performance OLEDs, appeared.[18,19] The breakthroughs that led to the exponential growth of this field and its first commercialized products can be traced back to two pioneering papers. The 1987 paper by Tang and VanSlyke demonstrated that the performance of green-emitting thin film bilayer OLED based on the small organic molecule tris(8-hydroxy quinoline) Al (Alq_3) was sufficiently promising to warrant extensive research on a wide variety of thin film small-molecule OLEDs (SMLEDs).[20]

The 1990 paper by Bradley, Friend, and co-workers described the first polymer OLED (PLED), which was based on poly(p-phenylene vinylene) (PPV), and demonstrated that such devices deserved a wider research attention.[21] Since then, the competition between small-molecular OLEDs (SMLEDs) and PLEDs continued in parallel with the overall important developments of this field.

In terms of scientific recognition, Shirakawa, Heeger and MacDiarmid were awarded in 2000 with the Nobel Prize in Chemistry for the discovery (1977) and development of conductive polymers, this fact vindicates the current interest of these materials and the new evolving industry of plastic electronics.[22]

Nowadays and as mentioned before, OLED displays are implemented mainly in short-lifetime applications such as mobile phones and mp3 players. Long-term organic optoelectronic devices are in their beginnings namely commercial TVs and prototype lamps. In 2007 Sony launched into the market the "OLED TV XEL-1" of 3 millimetres thick and 11 inches, Fig.1.3. In 2008, OSRAM developed a limited edition of the OLED lamp "Early Future" whose luminescent tiles measure 132 x 33 millimetres each.

Fig. 1.3 SONY XEL-1 OLED TV (2007)

Fig. 1.4 Early Future OSRAM OLED lamp (2008)

In summary, the fascination with OLED devices is due to several potential advantages for the development of an organic-based technology: (1) Relative

ease and low cost of fabrication, (2) their basic properties as active light-emitters (i.e., for self-luminescent panels), (3) flexibility, (4) transparency and (5) scalability. The necessary optimization of OLED devices stems from the intrinsic degradation of the organic materials. Charge transport mobility and the defect states of the compounds are widely studied to enhance the performance of the devices. In the forthcoming chapters, we present a theoretical approach by IS that allows, at once, the characterization of both physical properties in organic layers.

The structure of the thesis is divided into four major parts. The first two chapters (i.e., introduction and OLED fundamentals) are aimed to provide insight, a global and complete perspective, of the current research situation on OLEDs and its relationship with the present study. Particularly, the second chapter exposes the basis of OLED devices such as materials, fabrication procedures, OLED operation, notions of injection, transport and recombination, experimental techniques for the determination of mobility as well as the factors involved in the efficiency of OLEDs. Chapter number three (i.e., research methods) describes the specific tools implemented for obtaining the scientific results on charge transport mobility by IS. Results are the main body of the thesis and cover the ranging chapters from four to eight. Chapter four treats the discrepancy of the charge transport mobility dependence (i.e., field- and density-dependence) by means of a universal scaling law for each case. Chapter five applies the IS for the field-dependent mobility framework in organic layers to model experimental data of SY-copolymer. Chapter six interprets the influence of a single defect (i.e., a single-trap level) in mobility measurements by IS. Chapter seven reduces the field-dependent mobility transport, commonly found in experiments by IS, to a trap-controlled one. Chapter eight fully describes the trap-limited mobility in terms of an exponential density of defects (traps) capable of modelling a experimental data of capacitance spectra in a single layer of Alq_3.

Finally, the overall conclusions drawn in chapter nine summarize the whole research work carried out and outline future perspectives.

The thesis is based on the list of publications that is enclosed below:

1) J. Bisquert, G. Garcia-Belmonte, J. M. Montero, H. J. Bolink
Charge injection in organic light emitting diodes governed by interfacial states
Proceeding SPIE Int. Soc. Opt. Eng.6192, 619210 (2006)

2) J. Bisquert, J. M. Montero, H. J. Bolink, E. M. Barea and G. Garcia-Belmonte
Thickness scaling of space-charge-limited currents in organic layers with field- or density-dependent mobility
Physica Status Solidi a, 203, (15), 3762 (2006)

3) J. M. Montero, J. Bisquert, H. J. Bolink, E. M. Barea and G. Garcia-Belmonte
Interpretation of capacitance spectra and transit times of single carrier space-charge limited transport in organic layers with field-dependent mobility
Physica Status Solidi a, 204, (7), 2402 (2007)

4) G. Garcia-Belmonte, J. M. Montero, E. M. Barea, J. Bisquert and H. J. Bolink
Millisecond radiative recombination in poly(phenylene vinylene)-based light-emitting diodes from transient electroluminescence
Journal of Applied Physics, 101, (11), 114506 (2007)

5) G. Garcia-Belmonte, E. M. Barea, Y. Ayyad-Limonge, J. M. Montero, H. J. Bolink and J. Bisquert
Cathode effect on current-voltage characteristics of polyspiroblue CB02
Proceedings SPIE Int. Soc. Opt. Eng., 6999, 699990 (2008)

6) G. Garcia-Belmonte, J. M. Montero, Y. Ayyad-Limonge, E. M. Barea, J. Bisquert and H. J. Bolink
Perimeter leakage current in polymer light emitting diodes
Current Applied Physics, 9, 414 (2009)

7) J. M. Montero, J. Bisquert, G. Garcia-Belmonte, E. M. Barea and H. J. Bolink
Trap-limited mobility in space-charge-limited current in organic layers
Organic Electronics, 10, 305 (2009)

8) J. M. Montero and J. Bisquert
Trap origin of field-dependent mobility of the carrier transport in organic layers
Solid-State Electronics, submitted (2010)

9) J. M. Montero, J. Bisquert and G. Garcia-Belmonte
Interpretation of trap-limited mobility in space-charge-limited current in organic layers with an exponential density of traps
Manuscript in preparation (2010)

1.2. References

[1] W. E. Howard and O. F. Prache, IBM J. Res. Dev. **45**, 115 (2001).

[2] S. Reineke, F. Lindner, G. Schwartz, et al., Nature **459**, 234 (2009).

[3] "*The Promise of Solid State Lightning* " (Optoelectronics Industry Development Association, Report, 2002).

[4] S. Tonzani, Nature **459**, 312 (2009).

[5] R. Szeweda, III-Vs review. Adv. Semicond. Mag. **18**, 36 (2006).

[6] S. Forrest, Nature **428**, 911 (2004).

[7] P. W. M. Blom and M. C. J. M. Vissenberg, Mater. Sci. Eng. **27**, 53 (2000).

[8] B. K. Crone, P. S. Davids, I. H. Campbell, et al., J. Appl. Phys. **84**, 833 (1998).

[9] J. C. Scott, P. J. Brock, J. R. Salem, et al., Synth. Met. **111-112**, 289 (2000).

[10] R. H. Friend, R. W. Gymer, A. B. Holmes, et al., Nature **397**, 121 (1999).

[11] T. P. Nguyen, Phys. Status Solidi (a) **205**, 162 (2008).

[12] T. Okachi, T. Nagase, T. Kobayashi, et al., Appl. Phys. Lett. **94**, 043301 (2009).

[13] Q. Wang, S. Ito, M. Grätzel, et al., J. Phys. Chem. B **110**, 25210 (2006).

[14] J. Bisquert, Phys. Rev. B **77**, 235203 (2008).

[15] M. Bernanose, P. Comte and J. Vouaux, J. Chem. Phys. **50** (1953).

[16] M. Pope, H. P. Kallmann and P. Magnantte, J. Chem. Phys. **38**, 2042 (1963).

[17] C. K. Chiang, C. R. Fincher, Y. W. Park, et al., Phys. Rev. Lett. **39**, 1098 (1977).

[18] J. Shinar, "*Organic Light-Emitting Devices: A Survey*" (Springer, New York, 2004).

[19] K. Müllen and U. Scherf, "*Organic Light-Emitting Devices: Synthesis, Properties and Applications"* (WILEY-VCH, Singapore, 2006).

[20] C. W. Tang and S. A. VanSlyke, Appl. Phys. Lett. **51**, 913 (1987).

[21] J. H. Burroughes, D. D. C. Bradley, A. R. Brown, et al., Nature **347**, 539 (1990).

[22] F. Fabregat-Santiago, "*Study on thin film electrochemical devices with impedance methods"* (Universitat Jaume I, PhD Thesis, Castellón, 2001).

2

OLED Fundamentals

2.1. Properties of Organic Semiconductors

The semiconductor behaviour of these materials arises from the presence of conjugated molecules; the term conjugated refers to the existence of alternating single and double carbon-carbon bonds. Semiconductivity is exhibited in small molecules (see Fig. 2.1), short chain (oligomers), and organic polymers (see Fig. 2.2). Semiconducting small molecules (aromatic hydrocarbons) include the polycyclic aromatic compounds of pentacene, anthracene, and rubrene. Examples of polymeric semiconductors are poly(3-hexylthiophene), poly(p-phenylene vinylene), F8BT, as well as polyacetylene and its derivatives.[1]

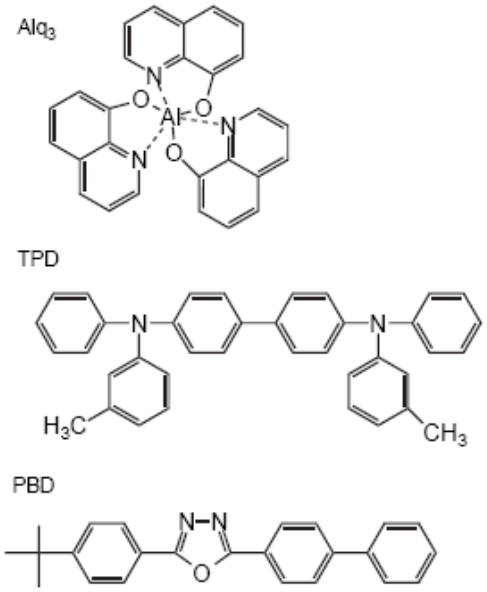

Fig. 2.1 Structure of some small molecule organic semiconductors that have been used for thin-film electroluminescence devices. Alq_3 is used as an emissive layer but also as hole transport layer, TPD is implemented as a hole transport layer, and PBD is used as an electron transport layer.

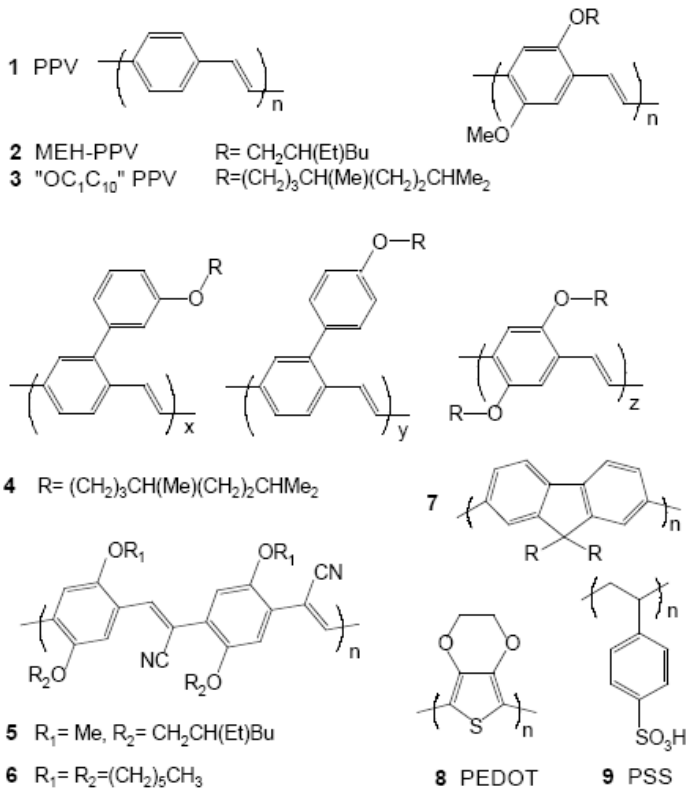

Fig. 2.2 Polymers used in electroluminescent diodes. The prototypical (green) fluorescent polymer is poly(p-phenylene vinylene) as labelled by number 1. The two best known (orange-red) solution-processable conjugated polymers are MEH-PPV (2) and OC_1C_{10} PPV (3). Copolymer 4 has a very high electroluminescence efficiency and cyano-derivatives of PPV 5 and 6 are used as electron transport materials. High purity polymers such as poly(dialkyfluorene)s show high luminescence efficiencies. Doped polymers e.g. poly(dioxyethylene thienylene), PEDOT (8), doped with polystyrenesulphonic acid, PSS (9), are widely used as hole-injection layers.

In organic semiconductors, and other molecules e.g. benzene, the carbon atoms can form the so-called sp_2 hybrid orbitals, with each carbon atom having three sp_2 orbitals forming a triangle within the plane surrounding the carbon atom. In addition, each carbon atom also has a p_z orbital which is perpendicular to the plane of the sp_2 orbitals (see Fig. 2.3). The basic structure of the molecule backbone is composed of σ bonds between the carbon atoms by overlapping sp_2

orbitals. Nevertheless, they are not responsible of the semiconducting properties of the organic materials whereas the bonds among p_z orbitals of neighbouring carbon atoms actually are. These orbitals overlap each other forming π-bonds that support the mobile charge carriers. The bonding orbital π, with lower energy, and the anti-bonding orbital π^*, with higher energy, form delocalized valence and conduction wavefunctions providing a well defined π-π* bandgap. The valence and conduction wavefunctions are also known as the HOMO (Highest Occupied Molecular Orbital) and LUMO (Lowest Unoccupied Molecular Orbital) energy levels, respectively. Due to the π conjugation, in the perfect isolated polymer chain the delocalized π electron cloud extends along the whole length of the chain. However, in the real structure various defects are present such as external impurities (i.e., atoms eliminating the double bonds among others) or intrinsic defects (i.e., torsion in the chain, kinks, etc) that can partially break the conjugation in the molecule.[2]

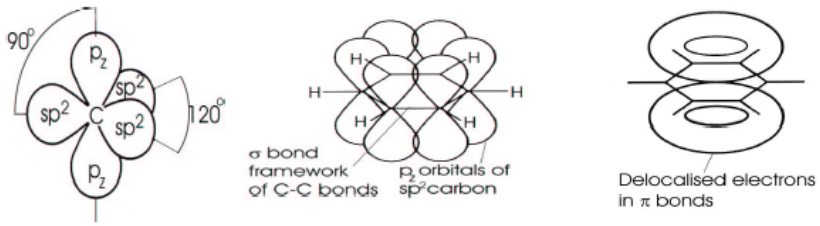

Fig. 2.3 Atom carbon orbitals : sp_2 hybrid orbitals an the p_z orbitals (left-hand-side), a benzen ring with the structural σ bonds originated by the sp_2 orbital overlappin (centre) and the delocalised electron cloud caused by the p_z orbital overlapping forming the π bonds.

Since the semiconducting behaviour of both conjugated polymers and small molecule semiconductors has its origin in the properties of carbon atoms, the physics of both classes of materials are fairly similar. An important characteristic of organic-based films is the disorder. Although polymer chains may be quite long, the π-conjugation is interrupted by defects, hence the conjugated polymers can be considered as an assembly of conjugated segments. The length of the segments varies randomly and that is a major reason for

energetic disorder implying inhomogeneous properties and a relatively broad density-of-states (DOS). The width of the DOS, to a large degree, determines the charge transport characteristics of the material and the tail states can in principle act as shallow trapping states for charge carriers (intrinsic localized states). On the other hand, extrinsic trapping, can also release charges back to the DOS. This continuous modelization based on a multiple-trapping scheme of charge carriers explains the transport in conjugated polymers that is governed by inter-chain hopping from one molecule to its neighbouring one.[3]

The major difference between organic semiconductors based on small-molecules and conjugated-polymers is the method of preparation. Thin films of small molecules are usually performed by means of vacuum evaporation techniques, meanwhile for conjugated polymers there is a wider range of fabrication methods available. Wet-coating techniques such as spin-coating or doctor blade are commonly used to perform polymer-based thin films as well as ink-jet printing. This latter technique eases fabrication at atmosphere conditions with low cost and a high-quality precision despite the substrate used.[4]

Currently, the only weakest point of implementing organic semiconductors found out is their lifetimes although longer term devices are already achieved by encapsulation to partially avoid degradation.[5]

2.2. Structure of OLEDs

The basic structure of a typical OLED consists of at least one layer of organic semiconductor sandwiched between two electrodes. A common trilayer OLED is shown in Fig. 2.4 with two additional organic layers aside the organic emitter compound. They are so-called organic transport layers either for electrons (ETL) or for holes (HTL).

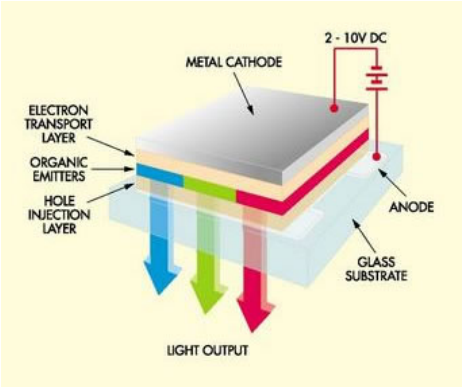

Fig. 2.4 Basic structure of OLEDs

Appropriate multilayer structures typically enhance the performance of the devices by lowering the energy barrier for hole or electron injection from the anode or cathode in order to balance the charge carrier distribution along the emitting layer. A wider uniform distribution of charge carriers enables control over the e^--h^+ recombination region responsible for the light output, e.g., moving it from the organic/electrode interfaces (where the defect states are higher) to the bulk emitter.[6]

The first layer above the glass substrate is a transparent conducting anode, commonly indium tin oxide (ITO) to allow the light outflow. Flexible OLEDs can also be performed with an anode made of a transparent organic compound, i.e., PEDOT:PSS, deposited on a suitable plastic.

The cathode is typically a low-to-medium workfunction (Φ) metal such as Ca (Φ=2.87 eV), Ba (Φ=2.7 eV), Al (Φ=4.3 eV) or $Mg_{0.9}Ag_{0.1}$ (for Mg, Φ=3.66 eV) deposited by either thermal or e-beam evaporation. The metal workfunction of the anode composed of ITO is estimated ranging from 4.7 to 5.2 eV. These metal workfunction values allow an effective injection for both charge carriers, electrons and holes, since their respective transport levels in the organic compounds are in a range of 0.5-0.6eV of difference.[7]

2.3. OLED Fabrication Procedures

2.3.1. Thermal Vacuum Evaporation

The vacuum thermal evaporation deposition technique (also known as vapour-phase deposition) consists in heating **small molecules** until evaporation of the organic material to be deposited. The material vapour finally condenses in form of thin film on the cold substrate surface and on the vacuum chamber walls. Usually low pressures are used, about 10^{-6} Torr or lower, to avoid reaction between the vapour and the atmosphere. At these low pressures, the mean free path of vapour atoms is the same order as the vacuum chamber dimensions, so these particles travel in straight lines from the evaporation source towards the substrate.

One of the most prominent advantages of thermal vacuum evaporation is that it enables fabrication of multilayer devices in which the thickness of each layer can be accurately controlled. In addition, 2-dimensional combinatorial arrays of OLEDs, in which two parameters (e.g., the thickness or composition of two of the layers) may be varied systematically across the array and can be relatively easy fabricated in a single deposition procedure. Furthermore, the vacuum deposition techniques employ the generally available vacuum equipment existing in the semiconductor industry.[4,8]

2.3.2. Wet-Coating Techniques

Since **conjugated polymers** frequently crosslink or decompose by heating, they can not be thermally evaporated in a vacuum chamber. Hence, they are generally deposited by wet-coating a thin film from a solution containing the organic compounds. That, however, imposes restrictions on the nature of the polymers and the sidegroups attached to the polymer backbone, because the polymers must be soluble. For example, PPV is insoluble, nevertheless it is fabricated by spin-coating of a soluble precursor which is annealed afterwards.

The process of applying a solution to a horizontal rotating disc, resulting in ejection and evaporation of the solvent and leaving a liquid or solid film, is called spin-coating, and has been studied and used since the beginning of the 20th century. Spin-coating is a unique technique in the sense that it is possible to apply a highly uniform film to a planar substrate over reduced area with a highly controllable and reproducible film thickness, Fig. 2.5. Although the thickness of spin-coating films may be controlled by: (1) the concentration of the polymer solution, (2) the spinning rate and (3) the spin-coating temperature, the achievement of uniform thicknesses constitutes the main drawback of this technique. Actually, it is very difficult to fabricate uniform and thick films for large area devices due to the procedure itself and the lack the thickness monitorization. In addition, no combinatorial fabrication methods have been developed for spin-coated PLEDs.[9]

To sum up, spin-coating is an established procedure in the semiconductor and display industries, widely used in photolithography of silicon and ITO and polycrystalline backplanes for liquid-crystal displays. However, it may not be used for large size single plane and full-colour displays.

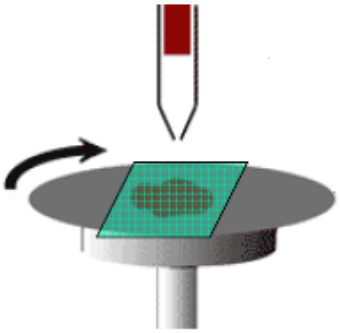

Fig. 2.5 Basic principle of the spin-coating technique where the organic compound is dropped over the glass substrate with ITO.

Doctor blade is an alternative technique to perform relatively thick films, however it is not appropriate for films with less thickness than 100 nm which

are commonly used in OLEDs. In this technique, a solution containing the soluble polymer is spread with uniform thickness over the substrate by means of a precision "doctor blade".

2.3.3. Ink-jet printing

An important development of the wet-casting is the ink-jet printing method achieved by Yang and co-workers. This technique is currently utilized by the most important companies in displays, e.g., Seiko, Epson, Philips, DuPont, Mitsubishi, Universal Display or Toshiba. This technique is nowadays leading the pursuit for commercially viable high-information content displays, since the organic layers are precisely deposited into fixed positions to fully perform an array of pixels independently of the substrate (see Fig. 2.6). These pixels are composed of different organic materials able to generate red, green and blue. Polyfluorene materials, among others, have demonstrated its versatility by this method which is considered as very efficient technique. High-quality resolution, thickness control and the possibility to work at atmospheric conditions of pressure and temperature are the strongest points of this manner to perform displays.[8,10]

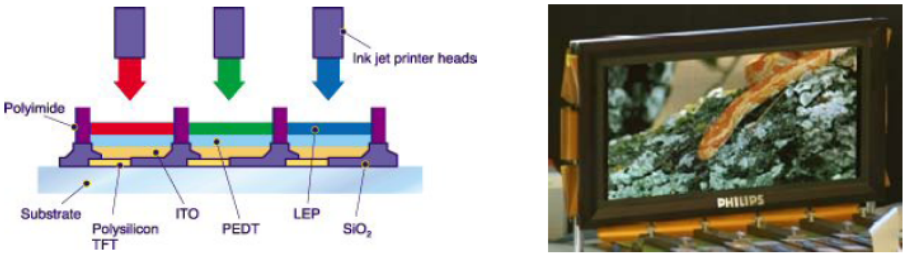

Fig. 2.6 Illustration of a simplified scheme of the ink-jet printing technique (left) and its outcome for a TV display prototype from Philips (right).

2.4. Basic Operation of OLEDs

The OLED device composed of a single layer of organic electroluminescent semiconductor consists of two additional electrodes with appropriate workfunctions (Φ_A and Φ_C for the anode and cathode, respectively) to ease the charge carrier injection to the HOMO and LUMO (see left-hand-side of Fig. 2.7). Once the electrodes are deposited on the device, the energy bands bend to achieve the equilibrium by establishing the same Fermi level along the sample (see centre of Fig. 2.7). Note that the band bending within the organic material is considerably different to their device counterparts made of inorganic compounds since the straight lines are more commonly shown for insulators in the literature. In this situation, charge injection does not occur therefore an applied voltage is required to force holes and electrons to overcome the energy barriers between the electrode workfunctions and their corresponding extended states, i.e., HOMO and LUMO. The band bending slope is negative in this configuration however by applying voltage the inclination gradually changes to positive values. An interesting intermediate situation is the flat-band configuration where the voltage applied is exactly the built-in potential which is defined as the difference between the metal electrodes workfunctions (see right-hand-side of Fig. 2.7).

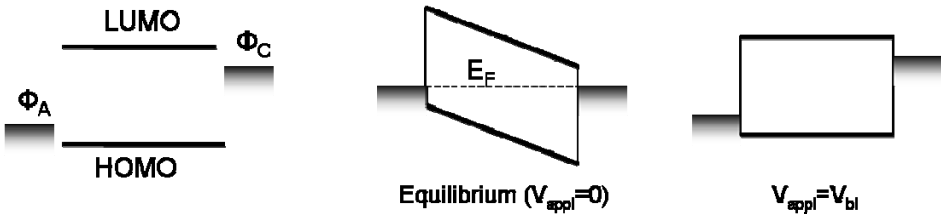

Fig. 2.7 Simple band structure for a single layer OLED. The figures displays three different situations: without any contact at the interfaces (left), once the contacts have been deposited and equilibrium is achieved (centre) and at non-equilibrium in the flat-band applied potential.

Once the voltage applied is over the built-in potential (see Fig. 2.8), charge injection from the electrodes does occur, leading the transport of electrons and holes through the material by drifting under the influence of the local electric

field. These carriers may then recombine to form a singlet or a triplet exciton (a Coulombically bound electron-hole pair) which may decay radiatively providing light output.[11,12] Fluorescence emitters (i.e., either PLEDs or SMLEDs) are based on the singlets decay whereas the phosphorescence emitters use the triplets decay (mainly in SMLEDs).[13]

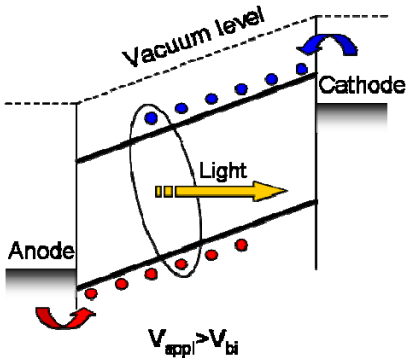

Fig. 2.8 Schematic energy band diagram illustrating the principle of a single layer device OLED.

The singlet to triplet exciton formation ratio is one of the most important issues regarding the electroluminescence (EL) of conjugated polymers. Since EL results exclusively from the decay of singlet excitons, can be considered as the theoretical limit for the efficiency of a polymer light-emitting diode (LED), particularly in the internal quantum efficiency (see section 2.8). Simple spin statistics predicts a singlet proportion of ¼ (i.e., one singlet and three triplets), but there have been some works which suggest that the exciton formation process could result in larger proportions.[14] The common energetic scheme for the singlet and triplet state decays is displayed in Fig. 2.9 where the intersystem crossing reduces the fluorescent emissions. However, additional singlet regeneration routes have been pointed out for the enhancement of singlet radiative decay such as the bimolecular triplet-triplet anhilation (TTA) that could be the responsible for the delayed fluorescence (DF) observed in experimental data.

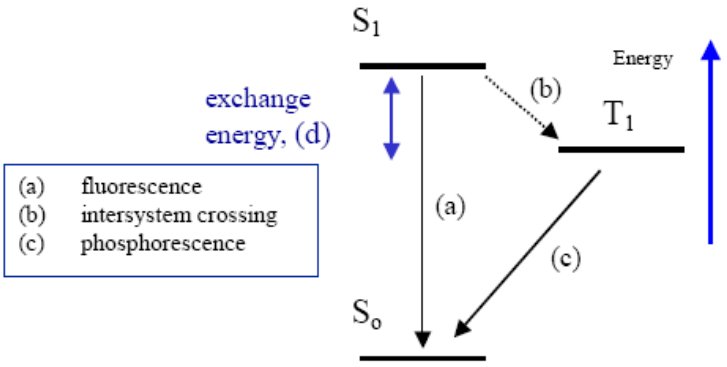

Fig. 2.9 Energy levels of the singlet and triplet states generated by electroluminescence and the route decays to the ground state.

Injection, *transport* and *efficiency* are the three crucial factors that have been widely studied to enhance the device performance of OLEDs (see next detailed subsections). On the one hand (see Fig. 2.10), the inclusion of hole transport layers (HTL) and electron transport layers (ETL) are aimed to ease injection and transport providing a more balanced charge distribution in the recombination region (see section 2.6.3). On the other hand, these two extra organic layers act as blocking layers for the opposite charge carrier not transport therefore it results in a positive feature that enhances the recombination rate and thereby improving the device efficiency.

Multilayer OLEDs can be extended to more than three layers to obtain a better device performance (i.e., injection, transport and efficiency) or even though to generate white light by stacking red, green and blue emitters with appropriate separating interlayers (see Fig. 2.11).

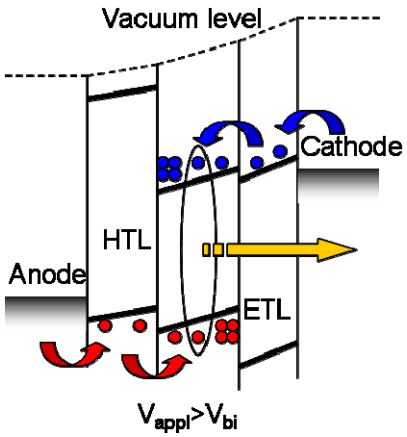

Fig. 2.10 Schematic energy band diagram of a trilayer OLED at forward bias.

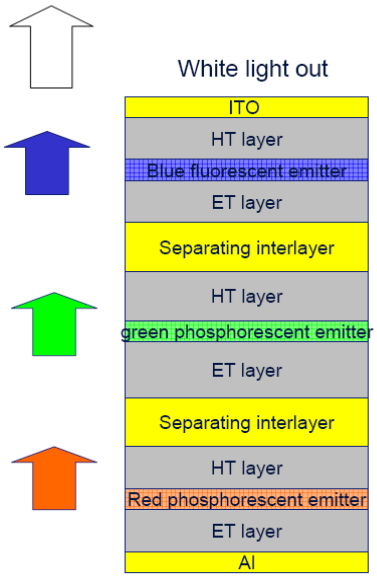

Fig. 2.11 Schematic structure of a standard white OLED by stacking RGB organic emitters.

2.5. Charge Injection into Organic Materials

The metal-organic semiconductor junctions are notably different to their inorganic counterparts and extensive research is reported in the literature. As commented in the previous subsection, OLED metal electrodes inject electrons and holes into opposite sides of the emissive organic layer. However, in the continuous models, the charge carriers must overcome the energy barriers that stems from the difference of the metal workfunctions and the extended states (i.e., HOMO and LUMO) as shown in Fig. 2.7.

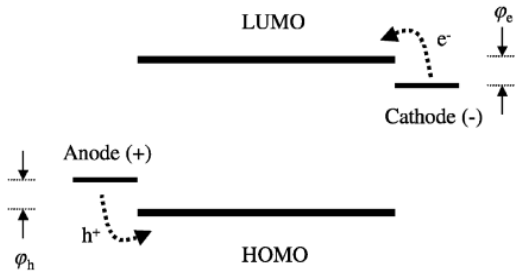

Fig. 2.12 Energy level diagram of a single layer organic light-emitting diode. Energy barriers either for hole injection (left) or electron injection (right) from the metal electrodes are shown.

The injection process may govern the performance of organic devices if the supply of carriers can not achieve the maximum that the material can transport. This would be the so-called injection-limited regime in contrast to the bulk-limited regime where the supply of injected carriers exceeds the transported ones.[15] In both regimes the *J-V* behaviour is quite different as shown in Fig. 2.13.

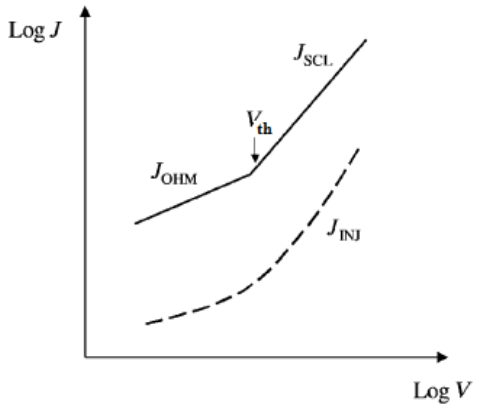

Fig. 2.13 Bulk-limited (solid line) and injection limited (dashed line) current density versus voltage characteristics for a trap-free semiconductor. The threshold voltage V_{th} indicates the turn from ohmic to space-charge limited current.

On the one hand, in the drift-diffusion model, the boundary condition for the injection of carriers can be considered by the flux of current entering the bulk material (i.e., a Neumann boundary condition). Scott and Malliaras established the expressions for injection currents into organic materials under the assumption of thermionic emission and a backflowing recombination rate in accordance with the detailed balance, therefore:[16]

$$J_p(anode) = C(N_v \exp(-\varphi_h / k_B T)\exp(f^{1/2}) - pS(E)) \tag{2.1}$$

where N_v is the density of chargeable sites, p the hole density, φ_h is the difference between the HOMO and the anode workfunction. C is a constant

$$C = 16\pi\varepsilon_r\varepsilon_0\mu_p(k_B T / e)^2 \tag{2.2}$$

and f is the reduced electric field given by:

$$f(E) = eE\frac{r_C}{k_B T} \tag{2.3}$$

where r_C is the Coulomb radius defined as,

$$r_C = \frac{e^2}{4\pi\varepsilon_r\varepsilon_0 k_B T} \tag{2.4}$$

and the recombination velocity for organic materials $S(E)$ is expressed by

$$S(E) = \frac{1/\psi^2 - f}{4} \tag{2.5}$$

with the custom variable ψ depending on the reduced electric field f as:

$$\psi = f^{-1} + f^{-1/2} - f^{-1}(1 + 2f^{1/2})^{1/2} \tag{2.6}$$

Nevertheless, the assumption of a Dirichlet boundary condition for modelling ohmic contacts is also quite appropriate since similar results are obtained when low energy barriers are present. In the more classical literature this condition is given for the electric field as:[17]

$$E(anode) = 0 \tag{2.7}$$

meanwhile, in some later publications,[7,18] the charge density is fixed at the contact

$$p(anode) = p_0 \tag{2.8}$$

by a quantity p_0, which is normally set to N_v (effective density of states in the HOMO) for the ohmic behaviour.[18] Both considerations, either for the electric field or for the charge density, provide the same results (for instance, *J-V* curves and electric distributions of field and charge density) for the high values of $p_0 = N_v$.

On the other hand, in the hopping models, charge carriers make a jump from the contact to the organic material over a distance x_0. It contributes to the injection current into a Gaussian distribution $g(\varepsilon)$ of states (DOS) unless it returns to the contact.

The expression proposed by Arkhipov is:[19,20]

$$J_{inj} = e\nu_0 \int_a^{\infty} dx_0 \exp(-2\gamma x_0) w_{esc}(x_0) \int_{-\infty}^{\infty} d\varepsilon' Bol(\varepsilon') g[U_0(x_0) - \varepsilon'] \tag{2.9}$$

where w_{esc} is the probability for a carrier to avoid surface recombination, a the distance from the electrode to the first hopping site in the bulk, ν_0 the attempt-to-jump frequency, γ the inverse localization radius, and the function *Bol(E)* is defined as

$$Bol(\varepsilon) = \begin{cases} \exp\{-\varepsilon/(k_B T)\}, & \varepsilon > 0 \\ 1, & \varepsilon < 0 \end{cases} \tag{2.10}$$

U_0 describes the electrostatic potential energy at distance x from the injecting electrode which includes the image potential and the external potential induced by the external field F_0,

$$U_0(x) = \Delta - \frac{e^2}{16\pi\varepsilon_r\varepsilon_0 x} - eF_0 x \tag{2.11}$$

The carrier escape probability w_{esc} is affected by the potential distribution $U_0(x)$. The expression determining its value ($0 < w_{esc} \leq 1$) is strongly depended on the distance x_0 (typically no less than 0.6-0.7 nm),

$$w_{esc} = \frac{\int_a^{x_0} dx \exp\left[-\frac{e}{k_B T}\left(F_0 x + \frac{e}{16\pi\varepsilon_r\varepsilon_0}\frac{1}{x}\right)\right]}{\int_a^{\infty} dx \exp\left[-\frac{e}{k_B T}\left(F_0 x + \frac{e}{16\pi\varepsilon_r\varepsilon_0}\frac{1}{x}\right)\right]} \tag{2.12}$$

Nevertheless, the study of electron injection through the metal-organic interface could be also rationalized in terms of the presence of a thin dipole layer aside the contact. Electron injection into the bulk may occur via a two hopping model. Firstly, carriers hop from the injecting electrode to an intermediate state that lies in dipole layer (defined by a Gaussian distribution).

The second hopping event takes place from the intermediate to the bulk LUMO states.[21] This model is capable to explain the phenomenon of negative capacitance observed in organic LEDs at low-frequencies by impedance spectroscopy.[22-24] Physically, the negative capacitance occurs because at high voltages the interfacial states are very far from equilibrium, and they need to become depopulated in order to accept electrons from the metal and transfer them to the bulk LUMO states.[25]

2.6. Charge Transport and Recombination in Organic Materials

2.6.1. Charge Transport Mobility

Most of the organic electroluminescent materials, either small molecules or conjugated polymers, display low-conductance behaviour. The hole mobility in these materials are typically ranging from 10^{-7} to 10^{-3} $cm^2/(Vs)$ (e.g., Silicon hole mobility is $1400 cm^2/(Vs)$), and the values for electron mobility are commonly reported lower by a factor of 10-100 (e.g., Silicon electron mobility is 450 $cm^2/(Vs)$). It is well established that the major reason of this disadvantage, in comparison with their inorganic counterpart materials, is the disorder in the amorphous or polycrystalline organic materials. The transport in the organic materials is usually described as subsequent intersite hops from localized-to-localized states assisted by the action of the electric field. In this framework, the jump rate between two transporting sites *i* and *j* is assumed to be of the Miller-Abrahams type:[26]

$$\nu_{ij} = \nu_0 \exp\{-2\gamma R_{ij}\} \begin{cases} \exp\{-(\varepsilon_j - \varepsilon_i)/(k_B T)\}, & \varepsilon_j > \varepsilon_i \\ 1, & \varepsilon_j < \varepsilon_i \end{cases} \qquad (2.13)$$

where R_{ij} is the intersite distance. When a field E is applied, the site energies also include the electrostatic energy. In addition to the energetic disorder of the transporting sites, positional disorder can be taken into account by regarding

the overlapping parameter γ. As a matter of fact, the transition rate ν_{ij} from one site to another depends on their energy difference and on the distance between them. The carriers may hop to a site with a higher energy only by absorbing a phonon of appropriate energy.

Furthermore, the charge-transporting sites distribution has been usually considered as a Gaussian one:

$$\rho(\varepsilon) = (2\pi\sigma^2)^{-1/2} \exp\left\{-(\varepsilon - \varepsilon_0)^2 / (2\sigma^2)\right\} \tag{2.14}$$

where the energy ε_0 and σ are the centre and the width of the density of states, respectively. In this model usually called the Gaussian disorder model (GDM), the field-dependent mobility, commonly found in time-of-flight experiments, is derived from random walk with Monte Carlo simulations.[27] The well-known Poole-Frenkel effect for mobility now arises again from this formalism, with the following expression:

$$\mu(E) = \mu_0 \exp\left\{\sqrt{E / E_0}\right\} \tag{2.15}$$

where μ_0 is the zero-field mobility for a particular carrier species in the material and E_0 a constant material which is temperature dependent. These parameters are found to fit in terms of other quantities closely related to the degree of disorder such as C, Δ, T_0 and D:[28]

$$\mu_0 = C \exp\left\{\Delta / (k_B T)\right\} \tag{2.16}$$

$$\frac{1}{E_0} = D\left[\frac{1}{k_B T} - \frac{1}{k_B T_0}\right] \tag{2.17}$$

The hopping transport model described up to now constitutes a coherent explanation of conduction in organic materials nevertheless it is not the only one. The multiple-trapping model, i.e. a continuum model rationalized in terms of transport of carriers via extended states repeatedly interrupted by trapping of

localized states, is also widely accepted. Both concepts of transport, either hopping or multiple-trapping, provide interpretation for experimental measurements of mobility by means of ToF (Time-of-Flight) among other different techniques to describe in the next subsection. The success of the multiple-trapping vision lies on its simplicity in contrast to the hopping model. In addition, both formalisms are interconnected since, by averaging the hopping rates over spatial and energy configurations, the dominated hopping events are determined by a transport level so-called E_{tr} as calculated by Arkhipov.[29] The occurrence of this effective transport level reduces the hopping transport to multiple trapping, with E_{tr} playing the role of the mobility edge.[30]

Despite the widely application of field-dependent mobility in organic layers for devices such as light-emitting diodes (OLEDs), mobility measurements in field-effect transistors (FETs) showed an enhancement up to three orders of magnitude.[31,32] This fact required a revision of the mobility field-dependence to include the carrier-concentration contribution, which was explained by the hopping percolation model in an exponential density of states by Vissenberg and Matters.[33] Thus, the density-dependent mobility becomes:[34]

$$\mu(n) = an^{b} \tag{2.18}$$

where a and b are model constants, particularly:

$$b = \frac{T_t}{T} - 1 \tag{2.19}$$

which is a coefficient that relates the operating temperature T to the characteristic trap temperature of the exponential distribution T_t.

A less-known mobility dependence on the frequency is also reported in the literature by impedance methods. This assumption is based on the dispersive transport (i.e., the existence of a broad distribution of transit times) of Sher and Montroll (SM) in ac techniques and is given by the expression:[35-37]

$$\mu(\omega) = \mu_{dc}\left(1 + M(i\omega\tau_{tdc})\right)^{1-\alpha} \tag{2.20}$$

where M and α (0< α <1) are dispersion parameters and τ_{tdc} is the classical expression for dc transit times (i.e., time needed for carriers to cross the sample electrode-to-electrode):[38]

$$\tau_{tdc} = \frac{4}{3}\frac{L^2}{\mu_{dc}\ V_{dc}} \tag{2.21}$$

where L is the sample thickness and V_{dc} voltage in the bulk. In the dc regime, the mobility is considered as a constant value.

2.6.2. Space-charge-limited Current (SCLC)

The charge transport in the bulk of an organic material, limiting the maximum current flowing through the device, is widely accepted to be space-charge-limited current (SCLC). In this regime, SCLC flow occurs when an electrode (normally an ohmic contact) can supply an unlimited number of carriers into the bulk causing a build-up of space charge in the device which is actually setting-up the electric field. SCLC.[39] Unipolar space-charge-limited current regime is present within the material (if no injection limitation occurs) and plays a crucial role for the analysis of the different models of carrier mobility exposed in the previous subsection.

SCLC described in terms of equations entails: continuity equation, drift current and Poisson equation. For a single-carrier device we have:[40]

$$\frac{dJ}{dx} = 0 \tag{2.22}$$

$$J = e \cdot \mu_n(x) \cdot n(x) \cdot E(x) \tag{2.23}$$

$$\frac{dE(x)}{dx} = -\frac{e}{\varepsilon} n(x) \tag{2.24}$$

In fact, the interpretation of current-density-voltage characteristics of single-layer devices is explained under the SCLC transport. The well-known Mott-

Gourney square law for trap-free and constant mobility can be obtained by integration of the electric field with the boundary condition *E(x=L)=0*,[41]

$$V = \int_0^L E(x)dx \tag{2.25}$$

Hence:

$$J_{M-G} = \frac{9}{8}\varepsilon \cdot \mu_n \frac{V^2}{L^3} \tag{2.26}$$

The alternative ohmic boundary condition is based on fixing the charge density at the injecting contact by n_0, which is normally quite high. In this case, the above formula is slightly modified:

$$V = \frac{\varepsilon J^2}{3e^3\mu_n^2}\left(\left(\frac{2e^2\mu_n L}{\varepsilon J} + \frac{1}{n_0^{\,2}}\right)^{3/2} - \frac{1}{n_0^{\,3}}\right) \tag{2.27}$$

when $n_0 \to \infty$ Eq. (2.27) reduces to Eq. (2.26). However, it is usually required to take into account the field-dependent mobility. For this case, the approximation of Murgatroyd holds:[42]

$$J \approx \frac{9}{8}\frac{\varepsilon\mu_n}{L^3}V^2 e^{0.89\sqrt{V/E_0 L}} \tag{2.28}$$

If shallow traps are present in the organic layer, the same expressions remain by only including a multiplying factor θ in the mobility parameter μ_p:[43]

$$\theta = \frac{n}{n + n_t} \tag{2.29}$$

where n_t is the density of trapped charge by the shallow traps and n the mobile carriers. In reality, traps are more likely to be distributed in energy rather than existing at discrete levels. For electrons, traps will be filled from the bottom to the top as far as more voltage is applied. The new injected carriers are expected to be trapped shifting the quasi-Fermi level upwards. In this regime, the

current-density behaves as $J \propto V^n$ with $n>2$ until all the traps are filled (i.e., the trap-filled limit regime TFL) up to a certain voltage where the coefficient n changes to $n=2$. Particularly, for an exponential density of trap states:

$$g_t(E_t) = \frac{N_t}{k_B T_t} e^{\frac{E_t - Ec}{k_B T_t}} \tag{2.30}$$

and under the approximation that all the trapping states are filled below the Fermi level, the current-potential characteristics are:[44]

$$J = e\mu_o N_c \left(\frac{\varepsilon}{eN_t}\right)^l \left(\frac{l}{l+1}\right)^l \left(\frac{2l+1}{l+1}\right)^{l+1} \frac{V^{l+1}}{L^{2l+1}} \tag{2.31}$$

where N_t is the effective density of traps, μ_0 the trap-free mobility, N_c the effective density of states in the transport level, T_t (commonly $T_t>T$) the characteristic trap temperature and $l=T_t/T$.

Let us now include the second charge carrier in the trap-free SCLC model. In the case of double-carrier devices, the SCLC is present for both types of carrier species and the following equations describe the system:

$$\frac{d}{dx}\left[p(x)\mu_p(x)E(x)\right] = -B \cdot p(x) \cdot n(x) \tag{2.32}$$

$$J = e \cdot \mu_p(x) \cdot p(x) \cdot E(x) + e \cdot \mu_n(x) \cdot n(x) \cdot E(x) \tag{2.33}$$

$$\frac{dE(x)}{dx} = \frac{e}{\varepsilon}(p(x) - n(x)) \tag{2.34}$$

where the first one (i.e., continuity equation) contains the recombination process, the second one involves an extra drift current that stems from the additional charge carrier, and the third one includes a modification of the field distribution caused by the extra charge within the material. B is the bimolecular recombination constant and can be expressed depending on mobilities as a Langevin type:[45]

$$B = \frac{e}{\varepsilon}(\mu_p + \mu_n) \tag{2.35}$$

The solution for this set of transport equations was firstly analytically solved by Parmenter-Ruppel in 1959 with the zero electric field boundary conditions at the electrodes. The full expression is rather complicated (see Ref.[17] p. 230) since all the variables are spatially mixed,

$$J = \frac{9}{8}\varepsilon \cdot \mu_{eff}\frac{V^2}{L^3} \tag{2.36}$$

$$\mu_{eff} = \frac{4}{9}\mu_R v_e v_h \left[\frac{\Gamma\left(\frac{3}{2}(v_e + v_h)\right)}{\Gamma\left(\frac{3}{2}v_e\right)\Gamma\left(\frac{3}{2}v_h\right)}\right]^2 \left[\frac{\Gamma(v_e)\Gamma(v_e)}{\Gamma((v_e + v_e))}\right]^2 \tag{2.36}$$

with the mobility ratios $v_e = \mu_e / \mu_R$, $v_h = \mu_h / \mu_R$ and the recombination mobility $\mu_R = \varepsilon B/(2e)$. In especial cases the system may be simplified. For instance, under the approximation of strong recombination at a certain position inside the organic sample, i.e., transport is dominated by electrons in a region close to the anode whereas holes do it in the rest, the analysis simplifies into the quadratic formula:

$$J = \frac{9}{8}\varepsilon \cdot (\mu_p + \mu_n)\frac{V^2}{L^3} \tag{2.37}$$

Nevertheless, in the opposite situation under the approximation of the so-called plasma limit, i.e., similar concentrations of electrons and holes are present within the organic layer ($p \approx n$), the Parmenter-Ruppel result stands as:[46]

$$J = \left(\frac{9\pi}{8}\right)^{1/2}\varepsilon \cdot \left(\frac{2e\mu_p\mu_n(\mu_p + \mu_n)}{\varepsilon B}\right)^{1/2}\frac{V^2}{L^3} \tag{2.38}$$

It is noteworthy to remark that the presence of the second charge carrier, being

ohmically injected, might increase noticeable the current within the device, as shown in the last two formulae. In fact, the plasma limit constitutes the theoretical maximum current-density that a device can bear along the voltage range.

In reality, the common experimental situation of recombination in organic layers is between both previous described regimes, strong and weak recombination, and the analysis of *J-V* curves becomes slightly more complicated. Furthermore, the SCLC starts to dominate the charge transport at a certain threshold voltage V_{th}, normally some millivolts, when the injected charges considerable exceed the intrinsic charges lying in the bulk n_0. Until then, the charge is mainly ohmically transported in the bulk by drifting the free-charge carriers n_0 from one electrode to the other. The classical expression of current-density-voltage governing in that minority regime entails a first order polynomial current-density dependence on the voltage as $J \propto V$. In the specific configuration of just a single carrier, the following expression describes the characteristics,

$$J = en_0\mu_n \frac{V}{L} \tag{2.39}$$

where n_0 stands for the free charges removed in the sample by the electric field until the SCLC regime widely occurs from the threshold voltage onwards, see Fig. 2.13.

2.6.3. Distribution of Charge Carriers, Electric Field and Recombination in Organic Layers

Charge carrier distributions have been studied for the development of OLEDs in order to enhance their performance and therefore the light emission. The non-uniform distributions within thickness are caused by the SCLC and limit the efficiency of the organic devices. The search of charge balanced in organic layers constitutes a key role for improving the stability and efficiency of OLEDs.[47,48]

In single-carrier organic layers with constant mobility, analytical expressions are available in the literature. Solving the system of Eqs. (2.22)-(2.24) for holes with constant mobility and an injecting contact at *x=0* (where the boundary condition is zero electric field) charge and electric field follows the spatial dependence:[49]

$$p(x) = \frac{\varepsilon}{2e}\sqrt{\frac{2J}{\varepsilon \cdot \mu_p}}x^{-1/2} \tag{2.40}$$

$$E(x) = \sqrt{\frac{2J}{\varepsilon \cdot \mu_p}}x^{1/2} \tag{2.41}$$

Note that hole concentration tends to infinity at the injecting contact (x→0) which means that the metallic contact behaves as an unlimited supplier of charge carriers (ohmic). Electric field vanishes at x→0. The multiplication of both magnitudes gives a constant that entails constant current-density. In the vicinity of the injection zone, most of the current is due to massive charge concentration supported by a weak electric field, whereas in the rest of the bulk fewer charge carriers are driven by a strong electric field, Fig. 2.14. Electric distributions become smoother within the organic layer the higher value of mobility is implemented, or in other words, a higher mobility value enables its charge carriers to easily penetrate deeper within the organic material.

If the ohmic condition is given throughout a fixed charge injected at the interface $p(x=0) = p_0$, the previous expressions bear a slight modification:

$$p(x) = \frac{1}{\sqrt{\frac{2e^2\mu_p}{J\varepsilon}x + \frac{1}{p_0}}} \tag{2.42}$$

$$E(x) = \frac{J}{e\mu_p}\sqrt{\frac{2e^2\mu_p}{J\varepsilon}x + \frac{1}{p_0^{\,2}}} \tag{2.43}$$

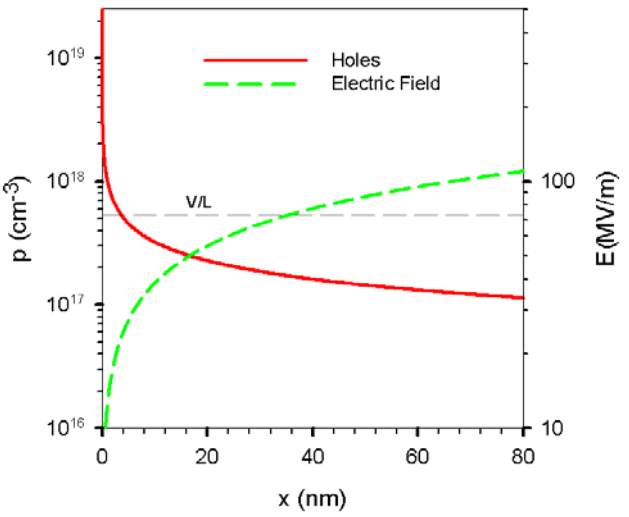

Fig. 2.14 Hole and electric field distributions in a single-carrier organic layer at at $J = 100\,\mathrm{A/m^2}$ and 5.86V. Device parameters are: $L = 80\,\mathrm{nm}$, $\mu_p = 5\times10^{-7}\,\mathrm{cm^2/(Vs)}$, $\varepsilon_r = 3$.

Since p_0 is considered a high number, typically $p_0 = N_v = 2.5\cdot10^{19}\,\mathrm{cm^{-3}}$, the correction becomes negligible and both conditions (zero electric field and high fixed injected charge) are equivalent. However, if p_0 is underestimated by several orders of magnitude, the bulk-limited regime may change to an injection-limited one.[50]

In dual-carrier devices charge concentrations (for holes and electrons) and the electric field distribution are obtained by solving the system composed of Eqs. (2.32)-(2.35) with the following boundary conditions:

$$\begin{aligned} p(x=0) &= N_v = 2.5\cdot10^{25}\,\mathrm{m^{-3}} \\ n(x=L) &= N_c = 2.5\cdot10^{25}\,\mathrm{m^{-3}} \end{aligned} \qquad (2.44)$$

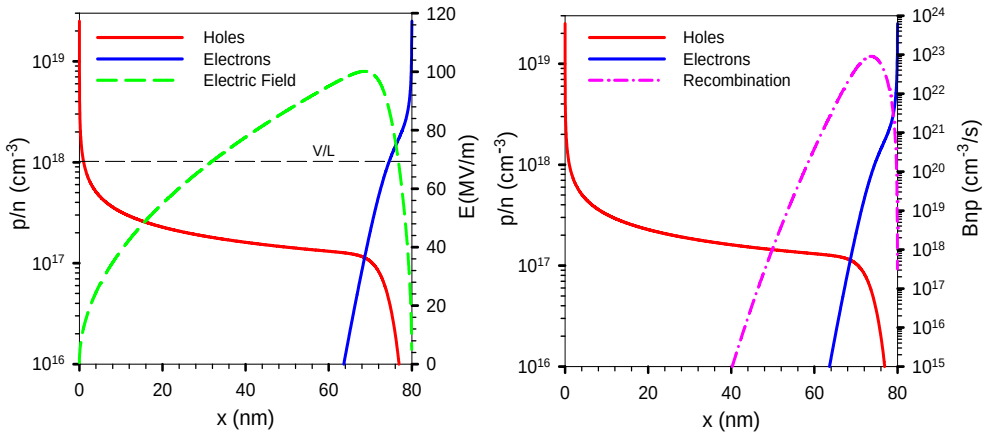

Fig. 2.15 Hole and electron carrier densities (left-hand side) and electric field distribution (green dashed line) at $J = 100\,\mathrm{A/m^2}$ and 5.54V. Right-hand-side figure shows recombination distribution. Device parameters are: $L = 80\,\mathrm{nm}$, $\mu_p = 5\times10^{-7}\mathrm{cm^2/(Vs)}$, $\mu_n = \mu_p / 10$, $\varepsilon_r = 3$ and $B = 2\cdot10^{-12}\mathrm{cm^3/s}$.

Figure 2.15 shows that the recombination region, where most of electron-hole encounters occur, is in the vicinity of the cathode as well as the generation of excitons. Some of them can be absorbed by the proximity of the contact resulting in a limitation of the device performance. The introduction of a hole transport layer (HTL) between the anode (typically ITO) and the light-emitting polymer (LEP), provokes a shift of the recombination zone towards the centre of the LEP.[50] The HTL not only slows down the faster charge carriers, i.e., the holes, but also improves the hole injection causing the necessary charge balanced.

2.7. Experimental Determination of Mobility

2.7.1. Time-of-Flight

The time-of-flight method (ToF) is the most widely used technique to measure mobility in organic semiconductors, which is a parameter of prime importance to describe the charge transport in the bulk of these materials.[51,52] The typical ToF set-up is composed of a relatively thin film sample sandwiched between two electrodes that may inject holes and electrons at forward bias. However, to measure a specific charge carrier mobility species, e.g., hole mobility, the device operation required is at reverse bias to obtain a non-injecting contact that must be transparent as well, Fig. 2.16. Once the electric field is established removing all the charges within the bulk, a laser pulse of a nitrogen laser penetrates from the side of the blocking contact and it is strongly absorbed in a short distance in its vicinity.[15] The photogenerated charge carriers are separated under the influence of the electric field and the holes are made to traverse the sample by drift. In a trap-free material, the photocurrent transient should exhibit a plateau during which the photoexcited holes move with constant velocity. When the holes arrive at the opposite electrode, the photocurrent drops to zero. This transit time τ (t_0 in the figure) for carriers to cross the sample is monitored in the oscilloscope and it is related to mobility via:[53]

$$\tau = \frac{L}{\mu_p E} \tag{2.45}$$

where L is the sample thickness, μ_p the hole mobility, and the electric field E may be approximated by the quotient of the voltage in the bulk (subtracting the threshold voltage) V_{th} and the thickness:

$$E = \frac{V_{dc} - V_{th}}{L} \tag{2.46}$$

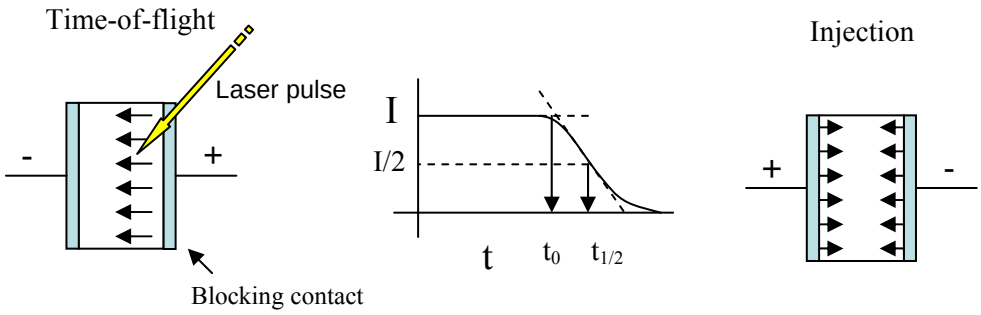

Fig. 2.16 Layout of a time-of-flight experiment to measure hole mobility (left). Photocurrent drift at reverse bias to measure mobility by means of transients (centre) whereas the device operation occurs at forward bias (right).

To sum up, the ToF method is based on the measurement of the carrier transit time, namely, the time required for a sheet of charge carriers photogenerated near one of the electrodes by pulsed light irradiation to drift across the sample to the other electrode under an applied electric field.

2.7.2. Current-Voltage Characteristics

Measurements of current-density-voltage characteristics, i.e., *J-V* curves, are commonly applied for the analysis of charge transport. The experimental set-up is quite simple and requires a single-carrier sample together with a potentiostat and its software implemented. The conventional manner to function is by ranging the voltage from 0 to several volts higher than the threshold voltage, when the SCLC mainly occurs. Once no injection limitation is checked over the *J-V* curves, fittings over the SCLC regime must be carried out according to the different mobility models. On the one hand, the consideration of the field-dependent mobility, Eq. (2.15), is taken into account by the approximation of Murgatroyd, Eq. (2.28), to obtain μ_0 and E_0 in trap-free organic layers.[54,55] That is the case of the measurements of PPV hole-only devices as shown in Fig. 5.7., below. On the other hand, by regarding an exponential density of traps in the band-gap, fittings over the bulk regime were carried out by means of the

Eq. (2.31). From these calculations on thick PPV single-carrier devices at different temperatures (see Fig. 2.17), Campbell et al. extracted the trap-free mobility μ_0 under the assumption of a reasonable effective density of states in the transport level N_v. Furthermore, the effective density of traps N_t and the characteristic trap temperature T_t were estimated.[56]

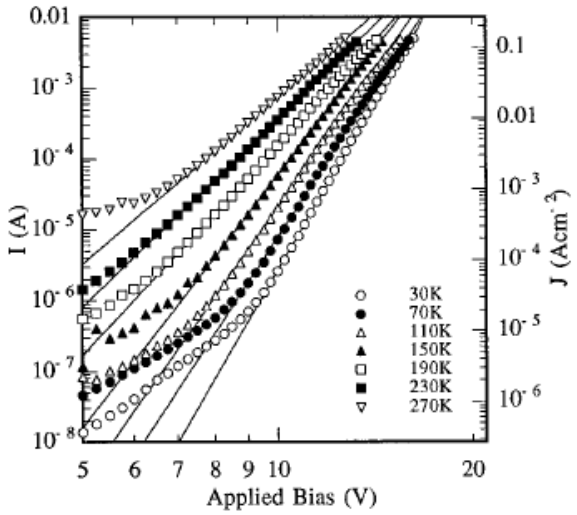

Fig. 2.17 Variation of the current I with applied bias V for one of the thinner (d=94 cm) devices at seven different temperatures in the high applied bias region. Thin broken lines are fits of Eq. (2.29) to the experimental results. Representation taken from Ref. [56]

2.7.3. Transient Electroluminescence

The transient electroluminescence technique is appropriate to study the charge transport in actual light-emitting layers. The experimental set-up requires a power source, able to emit a squared signal, connected to the device. A suitable photodetector is also needed to capture the light emission together with an oscilloscope so as to monitorize both signals, the voltage steps from the power source and the photosignal that stems from the photodetector. In fact, the method is based on the temporal evolution of the corresponding

electroluminescence (EL) occurring once the voltage step is applied across the light-emitting device, Fig. 2.18.[57]

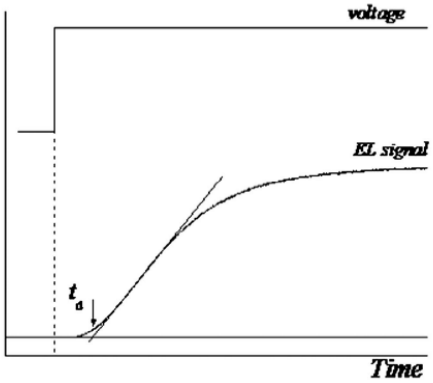

Fig. 2.18 Typical shape of the transient EL response and the voltage step above. Schematic representation taken from Ref. [58]

The time delay t_d between the onset of the EL response and the applied voltage stands for the time for electrons and holes to encounter within the bulk of the material. Under the assumption that charge injection time and recombination time are much faster than the transit time, t_d is related to the sum of both charge carrier mobility species, i.e., $(\mu_p + \mu_n)$.[59] Since in many organic materials one type of the carrier may exhibit mobility deviations of around two orders of magnitude, i.e., $\mu_p >> \mu_n$ thus the hole mobility (or the electron mobility depending on the material) can be determined by the application of Eq. (2.46) and Eq. (2.47), with t_d playing the role of the transit time τ for one of the charge carriers.

2.7.4. Dark Injection SCLC

The dark injection space-charge-limited transient current (DI SCLC) is a technique based on the measurement of the current transient *j(t)* stimulated by the application of a voltage step. The injection of charges through an ohmic contact is carried out in the dark. The experimental set-up is even simpler than

the transient EL method previously explained since the organic device may be connected to an oscilloscope in order to compare both signals, the voltage step and the transient current. Alternatively, a potentiostat with its corresponding software could be also utilized to monitore both transients.[60]

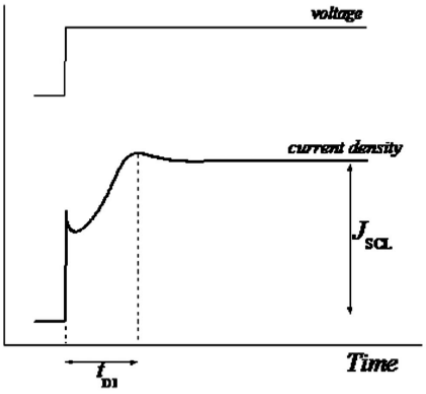

Fig. 2.19 Typical shape of the transient EL trap-free response and the voltage step above. Schematic representation taken from Ref. [58]

The method basically compares the temporal evolution of the transient current. Firstly, Fig. 2.19, the current keep up with the signal since its nature is purely ohmic by drifting the free charges present in the sample. Once they are removed in the bulk, the current slightly decreases, SCLC regime starts and the leading front of the charges takes some time to arrive at the collecting contact t_{DI} producing a maximum in the transient current. Finally, the stationary SCL current-density J_{SCL} is achieved for larger values in the time scale. The correlation between transit time in dark injection t_{DI} and charge transport mobility is given by the expression:[17]

$$t_{DI} = \frac{0.786 \cdot L^2}{\mu(V_{app} - V_{th})} \tag{2.47}$$

where L is the layer thickness, μ the mobility, V_{app}-V_{th} the voltage drop in the bulk of the organic material. DI can also be applied for the simultaneous measurement of mobility in dual carrier devices.

2.7.5. Impedance Spectroscopy

Impedance spectroscopy (IS) is a very useful technique for characterizing the electronic properties of materials.[61] In IS, the sample under investigation is subject to a small ac voltage harmonic modulation $v_{ac} = v_0 \cos(\omega t)$ and the complex impedance is measured by means of the ac induced current i_{ac}. Thus, the admittance $Y(\omega)$, which is simply the inverse of impedance $Z(\omega)$, can be obtained as a function of frequency and the dc biased voltage as,

$$Y(\omega) = i_{ac} / v_{ac} = G(\omega) + i\omega C(\omega) \tag{2.48}$$

where $\omega = 2\pi f$ is the linear frequency, $G(\omega)$ is the conductance, and $C(\omega)$ is the capacitance of the system.[38] On the one hand, the real part of complex admittance, i.e. conductance, is related to conduction processes within the device, such as translative motion of charge carriers. On the other hand, the imaginary part, i.e. the so-called susceptance $B(\omega) = \omega C(\omega)$, is linked to displacement processes, e.g., due to reorientation of electric dipoles within the material under the electric field.

The experimental set-up is composed of sample electronic device appropriately connected to a potentiostat provided with an impedance modulus and the corresponding software package. The measurements must be carried out by applying voltages above the built-in potential in order to inject charge carriers through the electrodes under the SCLC regime that results in additional contributions to device capacitance.[36]

In particular, an inductive contribution arises at low-frequencies from the fact that additional injected carriers are able to keep up with the signal to arrive at the collecting contact (see Fig. 2.20). However, for frequencies higher than the inverse of transit time τ^{-1} the ac carrier can not follow the signal oscillation displaying a step-up. Capacitance spectra for a trap-free single-carrier device has an analytical formula, see Eqs. (5.8)-(5.10), and the transit time can be

calculated by the maximum in the negative differential susceptance $-\Delta B(\omega) = -\omega(C(\omega) - C_g)$ by the expression, $\tau \approx 0.72 \cdot f_{\max}^{-1}$.[62,63]

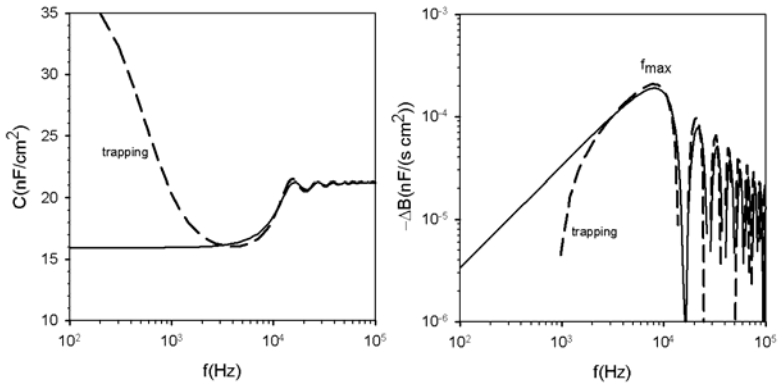

Fig. 2.20 Simulated capacitance and differential susceptance spectra to measure mobility. Effect of trapping is also shown by the dashed line.

Charge transport mobility can be finally obtained by,

$$\mu = \frac{4}{3} \frac{f_{\max} L^2}{0.72 \ (V_{app} - V_{th})} \tag{2.49}$$

where L is the layer thickness, $f_{\max}$ the frequency of the suscetance peak, μ the mobility, V_{app}-V_{th} the voltage drop in the bulk of the organic material.

To sum up, impedance spectroscopy constitutes a useful technique to measure mobility in single and double carrier devices at operative voltages, in forward bias,[64,65] meanwhile time-of-flight do it at a reverse bias.

2.7.6. CELIV Mobility

In contrast to the methods previously described, the CELIV technique (charge extraction by increasing voltage) is based on the study of the evolution of the transient current that stems from extraction of charges instead of injection. The measuring set-up is quite simple since only an oscilloscope, the sample, and a function generator, are required. The method works by applying

a linearly increasing voltage $U=At$ between the two electrodes, one ohmic and the other one blocking, in order to study the transient current $j(t)$, as shown in Fig. 2.21. By monitoring the peak in the transient current at t_{max}, charge carrier mobility can be obtained by the following expression,

$$\mu = \frac{2L^2}{3At_{\max}^2\left(1+0.36\frac{\Delta j}{j(0)}\right)} \tag{2.50}$$

where L is the sample thickness, A the voltage rate and Δj is the excess of transient current in the peak over the value at $t=0$, $j(0)$.[66,67]

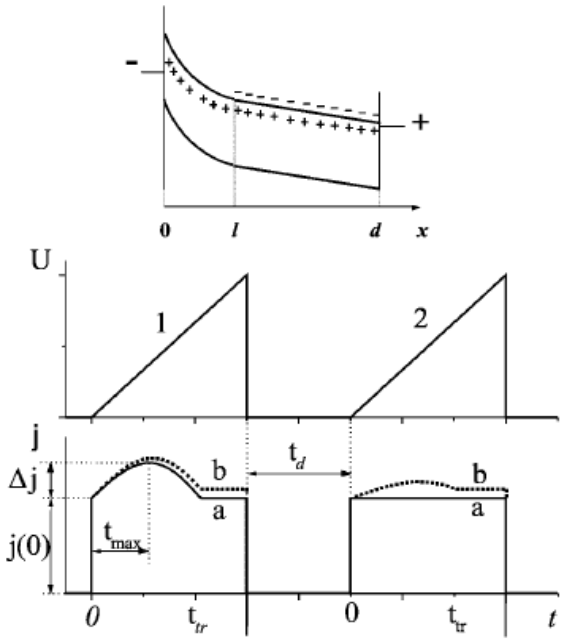

Fig. 2.21 Schematic illustration of the CELIV method. U is the form of the applied voltage to the sample, and j is the corresponding transient current. The upper panel displays the band diagram of the typical device. Representation taken from Ref. [66]

The CELIV method was initially aimed to measure charge carrier mobility in relatively conductive materials such as mycrocristalline silicon (μc-Si:H) where ToF fails due to a redistribution of electric field in a time shorter than the

transit time (i.e. the package of drifting charge disappears before its arrival to the collecting contact). The technique is also successfully applicable to low-mobility materials such as amorphous hydrogenated silicon (*a*-Si:H) and organic semiconductors (e.g. P3HT).[68]

2.7.7. OFET Mobility

Mobility is also measured by means of the field-effect in organic field-effect transistors, OFETs, but the value obtained by this procedure is normally higher (even three orders of magnitude) from others such as in ToF results.[32] This is mainly because the thin layer of semiconductor adjacent to the dielectric one determines the field-effect mobility. The ToF mobility probes the bulk mobility of the sample along a certain direction, whereas the field-effect configuration provides the surface mobility of the layers aside the dielectric gate, see Fig. 2.22. Morphological differences (e.g., depth and profile of traps) can influence the deviation of mobility values for bulk and surface transport.[69]

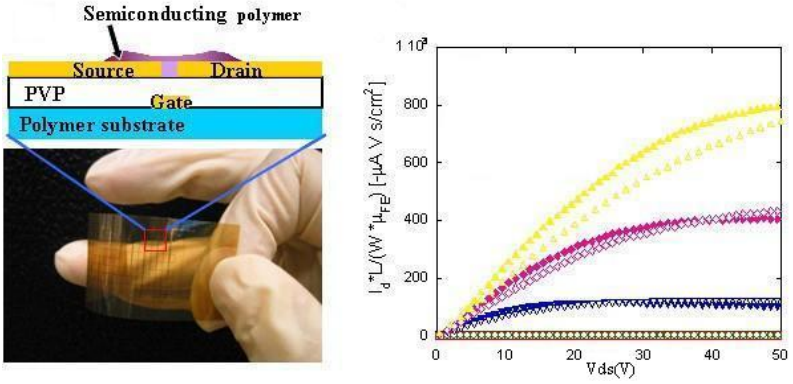

Fig. 2.22 Typical layout of an OFET (left) and its corresponding normalized drain current versus V_{dd} (right).

The bias voltage V_{ds} inside the drain-source channel of the OFET is understood by taking into account the formation of accumulation or depletion layers. The accumulation (depletion) layer corresponds to the excess (deficit) of majority carriers at the gate dielectric-semiconductor interface upon application

of bias a voltage V_{gs}, which results in a band bending. On the one hand, in the saturation regime (where the drain current I_d is independent of drain voltage V_{ds}) the drain current simplifies into the expression:

$$I_{d,Sat} = \frac{W}{2L}\mu_{FE}C_i\left(V_{gs} - V_t\right) \tag{2.51}$$

where C_i is the dielectric capacitance per unit area, V_{gs} and V_t are gate and threshold voltages, respectively, and W and L are the area and length of the channel, respectively. In this case operation regime, the mobility in OFETs can be calculated by,

$$\mu_{FE} = \frac{\partial I_{d,Sat}}{\partial V_{gs}}\frac{2L}{WC_i} \tag{2.52}$$

On the other hand, if the OFET is operating in the linear regime (where small drain voltages V_{ds} are applied), the transfer characteristics becomes,

$$I_{d,Lin} = \frac{W}{L}\mu_{FE}C_i\left(V_{gs} - V_t\right)V_{ds} \tag{2.53}$$

and consequently, the field-effect mobility is given by the following formula:

$$\mu_{FE} = \frac{\partial I_{d,Lin}}{\partial V_{gs}}\frac{L}{WC_iV_{ds}} \tag{2.54}$$

Measurements of charge transport mobility in OFETs contribute to the characterization and development of fast-response electronic devices.

2.8. The Efficiency of OLEDs

OLEDs are current-driven devices that utilize emissions from the electronically excited states of molecules. The operation of OLEDs involves charge injection from the anode and the cathode into the adjacent organic layers, transport of injected charge carriers through the organic layers, exothermic recombination of holes and electrons to generate excitons, followed

by their deactivation by the emission of either fluorescence or phosphorescence, which is taken out of the device as electroluminescence. Efficiency is a key issue not only for energy-consumption (OLEDs display low-drive voltage), but also for its effect on the longevity of the devices, since the ability to operate the device at a lower input power at a given luminance decreases the ohmic heating and increases the device lifetime.

The luminous power efficiency L_{eff} [lm W^{-1}] is one of the most common physical quantities to measure the efficiency of an electro-optical device and it is defined as:[53]

$$L_{eff} = \frac{\pi \ Lum}{JV} \tag{2.55}$$

where *Lum* is the luminance [$cd\ m^{-2}$], and *J* and *V* are the current density[$A\ m^{-2}$] and the applied voltage [*V*] required to obtain the luminance. A high power efficiency implies a low *J V* product for a given luminance. However, much of the analysis for the efficiency in the literature has been devoted to the external quantum efficiency η_{ext}, i.e., the number of photons emitted through the front face of the device per injected electron.

One of the forms in which the basic expression for the external quantum efficiency η_{ext} of an OLED is usually given in terms of four multiplying factor:[48]

$$\eta_{ext} = \alpha\eta_{\text{int}} = \alpha\eta_{rec}\eta_{spin}\eta_{PL} \tag{2.56}$$

where α is a light extraction factor that relates the external quantum efficiency η_{ext} to the internal quantum efficiency η_{int}, which is actually composed of three factors: η_{rec}, η_{spin} and η_{PL}. On the one hand, the out-coupling factor α depends on the refractive index *n* of the layer emitter and it is commonly approximated by:

$$\alpha \approx \frac{0.5}{n^2} \tag{2.57}$$

Hence, for $n \approx 1.6$, $\alpha \approx 0.2$. On the other hand, the internal quantum efficiency η_{int} comprises the following three quantities with their physical significance. (1) The recombination probability $\eta_{rec} \leq 1$ basically represents a measure of the balance between h^+ and e^-, and the ratio of exciton-forming events to the electrons flowing in the device. In other words, it is the fraction of electrons and holes which recombine with each other. This factor can be optimized by varying the composition and thickness of the different organic layers composing the OLED. (2) The spin-statistics factor η_{spin} is the generation probability of either electronically excited singlet or triplet state, which are, in principle, 0.25 and 0.75, respectively, if no intersystem crossing processes occur between states. Finally, (3) the photoluminescence PL quantum yield η_{PL} gives the ratio of the radiative decay events to the total ones (i.e., the sum of radiative and non-radiative pathways) that can be present in the material. When fluorescent emitters are employed, only 25% of the generated excitons might participate in radiative emissions, however, for the phosphorescent emitters, an internal quantum efficiency η_{int} up to 100% may be achieved. To sum up, an internal quantum efficiency $\eta_{\text{int}} \approx 1$ can be present in some phosphorescent material however, the out-coupling factor $\alpha \approx 0.2$ reduces the external quantum efficiency up to $\eta_{ext} \approx 20\%$.

Another more experimental and important device parameter, usually found in the literature for the characterization of OLEDs, is the conversion efficiency (CE), which is defined as the ratio between the EL intensity collected and the electric current. It gives the proportion of the number of photons taken out of the device to the charge flowing in the external circuit.[70]

2.9. References

[1] R. H. Friend, R. W. Gymer, A. B. Holmes, et al., Nature **397**, 121 (1999).

[2] S. J. Martin, "*Simulations of Charge Transport in Organic Light Emitting Diodes"* (University of Bath, PhD Thesis, Bath, 2002).

[3] K. Müllen and U. Scherf, "*Organic Light-Emitting Devices: Synthesis, Properties and Applications"* (WILEY-VCH, Singapore, 2006).

[4] J. Shinar, "*Organic Light-Emitting Devices: A Survey"* (Springer, New York, *2004*).

[5] B. K. Cumpston and K. F. Jensen, Trends in Polymer Science **4**, 151 (1996).

[6] K. Meerholz, Nature **437**, 327 (2005).

[7] P. W. M. Blom and M. C. J. M. Vissenberg, Materials Science & Engineering **27**, 53 (2000).

[8] S. Forrest, Nature **428**, 911 (2004).

[9] K. Norrman, A. Ghanbari-Siahkali and N. B. Larsen, Annu. Rep. Prog. Chem. Sect. C: Phys. Chem. **101**, 174 (2005).

[10] P. Chamorro, J. Martín, P. Martín, et al., "*Fundamentos de la Tecnología OLED"* (Mata Digital SL, Valladolid, 2008).

[11] H. Ishii, K. Sugiyama, E. Ito, et al., Adv. Mat. **11**, 605 (1999).

[12] I. D. Parker, J. Appl. Phys. **75**, 1656 (1994).

[13] F. So, B. Krummacher, D. Poplavskyy, et al., J. Appl. Phys. **102**, 091101 (2007).

[14] L. C. Lin, H. F. Meng, J. T. Shy, et al., Phys. Rev. Lett. **90**, 036601 (2003).

[15] Y. Shen, A. R. Hosseini, M. H. Wong, et al., ChemPhysChem **5**, 16 (2004).

[16] J. C. Scott and G. G. Malliaras, Chem. Phys. Lett. **299**, 115 (1999).

[17] M. A. Lampert and P. Mark, "*Current Injection in Solids"* (Academic Press, Inc., New York, 1970).

[18] P. W. M. Blom, M. J. M. de Jong and M. G. van Munster, Phys. Rev. B **55**, R656 (1997).

[19] V. I. Arkhipov, E. V. Emelianova, Y. H. Tak, et al., J. Appl. Phys. **84**, 848 (1998).

[20] V. I. Arkhipov, U. Wolf and H. Bässler, Phys. Rev. B **59** (1999).
[21] M. A. Baldo and S. R. Forrest, Phys. Rev. B **64**, 085201 (2001).
[22] H. H. P. Gommans, M. Kemerink and R. A. J. Janssen, Phys. Rev. B **72**, 235204 (2005).
[23] J. Bisquert, G. Garcia-Belmonte, A. Pitarch, et al., Chem. Phys. Lett. **422**, 184 (2006).
[24] J. Bisquert, G. Garcia-Belmonte, J. M. Montero, et al., Proc. SPIE Int. Soc. Opt. Eng. **6192**, 619210 (2006).
[25] G. Garcia-Belmonte, H. Bolink and J. Bisquert, Phys. Rev. B **75**, 085316 (2007).
[26] A. B. Walker, A. Kambili and S. J. Martin, J. Phys.: Condens. Matter **14**, 9825 (2002).
[27] H. Bässler, Phys. Status Solidi (b) **175**, 15 (1993).
[28] M. C. J. M. Vissenberg and P. W. M. Blom, Synth. Met. **102**, 1053 (1999).
[29] V. I. Arkhipov, E. V. Emelianova and G. J. Adriaenssens, Phys. Rev. B **64**, 125125 (2001).
[30] A. L. Alvarez, B. Arredondo, B. Romero, et al., IEEE Trans. Electron Devices **55**, 674 (2008).
[31] C. Tanase, P. W. M. Blom, E. J. Meijer, et al., Mater. Res. Soc. Symp. Proc. **725**, P10.9.1 (2002).
[32] C. Tanase, E. J. Meijer, P. W. M. Blom, et al., Phys. Rev. Lett. **91**, 216601 (2003).
[33] M. C. J. M. Vissenberg and M. Matters, Phys. Rev. B **57**, 12964 (1998).
[34] B. Ramachandhran, H. G. A. Huizing and R. Coehoorn, Phys. Rev. B **73**, 233306 (2006).
[35] H. Scher and E. W. Montroll, Phys. Rev. B **12**, 2455 (1975).
[36] S. W. Tsang, S. K. So and J. B. Xu, J. Appl. Phys. **99**, 013706 (2006).
[37] H. C. F. Martens, H. B. Brom and P. W. M. Blom, Phys. Rev. B **60**, R8489 (1999).
[38] A. Van der Ziel, "*Solid State Physical Electronics*" (Prentice-Hall, Englewood Cliffs, 1976).

[39] P. R. Emtage and J. J. O'Dwyer, Phys. Rev. Lett. **16**, 356 (1966).

[40] J. M. Montero, J. Bisquert, G. Garcia-Belmonte, et al., Phys. Status Solidi (a) **204**, 2402 (2007).

[41] N. F. Mott and R. W. Gurney, "*Electronic processes in ionic crystals"* (Oxford University Press, London, 1940).

[42] P. N. Murgatroyd, J. Phys. D: Appl. Phys. **3**, 151 (1970).

[43] A. Rose, "*Concepts in Photoconductivity and Allied Problems"* (John Wiley & Sons, New York, 1963).

[44] M. M. Mandoc, B. de Boer, G. Paasch, et al., Phys. Rev. B **75**, 193202 (2007).

[45] P. Langevin, Ann. Rev. Phys. Chem. **28**, 289 (1903).

[46] P. W. M. Blom, M. J. M. Dejong and S. Breedijk, Appl. Phys. Lett. **71**, 930 (1997).

[47] P. S. Davids, I. H. Campbell and D. L. Smith, J. Appl. Phys. **82**, 6319 (1997).

[48] B. K. Crone, P. S. Davids, I. H. Campbell, et al., J. Appl. Phys. **84**, 833 (1998).

[49] A. Pitarch, G. Garcia-Belmonte and J. Bisquert, J. Appl. Phys. **100**, 084502 (2006).

[50] J. M. Montero, "*Injection and Transport in Organic Light-Emitting Diodes (OLEDs)"* (Universitat Jaume I, MSc Thesis, Castellón, 2007).

[51] E. H. Magin and P. M. Borsenberger, J. Appl. Phys. **73**, 787 (1993).

[52] I. H. Campbell, D. L. Smith, C. J. Neef, et al., Appl. Phys. Lett. **74**, 2809 (1999).

[53] S. Shirota and H. Kageyama, Chem. Rev. **107**, 953 (2007).

[54] W. Xu, Khizar-ul-Haq, Y. Bai, et al., Solid State Commun. **146**, 311 (2008).

[55] V. Kumar, S. C. Jain, A. K. Kapoor, et al., J. Appl. Phys. **92**, 7325 (2002).

[56] A. J. Campbell, D. D. C. Bradley and D. G. Lidzey, J. Appl. Phys. **82**, 6326 (1997).

[57] J. Kovac, T. C. Wong, M. K. Fung, et al., Mat. Sci. Eng. B **85**, 172 (2001).

[58] F. So, B. Krummacher, D. Poplavskyy, et al., Journal of Applied Physics **102**, 091101 (2007).

[59] J. W. Jang, C. E. Lee, D. W. Lee, et al., Solid State Commun. **130**, 265 (2004).
[60] S. C. Tse, S. W. Tsang and S. K. So, J. Appl. Phys. **100**, 063708 (2006).
[61] R. Memming, "*Semiconductor Electrochemistry*" (Wiley-VCH, Weinheim, 2001).
[62] D. Poplavskyy and F. So, Proceedings SPIE **5937**, 12 (2005).
[63] D. Poplavskyy and F. So, J. Appl. Phys. **99**, 033707 (2006).
[64] H. C. F. Martens, J. N. Huiberts and P. W. M. Blom, Appl. Phys. Lett. **77**, 1852 (2000).
[65] M. Schmeits, J. Appl. Phys. **101**, 084508 (2007).
[66] G. Juška, K. Arlaukas and M. Viliunas, Phys. Rev. Lett. **84**, 4946 (2000).
[67] G. Juška, M. Viliunas, K. Arlaukas, et al., Appl. Phys. Lett. **89**, 4971 (2001).
[68] A. J. Mozer, N. S. Sariciftci, A. Pivrikas, et al., Phys. Rev. B **71**, 035214 (2005).
[69] M. Jaiswal and R. Menon, Polym. Int. **55**, 1371 (2006).
[70] P. W. M. Blom and M. C. J. M. Vissenberg, Mater. Sci. Eng. **27**, 53 (2000).

3

Research Methods

3.1. Simulations

Computational simulations are widely used in the literature to explore the limits of the physical models proposed and to provide explanations of different experimental issues. Furthermore, in the case of organic materials, intrinsic physical variables can be predicted since some of them are not able to be measured directly. In the present thesis, the solution of charge transport models is obtained by numerical algorithms applied on a system of ordinary differential equations (ODEs) of first order. For a single equation:

$$\left.\begin{aligned} \frac{dy}{dx} &= f(x,y) \\ y(x_0) &= y_0 \end{aligned}\right\} \tag{3.1}$$

The methods utilized in the physical models are well-known and covers the simplest (i.e., the Euler method) and the most optimum one (i.e., the 4th order Runge-Kutta).[1] The latter one exhibits a notable output regarding the two most important factors in any simulation process: time-consumption and result precision. The algorithm is based on the formation and evaluation of four coefficients every iteration:

$$\left.\begin{aligned} K_1 &= hf(x,y) \\ K_2 &= hf(x+h/2, y+K_1/2) \\ K_3 &= hf(x+h/2, y+K_2/2) \\ K_4 &= hf(x+h, y+K_3) \end{aligned}\right\} \tag{3.2}$$

where h is the discretization of the independent variable x to reach the solution:

$$y(x+h) = y(x) + (K_1 + 2K_2 + 2K_3 + K_4)/6 \tag{3.3}$$

In simulations of organic devices, it is fairly common to find opposite boundary conditions due to the location of the contacts at the extremes of the thickness organic layer, i.e., a two point boundary value problem is addressed. In this case, the numerical resolution begins with an initial guess that is

improved iteration by iteration. On the one hand, the most intuitive technique is the shooting method since it solves the whole system until the output is nearby the opposite boundary condition by considering an appropriate guess. On the other hand, the matrix technique of the relaxation method is more complex and precise since the improvement occurs at every point at once.[2]

Although the numerical algorithms were manually programmed with Mathematica software for the present thesis, powerful and user friendly commercial packages have been recently developed such as COMSOL Multiphysics[3] and SETFOS[4] (specific for organic devices), which are advisable for further research in the field.

3.2. Experiments

The typical measurements to characterize organic LEDs are in relation with the electrical and optical responses when a certain bias is applied. In this study PPV co-polymer has been used, "super yellow" (SY) prepared by Merck OLED Materials GmbH, as the light emitting polymer. Different device layouts have been investigated, double carrier injecting devices, using a 200 nm (polyethylenethioxythiophene: polystyrenesulfonic acid, PEDOT:PSS) hole injection layer over indium-doped tin oxide (ITO), and either a 80 or a 150 nm thick SY layer which was covered with a 5 nm barium and a 100 nm aluminium layer as cathode, Fig.3.1.

Hole only devices were prepared by using gold as the cathode. The PLEDs were prepared by spincoating the PEDOT:PSS and SY in clean room conditions in ambient atmosphere, after which they are transferred to a vacuum chamber integrated in a N_2 atmosphere. To remove any adsorbed moisture from the organic surface, the films were evacuated to a high vacuum of $<10^{-6}$ mbarr for several hours. After this procedure Ba and Al, or Au were evaporated subsequently and the samples were encapsulated in inert atmosphere. To enhance the stability of the sealed devices, a getter material is added in the

cavity between the cathode and the cover plate. This device structure prevents oxidation of the cathode for at least one year. However, to ensure that really all moisture is removed prior to cathode deposition, reference devices were prepared, including the spincoating process, from extensively dried solvents, and analysed in N_2 atmosphere.[5,6] Current density–potential (*J–V*) characteristics and impedance spectra were collected using an AutoLab PGSTAT30 equipment, Fig. 3.2.

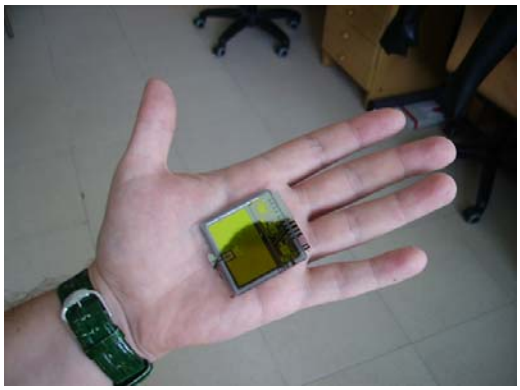

Fig. 3.1 SY-OLED from Merck OLED Materials

Experimental results of single-carrier devices (i.e., *J-V* curves and capacitance-impedance spectra) are modelled in chapter 5, however dual carrier devices exhibit interesting features as regards (1) static responses: *J-V* curves and luminance-voltage characteristics (*Lum-V*); and (2) dynamic responses such as transient electroluminescence and capacitance responses (*C-f*). Electroluminescence data were collected using a fast enough photodiode (Centronic OSD100-7, response time 6 μs) appropriately assembled to laboratory equipment for luminescence measurements: an integrating sphere Labsphere and a Faraday cage, see Fig. 3.3.

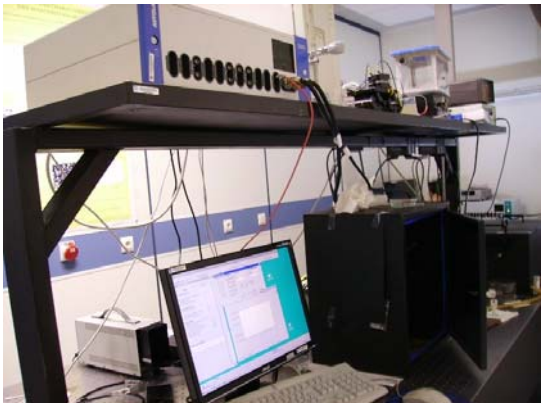

Fig. 3.2. Set-up for measurements of *J-V* and impedance: potentiostat (upper-left), computer and Faraday cage (right).

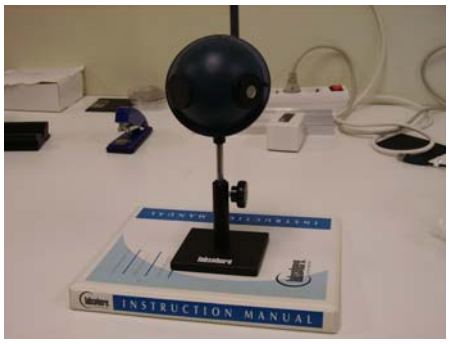

Fig. 3.3 Electroluminescence equipment for electro-optical measurements in organic-based devices: Integrating sphere (left-hand side) and Faraday cage (righ-hand side), respectively.

Current-density voltage characteristics (recorded at a scan rate of 0.01V/s and a step voltage of 1.525 mV) show two different regimes as previously pointed out in section 2.5. Figure 3.4.(a) pictures *J-V* and *Lum-V* curves. At low voltages, the ohmic regime dominates the charge transport in the present OLED device, up to approximately 1.9V where the SCLC transport becomes noticeable. In the range of 2.4V, and 6V, SCLC widely governs the charge transport and the electroluminescence in all the devices depicted.[7] Surprisingly, the interval of the ohmic regime depends on the active area (i.e., the turn on threshold voltage varies) as well as the magnitude of the current density whereas not their shape. This behaviour is attributed to the existence of a

perimeter leakage current whose contribution is proportionally more important to device total current in smaller emitting areas due to a higher value of the quotient perimeter-area.[8] Luminescence dependence on the applied voltage (gathered with the aid of the integrating sphere assembled to the photodiode) displays similar shape to the *J-V* curves. Figure 3.4.(b) displays the behaviour of capacitance spectra at several operating voltages obtained from IS and the set-up previously described of Fig. 3.2. An oscillating amplitude of 10 mV was added to the dc bias voltage using frequencies within the range of 1 MHz down to 1 Hz. The negative capacitance, commonly found in OLEDs at low frequency, is surprisingly different to that of hole only devices (see chapter 5, section 5.2) where it always remains positive.

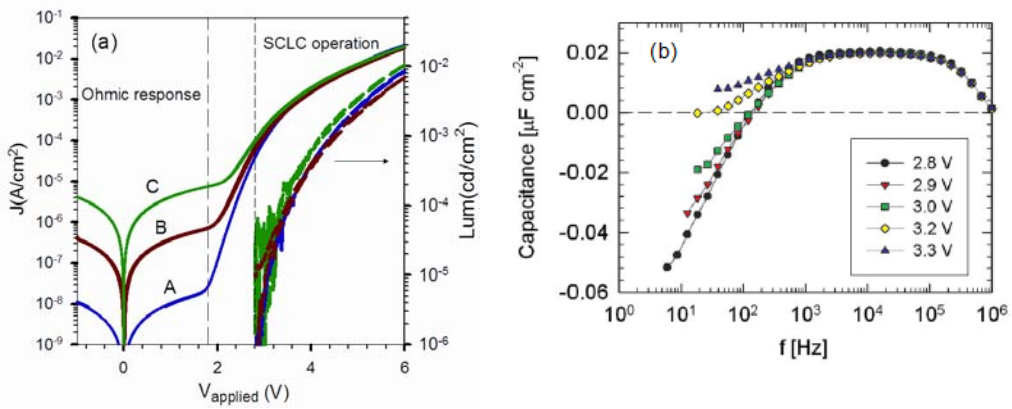

Fig. 3.4 Experimental measurements of an OLED with structure ITO/PEDOT:PSS/SY/Ba. (a) Representation of current density J and luminance Lum versus applied voltage V for devices with different active area A(6.03 cm^2), B(0.11cm^2) and C(0.01cm^2). (b) Capacitance spectra at different operating voltages *C-f* .

As regards the dynamic analysis, Figure 3.5 shows the experimental set-up for measurements of transient EL responses. The OLED sample is conveniently preserved in a Faraday cage where the luminescence, induced by the application of a wave generator signal connected to the device, is collected.

Fig. 3.5 Experimental set-up for measurements of transient responses: Faraday cage (down), wave generator (up-right), amplifier with power source (up-centre), and oscilloscope (up-left)

OLED transient current and EL response, generated by a rectangular voltage pulse of 6V, are monitorized by a digital oscilloscope (Hewlet Packard Infinium 1 Gsample/s). Meanwhile EL rise response is able to keep up with the perturbation, the EL decay depicts a much slower dynamics, Fig. 3.6 in the order of milliseconds. This delayed fluorescence (DF) process was interpreted in terms of the charge carrier dynamics.[9]

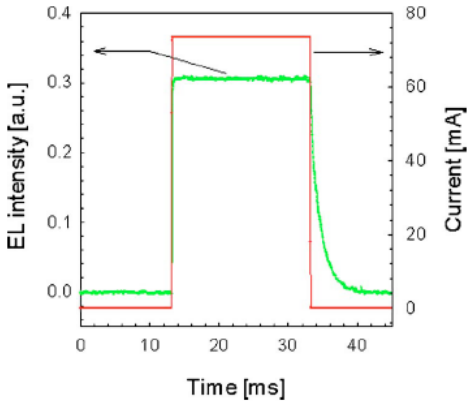

Fig. 3.6 Example of current and EL transients driven by a bias voltage pulse between 0 and 6V for device A with (area of 6.03 cm^2).

Figure 3.7 shows in a great detail the rise and fall behaviours of the transient EL at different frequencies ranging from 10KHz to 1Hz under the application of 5V with a duty cycle of 50%. On the one hand, at lower frequencies, the rise EL display an initial maximum characterized by two peaks that exceed the average value at the top voltage. However, these peaks become softer the more frequency is selected for the voltage perturbation. On the other hand, the fall DF depicts a similar behaviour and the same fall time. A slight peak in the decay is also observed for all the frequencies. Transient EL has been successfully modelled by an electro-optical model that comprises: charge carrier dynamics (drift-diffusion model), exciton dynamics and the optical transfer matrix formalism.[10]

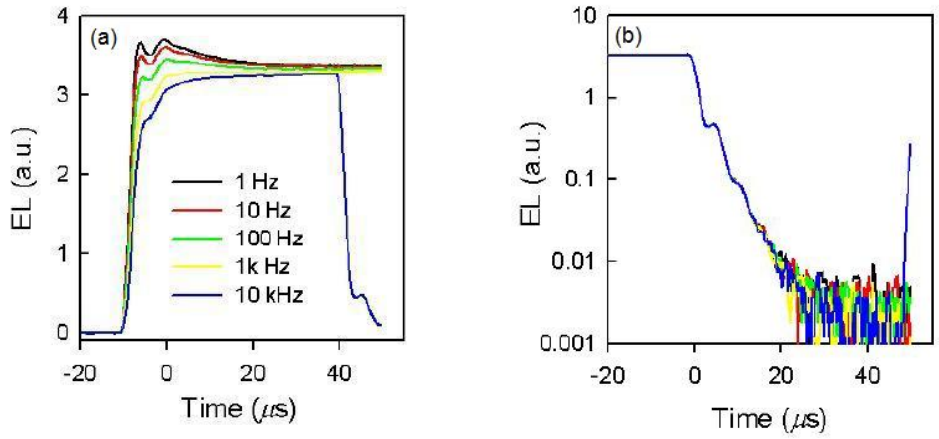

Fig. 3.7 Representation of transient EL responses driven by a squared voltage pulse between 0 and 5V at different frequencies: (a) rise and (b) fall parts of the EL step.

In conclusion, the implementation of computational simulations is required for the physical description of the experimental response in organic-based devices, either static or dynamic ones. Both research methods are complementary to tailor consistent physical models.

3.3. References

[1] D. Kincaid and W. Cheney, "*Análisis numérico: la matemáticas del cálculo científico"* (Addison-Wesley Iberoamericana SA, Buenos Aires, 1994).

[2] W. H. Press, B. P. Flannery, S. A. Teukolsky, et al., "*Numerical Recipes in FORTRAN 77: The Art of Scientific Computing"* (Cambridge University Press, Cambridge, 1992).

[3] http://www.comsol.com/.

[4] http://www.fluxim.com/.

[5] J. M. Montero, J. Bisquert, G. Garcia-Belmonte, et al., Phys. Status Solidi (a) **204**, 2402 (2007).

[6] J. Bisquert, G. Garcia-Belmonte, A. Pitarch, et al., Chem. Phys. Lett. **422**, 184 (2006).

[7] J. M. Montero, "*Injection and Transport in Organic Light-Emitting Diodes (OLEDs)"* (Universitat Jaume I, MSc Thesis, Castellón, 2007).

[8] G. Garcia-Belmonte, J. M. Montero, Y. Ayyad-Limonge, et al., Curr. Appl. Phys. **9**, 414 (2009).

[9] G. Garcia-Belmonte, J. M. Montero, E. M. Barea, et al., J. Appl. Phys. **101**, 114506 (2007).

[10] B. Ruhstaller, S. A. Carter, S. Barth, et al., J. Appl. Phys. **89**, 4575 (2001).

Thickness Scaling of Space-charge Limited Currents in Organic Layers with Field- or Density-dependent Mobility

4. Thickness Scaling of Space-charge-limited Currents in Organic Layers with Field- or Density-dependent Mobility

4.1. Introduction

Space-charge limited current (SCLC) is observed in the current density-potential (*J*-*V*) characteristics of organic light emitting diodes (OLEDs). In these materials it is often found that the mobility depends on the local electrical field E as[1-5]

$$\mu(E) = \mu_0 \exp(\gamma\sqrt{E}) \tag{4.1}$$

where μ_0 denotes the mobility of electrons or holes at zero field and γ is the parameter describing the field dependence. Equation (4.1) can be inferred either from a Poole-Frenkel model or a Gaussian disorder model.[6]

The current in organic layers may be controlled either by injection at the contacts, or by the electrical field formed by the injected carrier distribution, in SCLC regime. If both contacts have a low barrier to injection of a single carrier but prevent the injection of the other one, unipolar (hole-only or electron-only) devices are formed in which the current is SCL and a direct measure of carrier mobility can be obtained from *J*-*V* curves. For the light emitting devices the injection of both carriers is required and it is important to distinguish if the device is controlled by injection at the contact or by currents in the bulk of the organic layer. To determine the dominant mechanism, an understanding of the thickness scaling of *J*-*V* curves is required.[7,8]

There are well known analytical models[9] for SCLC transport with constant mobility, without and with traps, but to our knowledge no exact solutions of SCLC are available considering the field-dependent mobility. An approximate solution was given by Murgatroyd:[10]

$$J = \frac{9}{8}\frac{\varepsilon\mu_0}{L^3}V^2 e^{0.89\gamma\sqrt{V/L}} \tag{4.2}$$

Here analytical expressions are derived and the scaling relationship of $J-V$ characteristics is discussed, which allows to distinguish injection-limited from SCL devices, when the mobility depends on the field.

Recently, from measurements at high carrier concentration in organic field-effect transistors (OFETs) it was suggested that in disordered organic semiconductors the mobility depends on the density of carriers, rather than on the local electric field.[11-13] In a later paper[14] it was concluded that mobility depends on both, electrical field and carrier concentration. Therefore, it is important to clarify the thickness scaling relationships for *J-V* characteristics that may distinguish these dependencies of the mobility in organic materials.

4.2. Field-dependent Mobility

We first consider the mobility as described by Eq. (4.1). The SCLC is determined by the drift equation

$$J = p(x)e\mu\left[E(x)\right]E(x) \tag{4.3}$$

and the Poisson equation

$$\frac{\varepsilon}{e}\frac{dE(x)}{dx} = p(x) \tag{4.4}$$

where $p(x)$ is the carrier density at x distance from the injecting contact, $\varepsilon = \varepsilon_0\varepsilon_r$ the permittivity of the polymer, and e the positive elementary charge. Combining Eqs. (4.1), (4.3) and (4.4) we obtain the expression

$$J\,dx = \varepsilon\mu_0 e^{\gamma\sqrt{E}}\,E\,dE \tag{4.5}$$

Since the current is constant across the film, an integral of Eq. (4.5) gives

$$L = \frac{\varepsilon\mu_0}{J}\int_0^{E_L} e^{\gamma\sqrt{E}}\,E\,dE \tag{4.6}$$

where L is the film thickness and E_L is the electric field at the collecting contact at $x = L$. The electric potential relates to the electric field as

$$V = \int E\, dx \tag{4.7}$$

Note that V in Eq. (4.7) denotes the potential driving the SCLC in the bulk organic layer, after subtraction of the built-in potential, from the applied potential, i.e., $V = V_{app} - V_{bi}$. Introducing Eq. (4.5) in (4.7) we obtain

$$V = \frac{\varepsilon\mu_0}{J}\int_0^{E_L} e^{\gamma\sqrt{E}} E^2\, dE \tag{4.8}$$

The integrals in Eq. (4.6) and (4.8) have the form

$$I_n(y) = \int_0^y e^{\gamma\sqrt{u}} u^n\, du = \frac{2\Gamma[2(n+1)]}{\gamma^{2(n+1)}} P[2(n+1), -y] \tag{4.9}$$

in terms of the gamma function Γ and the incomplete gamma function P. Using the explicit form[15]

$$P(n,r) = 1 - \left(1 + r + \frac{r^2}{2!} + \ldots + \frac{r^{n-1}}{(n-1)!}\right) e^{-r} \tag{4.10}$$

we obtain from Eqs. (6) and (8) the results

$$L = \frac{\varepsilon\mu_0}{J}\frac{12}{\gamma^4}\left[1 - \left(1 - t + \frac{t^2}{2!} - \frac{t^3}{3!}\right)e^t\right] \tag{4.11}$$

$$V = \frac{\varepsilon\mu_0}{J}\frac{240}{\gamma^6}\left[1 - \left(1 - t + \frac{t^2}{2!} - \frac{t^3}{3!} + \frac{t^4}{4!} - \frac{t^5}{5!}\right)e^t\right] \tag{4.12}$$

These two expressions when combined give an exact solution to the $J - V$ characteristic, parametric in $t = \gamma\sqrt{E_L}$.

At very low fields, $t << 1$, we expand the exponential in both Eq. (4.11) and (4.12), up to one order higher than the polynomial in each case, and we get the expressions

$$L = \frac{1}{2}\frac{\varepsilon\mu_0}{J}E_L{}^2 \tag{4.13}$$

$$V = \frac{1}{3}\frac{\varepsilon\mu_0}{J}E_L{}^3 \tag{4.14}$$

These results follow directly from Eqs. (4.6) and (4.8) for $\gamma = 0$. Combining Eqs. (4.13) and (4.14) we arrive at

$$J = \frac{9}{8}\frac{\varepsilon\mu_0}{L^3}V^2 \tag{4.15}$$

the standard result for SCLC with field-independent mobility.[9]

Equation (4.15) predicts a scaling relationship of the current with L^3/V^2. In previous work it was shown by numerical calculation[4] that the current-potential curves with field-dependent mobility do not follow such a relationship. The general, exact scaling with the length for single carrier devices is deduced from Eqs. (4.11) and (4.12).[8] Defining the variables

$$y = JL \;;\; u = V/L \tag{4.16}$$

all the $J-V$ curves of layers with different thicknesses should collapse into a single curve. Obviously, the statement applies to the particular case in Eq. (4.15). More generally, let the mobility be an arbitrary function of the electrical field, $\mu = \mu_0 m(E)$. Then Eq. (4.5) can be written

$$J\,dx = \varepsilon\mu_0 m(E)E\,dE \tag{4.17}$$

and we obtain equations

$$JL = \varepsilon\mu_0 \int_0^{E_L} m(E)E\,dE \tag{4.18}$$

$$VL = \varepsilon\mu_0 \int_0^{E_L} m(E)E^2\,dE \tag{4.19}$$

that upon integration provide an exact solution of the *J-V* curve in terms of the parameter E_L. It follows that the scaling in terms of the variables of Eq. (4.16) or any combination of them provides a universal curve for different layer thicknesses whatever the field-dependence of the mobility.[5,16]

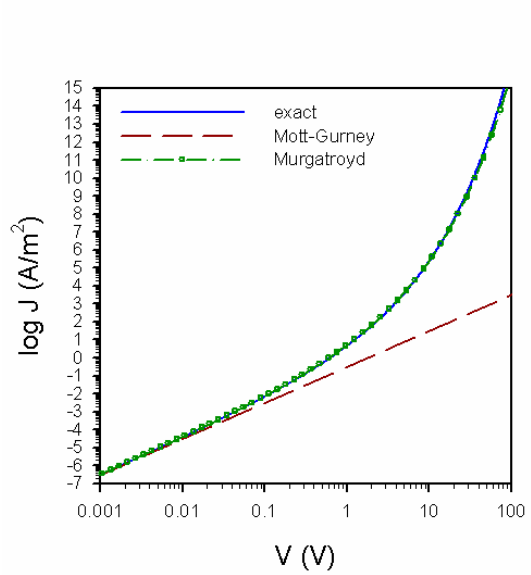

Fig. 4.1. Simulations of current density J versus voltage V for carriers with $\mu_0 = 10^{-11}$ m^2/Vs, $\gamma = 10^{-3}$ (m/V)$^{1/2}$, $\varepsilon_r = 3$ in a organic layer of thickness L=100nm. Shown are the exact analytical solution, the approximation of Eq. (4.2), and the low voltage Mott-Gurney approximation.

Figure 4.1 illustrates the *J-V* curve of SCLC of carriers with field-dependent mobility. For comparison the Mott-Gurney expression, Eq. (4.15), is plotted as well. As a remark, it should be observed that the exact expression departs

significantly from the Mott-Gurney one even at low fields, in which the curvature of the *J-V* line is very small. Therefore applying Eq. (4.15) in a restricted range of voltage may introduce a significant error in the determination of the charge carrier mobilities. Also shown in Fig.4.1 is the formula of Murgatroyd, which gives an excellent approximation to the exact result over a wide range of potentials. Since Eq. (4.2) can be written

$$yu^{-2} = \frac{9}{8}\varepsilon\mu_0 e^{0.89\gamma\sqrt{u}} \tag{4.20}$$

it follows that plotting the *J-V* curves as $\log\left(yu^{-2}\right)$ vs. $u^{1/2}$ will give a straight line, independent of thickness. This procedure was applied by Malliaras and Scott.[16]

4.3. Density-dependent Mobility

As commented above, it has also been suggested[11-14] that the mobility in organic semiconductors depends on the local density of charge carriers, $\mu = h(p)$. Let $\theta(z)$ be the inverse of the function h, such that $h[\theta(z)] = z$. From Eq. (4.3), Poisson equation (4.4) can be written as

$$\frac{\varepsilon}{e}\frac{dE}{dx} = \theta\left(\frac{J}{qE}\right) \tag{4.21}$$

Using Eq. (4.21) we obtain the following results

$$L = \frac{\varepsilon}{q}\int_0^{E_L}\theta^{-1}\left(\frac{J}{qE}\right)dE \tag{4.22}$$

$$V = \frac{\varepsilon}{q}\int_0^{E_L}E\,\theta^{-1}\left(\frac{J}{qE}\right)dE \tag{4.23}$$

As above in the Eqs. (4.18) and (4.19), the Eqs. (4.22) and (4.23) provide an exact solution of the *J-V* curve in terms of the parameter E_L, for any density-

dependence of the mobility. Let us consider the implication of Eqs. (4.22) and (4.23) for the thickness scaling of the *J-V* curves. Suppose that the mobility function $\mu = h(p)$ has a scaling form such that

$$h(\lambda p) = \lambda^{\beta} h(p) \tag{4.24}$$

Then $\theta(\lambda z) = \lambda^{1/\beta}\theta(z)$. Applying this relationship in Eqs. (4.22) and (4.23) we obtain

$$J^{1/\beta}L = \frac{\varepsilon}{q}\int_0^{E_L} \theta^{-1}\left(\frac{1}{qE}\right)dE \tag{4.25}$$

$$J^{1/\beta}V = \frac{\varepsilon}{q}\int_0^{E_L} E\,\theta^{-1}\left(\frac{1}{qE}\right)dE \tag{4.26}$$

Therefore, thickness rescaling of the *J-V* curves to a single curve is obtained with the variables

$$y = J^{1/\beta}L \;;\; u = V/L \tag{4.27}$$

Vissenberg and Matters[17] calculated an analytical expression for the hopping conductivity in an exponential density of states. The resulting mobility has a form[18]

$$\mu = ap^{b} \tag{4.28}$$

where a is a prefactor depending on temperature and $b = (T_0/T) - 1$, with T_0 a characteristic temperature determining the width of the distribution. Equation (4.1) gives good agreement with Monte Carlo calculations at low temperature[19] and describes well the mobility in OFETs.[18] Exact solution of *J-V* curves for SCLC under Eq. (4.28) have been given by Coehoorn et al.[20] Materials obeying Eq. (4.28) should display the scaling law of Eq. (4.27) when the SCLC is measured in a layer sandwiched between two electrodes. Since T_0 is typically

around 500 K,[18] the exponent β should be near to 0.6 at room temperature. There is a significant difference between Eq. (4.16) and Eq. (4.27) that could be observed experimentally. Therefore the thickness scaling of *J*-*V* curves is able to distinguish clearly between a field- and density-dependence of the mobility in organic layers.

The exception to the preceding statement is the case $b = 1$ in Eq. (4.28), i.e. when the mobility is linear on carrier density. In this case, and only in this case, field- and density-dependence provide the same scaling law, Eq. (4.16). On another hand, suggested forms[21] of the mobility in a gaussian distribution of states, such as $\mu = \mu_0 \exp\left(c(p/p_0)^{\nu}\right)$, do not satisfy a scaling of the type of Eq. (4.24), and the thickness rescaling of Eq. (4.27) does not apply.

4.4. Conclusion

In summary an exact solution of the *J*-*V* curve for SCLC with field-dependent mobility has been given, allowing an exact simulation of the *J*-V characteristics. The method can be easily extended to other functional dependencies of the mobility on the electric field, and the general scaling relationship for field-dependent mobility, in terms of the variables JL and V/L, holds in all the cases. This thickness scaling of the SCLC does not generally occur for density-dependent mobility. For the density dependence of the mobility proposed in OFET materials[17,18] the thickness scaling occurs in terms of the variables $J^{1/\beta}L$ and V/L. Therefore the proposed scaling is a useful test for distinguishing field- and density-dependent mobility in SCLC in disordered organic semiconductors.

4.5. References

[1] D. M. Pai, J. Chem. Phys. **52**, 2285 (1970).

[2] P. W. M. Blom, M. J. M. de Jong and M. G. van Munster, Phys. Rev. B **55**, R656 (1997).

[3] P. S. Davids, I. H. Campbell and D. L. Smith, J. Appl. Phys. **82**, 6319 (1997).

[4] B. K. Crone, P. S. Davids, I. H. Campbell, et al., J. Appl. Phys. **84**, 833 (1998).

[5] W. Brütting, S. Berleb and A. G. Mücki, Org. Electron. **2**, 1 (2001).

[6] H. Bässler, Phys. Status Solidi (b) **175**, 15 (1993).

[7] W. Brütting, S. Berleb and A. G. Mücki, Synth. Met. **122**, 99 (2001).

[8] D. Natali and M. Sampietro, J. Appl. Phys. **92**, 5310 (2002).

[9] M. A. Lampert, "*Current Injection in Solids"*, 1970).

[10] P. N. Murgatroyd, J. Phys. D: Appl. Phys. **3**, 151 (1970).

[11] C. Tanase, P. W. M. Blom, D. M. de Leeuw, et al., Phys. Status Solidi (a) **201**, 1236 (2004).

[12] C. Tanase, P. W. M. Blom and D. M. Leeuw, Phys. Rev. B **70**, 193202 (2004).

[13] P. W. M. Blom, C. Tanase, D. M. Leeuw, et al., Appl. Phys. Lett. **86**, 092105 (2005).

[14] W. F. Pasveer, J. T. J. Cottaar, C., R. Coehoorn, et al., Phys. Rev. Lett. **94**, 206601 (2005).

[15] M. Abramowitz and I. A. Stegun, "*Handbook of Mathematical Functions"* (Dover Publications, New York, 1964).

[16] G. G. Malliaras and J. C. Scott, J. Appl. Phys. **85**, 7426 (1999).

[17] M. C. J. M. Vissenberg and M. Matters, Phys. Rev. B **57**, 12964 (1998).

[18] C. Tanase, E. J. Meijer, P. W. M. Blom, et al., Phys. Rev. Lett. **91**, 216601 (2003).

[19] S. D. Baranovskii, H. G. A. Huizing and R. Coehoorn, Thin Solid Films **487**, 2 (2005).

[20] B. Ramachandhran, H. G. A. Huizing and R. Coehoorn, Phys. Rev. B **73**, 233306 (2006).

[21] R. Coehoorn, W. F. Pasveer, P. A. Bobbert, et al., Phys. Rev. B **72**, 155206 (2005).

Interpretation of Capacitance Spectra and Transit Times of Single Carrier Space-charge-limited Transport in Organic Layers with Field-dependent Mobility

5.1. Introduction

Organic materials are being investigated to develop modern optoelectronic devices such as organic field effect transistors, organic solar cells and organic light emitting diodes (OLEDs) by simple spin-coating techniques. In these devices the charge injection and transport determines to a large extent their performances. If carriers can easily overcome energy barriers at the interfaces (anode and cathode), the current should be bulk-limited and not injection-limited. In this situation, the ohmic regime has a narrow initial dominium (milivolts) whereas space-charge limited current (SCLC) regime dominates widely the charge transport within the organic layer. In a dual carrier device (in which both holes and electrons are injected) it is complicated to derive independent transport parameters for the separate electronic carriers. To overcome this hurdle, hole-only devices can be prepared by using a high workfunction cathode that prevents the injection of electrons. These devices exhibit an unipolar current that is SCL as well.

SCLC regime is often observed in the current density-potential (*J*-*V*) characteristics of polymer light emitting diodes (PLEDs). The ac impedance measurement has the advantage that it provides additional information, i.e. capacitance and transit time, with respect to dc methods, and some authors have applied these methods to obtain parameters governing single carrier transport in organic layers[1-5] These works apply the standard SCLC impedance model that is valid for constant mobility,[6,7] in some cases extended with a dispersive (frequency-dependent) mobility[1,2] and for bipolar devices.[1,3-5,8] It is well established that in organic layers the mobility depends on the local electrical field E as[9-13]

$$\mu(E) = \mu_0 \exp(\gamma\sqrt{E}) \tag{5.1}$$

where μ_0 denotes the mobility of electrons or holes at zero field and γ is the parameter describing the field dependence.[14] Many studies have shown that

Eq. (5.1) produces a dramatic change of the dependence of steady-state current-potential characteristics. It is therefore likely that the field-dependent mobility introduces significant changes in the ac impedance model of SCLC. To our knowledge, only Berleb and Brütting have considered this effect,[2] but their study is not completely correct, because they fail to include the modulation of the field in the expression of the mobility, see Eq. (5.12), below. Here we provide the solution to this problem and discuss the characteristics of ac impedance of a single carrier in SCLC, with a view to the interpretation of capacitances and transit times in PLEDs and other organic electronic devices. Steady-state and capacitance measurements of hole-only devices are discussed as well, to check the application of the model. A recent study by Coehoorn et al.[15] takes all the relevant aspects into account, however they consider a density-dependent mobility, with an exponential distribution of traps, and they are able to produce an analytic solution for the impedance. Their study and ours may be regarded as complementary, covering the most important expressions generally used to describe variations of the mobility in organic layers.

5.2. Theory

5.2.1. AC Impedance and capacitance spectra

The SCLC for unipolar transport (neglecting diffusion) is described by the continuity equation, the drift current equation and the Poisson equation, respectively:

$$\frac{dJ}{dx} = 0 \tag{5.2}$$

$$J = p(x)e\mu\left[E(x)\right]E(x) + \varepsilon\frac{\partial E(x)}{\partial t} \tag{5.3}$$

$$\frac{\varepsilon}{e}\frac{dE(x)}{dx} = p(x) \tag{5.4}$$

where $p(x)$ is the carrier density at position x, $\varepsilon = \varepsilon_0 \varepsilon_r$ the permittivity of the polymer, and e the positive elementary charge. The collecting contact is at $x = L$. The electric potential relates to the electric field as

$$V = \int_0^L E(x)dx \tag{5.5}$$

The impedance is defined as the quotient of potential to current density

$$Z(\omega) = \hat{V}(\omega) / \hat{j}(\omega) \tag{5.6}$$

where the tilde denotes a small ac perturbation of angular frequency ω over a steady-state. The frequency-dependent capacitance is defined as

$$C'(\omega) = \mathrm{Re}\left[1 / i\omega Z(\omega)\right] \tag{5.7}$$

The impedance model for SCLC with a constant mobility is well known[6,7] and it has the expression

$$Z(\omega) = \frac{6}{g_0 (i\omega\tau_{tr})^3}\left[1 - i\omega\tau_{tr} + \frac{1}{2}(i\omega\tau_{tr})^2 - e^{-i\omega\tau_{tr}}\right] \tag{5.8}$$

where

$$\tau_{tr} = \frac{4}{3}\frac{L^2}{\mu V_{dc}} \tag{5.9}$$

$$g_0 = \frac{9}{4}\varepsilon\mu_0 \frac{V_{dc}}{L^3} = \frac{dj_{dc}}{dV_{dc}} \tag{5.10}$$

$$C_g = \frac{\varepsilon}{L} \tag{5.11}$$

are the transit time, dc conductance and geometrical capacitance, respectively. The capacitance obtained from Eq. (5.7) takes the value of the geometric

capacitance C_g at high frequencies, and at the frequency of the transit time, τ_{tr}, decreases to $3C_g/4$ towards low frequencies.

Let us consider the ac impedance model of SCLC for a single carrier with field-dependent mobility as stated in Eq. (5.1). It is formulated separating the stationary components from the small perturbation ac parts in the drift equation. The mobility dependence on the field implies, up to first order, the following expression

$$\mu\left(E_{dc}+\hat{E}\right)=\mu\left(E_{dc}\right)+\frac{\partial\mu}{\partial E}\hat{E} \tag{5.12}$$

Therefore we obtain the equation

$$J_{dc}+\hat{j}=e\left[p_{dc}+\hat{p}\right]\left[\mu\left(E_{dc}\right)+\frac{\partial\mu}{\partial E}\hat{E}\right]\left[E_{dc}+\hat{E}\right]+i\omega\varepsilon\hat{E} \tag{5.13}$$

The zero order gives the steady state equation

$$J_{dc}=p_{dc}e\mu\left(E_{dc}\right)E_{dc} \tag{5.14}$$

In combination with Eq. (5.1), the *J(V)* dependence from this last equation has been solved in a parametric form in the previous chapter[16,17] and corroborates the very accurate explicit approximation of Murgatroyd:[18]

$$J=\frac{9}{8}\frac{\varepsilon\mu_0}{L^3}V^2e^{0.89\gamma\sqrt{V/L}} \tag{5.15}$$

The small signal terms in Eq. (5.13), in combination with Poisson's equation, provide the equation

$$\hat{j}=ep_{dc}\mu'(E_{dc})\hat{E}+\varepsilon\mu(E_{dc})E_{dc}\frac{\partial\hat{E}}{\partial x}+i\omega\varepsilon\hat{E} \tag{5.16}$$

where

$$\begin{aligned}\mu'(E_{dc}) &= \mu + \frac{\partial \mu}{\partial E} E_{dc} \\ &= \mu_0 \left[1 + \frac{\gamma}{2} \sqrt{E_{dc}} \right] \exp(\gamma \sqrt{E_{dc}})\end{aligned} \tag{5.17}$$

The impedance is obtained from the solution of Eq. (5.16) with respect to $\hat{V}$, which is obtained numerically. Figure 5.1 shows capacitance spectra at different bias potentials. In contrast to the constant mobility case, the shape of the spectra depends on the stationary operation point. The transition from low (C_{lf}) to high frequency (C_g) value is displaced to higher frequency at higher bias potential, indicating a reduction of the transit time. In addition, the low frequency capacitance increases with applied bias and its values are higher than $3C_g/4$. For the high frequency regime, capacitance amounts to C_g as in the constant mobility case. In an early study,[19] the values of low frequency capacitance are found to be sensitive to the specific dependence of mobility on the local field, although the characteristic formula Eq. (5.1) for organic conductors was not described at that time. The origin of the low frequency capacitance being lower than C_g is discussed by Kassing[20] in terms of three contributions to the capacitance that arise in Eq. (5.16): velocity modulation, density modulation, and a displacement term, respectively. It is noteworthy that in the study of Coehoorn et al.[15] with density-dependent mobility, the low frequency capacitance is lower than the constant mobility case value, i.e., $C_{lf} < 3C_g/4$, while for Eq. (5.1), we have remaked that it is always $3C_g/4 < C_{lf} < C_g$.

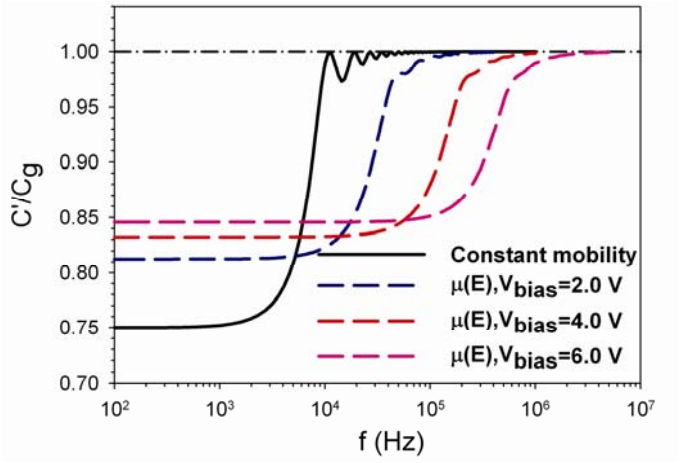

Fig. 5.1 Simulations of capacitance spectra of a single carrier injected in an organic layer of thickness $L = 125\,\text{nm}$ with parameters $\mu_0 = 4.6\times10^{-7}\ \text{cm}^2/\text{Vs}$, $\gamma = 5.4\times10^{-3}(\text{cm/V})^{1/2}$, $\varepsilon_r = 3$ and for different applied bias.

5.2.2. Transit Times

The dc transit time is obtained integrating the reciprocal of the drift velocity as:

$$\tau_{trdc} = \int_0^L \frac{1}{\mu(E)E}\,dx \tag{5.18}$$

A lower transit time is expected with respect to the constant mobility case because carriers drift velocity is increased with the exponential dependence of the mobility on the field. Figure 5.2 shows the electric field distribution for a given bias potential in different cases:

- $\gamma = 0$ describes the constant mobility electric field distribution.
- $\gamma = \gamma_0$ describes the field-dependent mobility electric field distribution for characteristic γ values.

- $\gamma = 6 \times \gamma_0$ describes the field-dependent mobility electric field distribution for extreme γ values.

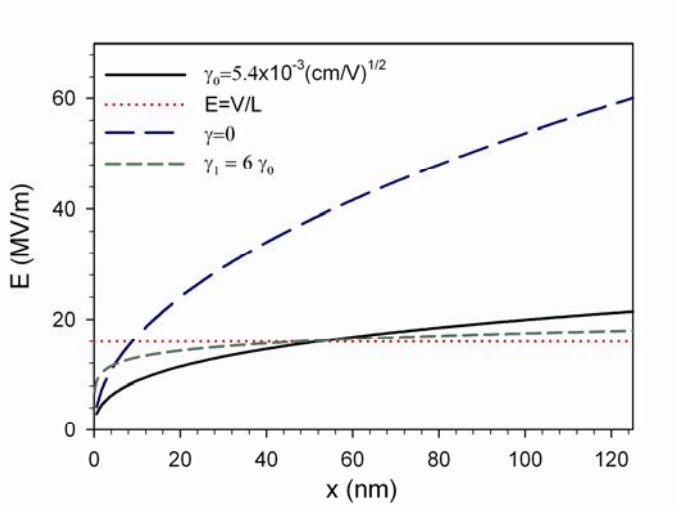

Fig. 5.2. Distribution of electric field for single carrier injected in an organic layer of thickness $L = 125\,\text{nm}$ with a bias voltage 2.0 V, with parameters $\mu_0 = 4.6\times10^{-7}\ \text{cm}^2/\text{Vs}$, $\varepsilon_r = 3$ and various values of γ as indicated. An approximation to the ohmic regime is shown also.

As shown in Fig. 5.2, when the mobility increases rapidly with the field, the field increases more slowly towards the extracting contact. Since carriers mobility is increased by their field-dependence, more of them can penetrate in the material and establish a larger carrier distribution with regard to the constant mobility case. In order to maintain a constant current, Eq. (5.2), the system reacts decreasing the electric field. This causes the electric field distribution with a stronger field-dependent mobility to approach a uniform electrical field. Therefore, we can apply the following approximations in order to obtain a simplified expression for the transit time.

Assuming:

$$\sqrt{E(x)} \approx \sqrt{V / L} \tag{5.19}$$

Equation (5.1) becomes a field-independent mobility with a correcting exponential factor,

$$\mu(E) \approx \mu_0 \exp(\gamma\sqrt{V/L}) \tag{5.20}$$

Finding the stationary solution for the system of Eqs.(5.2)-(5.4) with Eq.(5.20), we obtain the well known Child's law and electric field distribution in space with the corrected constant mobility by using the same derivation as for constant mobility[21]

$$J \approx \frac{9}{8}\varepsilon\mu_0 \exp\left[\gamma\sqrt{V/L}\right]\frac{V^2}{L^3} \tag{5.21}$$

$$E(x) \approx \left(\frac{2Jx}{\varepsilon\mu_0 \exp\left[\gamma\sqrt{V/L}\right]}\right)^{1/2} \tag{5.22}$$

Replacing the current, Eq. (5.21), in Eq. (5.22), we obtain

$$E(x) \approx \frac{3}{2}\frac{V}{L^{3/2}}\sqrt{x} \tag{5.23}$$

Substituting Eqs. (5.20) and (5.23) in Eq. (5.18) and integrating, we arrive at

$$\tau_{dctr} \approx \frac{4}{3}\frac{L^2}{\mu_0 \exp\left[\gamma\sqrt{V/L}\right] V} \tag{5.24}$$

which is simply the classical expression for transit times with constant mobility, Eq. (5.9), including an exponential dependence due to field-dependent mobility.

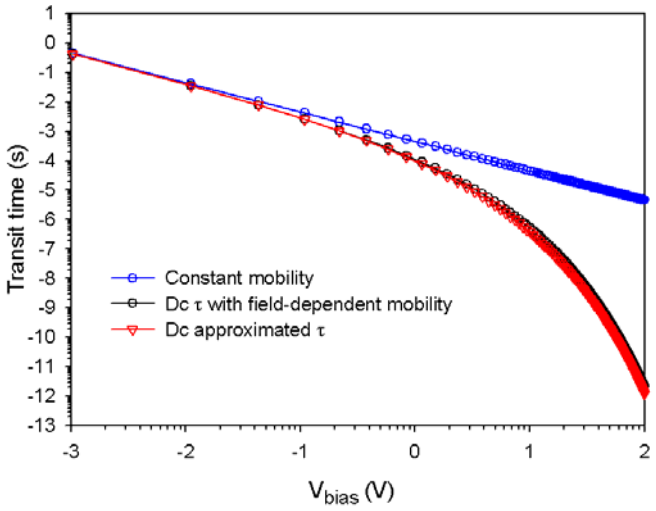

Fig. 5.3 Transit times of single carriers in an organic layer with different integrated expressions described in the main text. Deviation from the constant mobility case is shown.

In Fig. 5.3 the dc-transit times have been represented using different formulas: Constant mobility transit time, Eq. (5.9); the field-dependent mobility transit time, Eq. (5.8), and the approximated expression of field-dependent transit time, Eq. (5.24). The results in Fig. 5.3 show that the dc transit time with a field-dependent mobility departs strongly from the constant mobility transit time. In addition it is observed that Eq. (5.24) gives an excellent approximation to the exact dc transit time in Eq. (5.18).

As mentioned above, the time needed for carriers to cross the device thickness can also be obtained from the frequency of change of capacitance spectrum in the transition form high to low frequency values. For low frequencies, ac-carriers injected have enough time to reach the opposite electrode under the influence of background dc electric field and the capacitance has a low value. Increasing the voltage modulation, ac-carriers can not keep up with the signal at a critical frequency that marks the capacitance step. A common method to define an ac-transit time consists in analyzing the

change of susceptance $-\Delta B = -\omega(C' - C_g)$ which gives the critical frequency at the maximum of the susceptance plots.[3,4] The ac-transit time is given approximately by

$$\tau_{actr} \approx 0.72 \cdot f_{\max}^{-1} \tag{5.25}$$

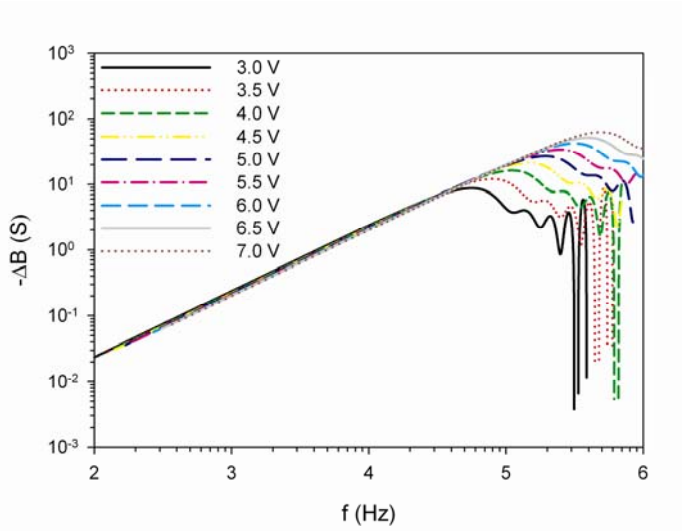

Fig. 5.4 Susceptance spectra for a single carrier in an organic layer of thickness L=125nm, calculated numerically with parameters $\mu_0 = 4.6\times10^{-7}$ cm^2/Vs, $\gamma = 5.4\times10^{-3}(cm/V)^{1/2}$, $\varepsilon_r = 3$, with different values of applied bias potential as indicated.

Figure 5.4 shows the calculated susceptance spectra at different bias values for characteristic mobility parameters μ_0, γ. Using Eqs. (5.24) and (5.25) we can obtain mobility values $\mu_0 \exp\left[\gamma\sqrt{V/L}\right]$ from the peak frequency and compare them with the originally postulated values. This is shown in Fig. 5.5. The results indicate that expressions (5.24) and (5.25) are suitable for derivation of the mobility from ac impedance data.

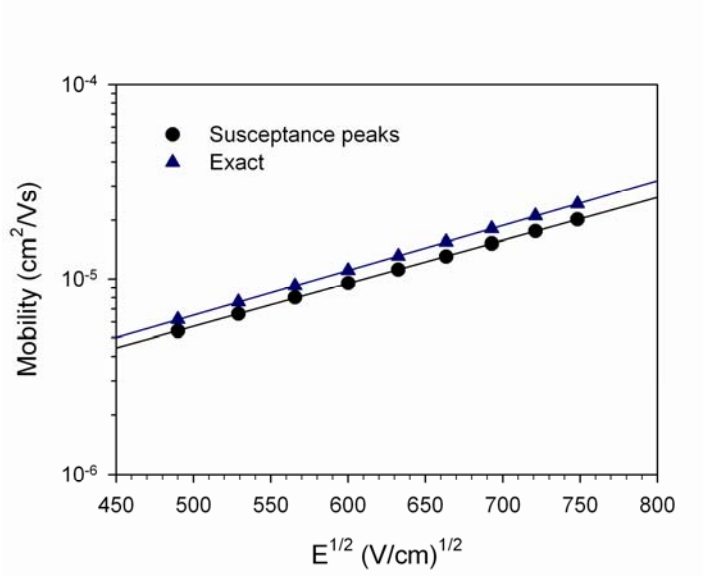

Fig. 5.5 Mobility values obtained from susceptance peaks (linear fit gives $\mu_0 = 4.5\times10^{-7}$ cm^2/Vs, $\gamma = 5.1\times10^{-3}(cm/V)^{1/2}$) compared to the initial values used in the simulation, $\mu_0 = 4.6\times10^{-7}$ cm^2/Vs, $\gamma = 5.3\times10^{-3}(cm/V)^{1/2}$.

In order to further test the suggested approximations, rather high γ and bias-potential values $\gamma\sqrt{E} \approx 20$ are used to generate a set of transit times. These values are expected to provide a very strong departure from the field-independent mobility expressions. Figure 5.6 shows transit times provided by the ac method from susceptance peaks, Eq. (5.25), by the dc integrated expression, Eq. (5.18), and by the postulated approximated expression, Eq. (5.24). It is observed that the different methods provide similar values and the same bias-dependence of the transit time, even in this extreme case simulation, though the different values are offset by a factor 2-4.

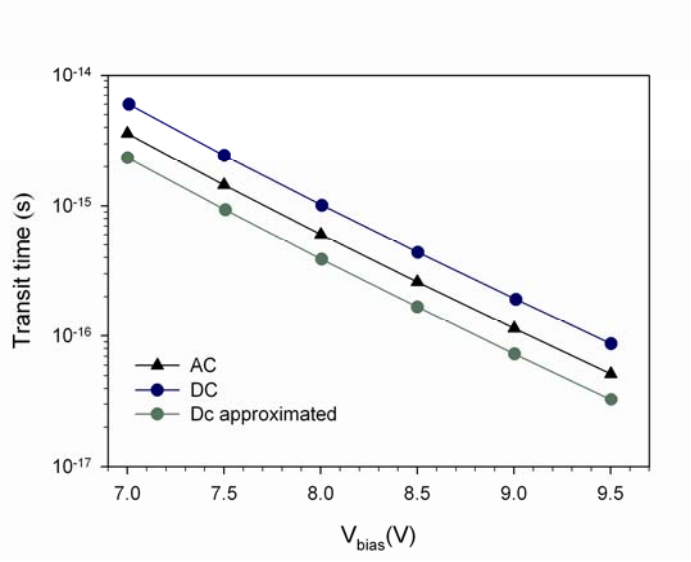

Fig. 5.6 Transit times of a single carrier in an organic layer with extreme values of field-dependent mobility ($\gamma\sqrt{E} \approx 20$) using different calculation methods as described in the main text.

5.2.3. Trapping Effects

Trapping and subsequent release of charges from trap states result in an additional contribution to capacitance at low frequencies. For a single trap level with a relaxation time τ_{trap} the frequency dependence of the excess capacitance is given by:

$$\Delta C_t \propto \frac{1}{1+(\omega\tau_{trap})^2} \tag{5.26}$$

i.e., the capacitance due to trapping increases and saturates at low frequencies ($\omega < \tau_{trap}^{-1}$). At higher frequencies the release rate from the traps can not keep up with the voltage modulation and the contribution due to trapping becomes negligible.

5.3. Experiment

Sample preparation of hole-only devices with SY-copolymer and the electric measurements carried out on them are described in chapter 3. Current density-potential (*J-V*) characteristics and impedance spectra were collected using an AutoLab PGSTAT30 equipment. An oscillating amplitude of 10 mV was added to the dc bias using frequencies within the range of 1 MHz down to 1 Hz

5.4. Modelling Results

A representative experimental *J-V* curve of a device ($L = 80\,\text{nm}$, active area $9.5\times10^{-2}\ \text{cm}^2$) is shown in Fig. 5.7 and it is very well described by Eq. (5.15), indicating a field-dependent mobility. The fit of the data provides the mobility parameters ($\mu_0 = 1.73\cdot10^{-7}\,cm^2/(Vs)$ and $\gamma = 1.91\cdot10^{-3}(cm/V)^{1/2}$).

Using these values and extracting the permittivity ($\varepsilon_r = 2.34$) from the maximum value of the high frequency capacitance, see Eq. (5.11), capacitance spectra have been generated and compared with the experimental data as shown in Fig. 5.8. It is observed that the measured spectra display the onset of the geometric capacitance value at the frequencies predicted by the theory, which gives a confirmation of the applicability of the SCLC impedance model that has been proposed above. Two deviations are observed between experimental curves and the model proposed, which are due to additional effects that were not included in this model. (1) The high frequency part of the capacitance exhibits a pronounced frequency dependence, in contrast with our assumption of a constant geometric (dielectric) capacitance. The dielectric response of disordered polymers is known to be modelled by using empirical relaxation functions[1,22] that account for the slight decrease in the capacitance value. Such effect is then dielectric in nature and so it is not considered in our ac transport model. We have used a permittivity value corresponding to the maximum reached by the capacitance spectra in the simulation shown in Fig. 5.8.

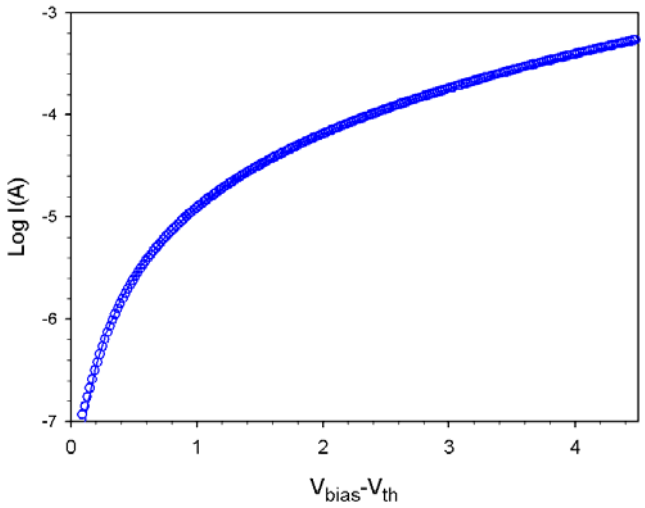

Fig. 5.7. Experimental results (points) of current versus voltage V in a hole-only device with L = 80 nm. The line is a fit using the formula of Murgatroyd in the SCLC regime with a threshold voltage $V_{th} = 0.5V$.

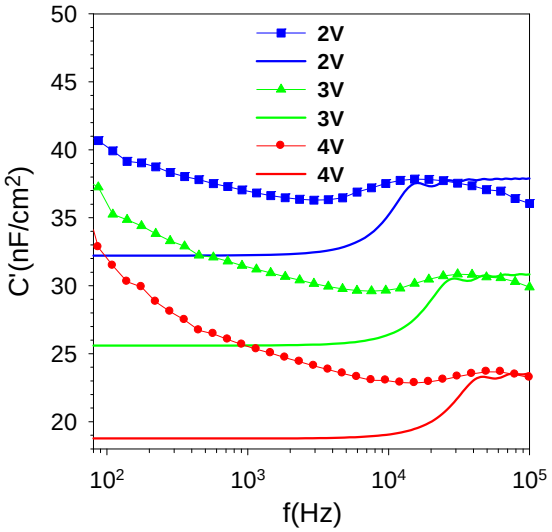

Fig. 5.8. Experimental results of capacitance spectra at different bias potentials ranging from 2V to 4V (line and scatter plots) with their respective numerical calculations of the SCLC capacitance using the parameters from the fit in Fig. 5.7 (line plots). An offset of 6nFcm^{-2} between every curve has been taken in the picture.

It has been verified that the transit frequency is not much affected by the permittivity value used around 2. (2) A strong contribution of traps, is appreciated at low frequency in the experimental data. This fact prevents us from observing the low frequency value of the capacitance, which would be an interesting additional check of the mobility dependence on electrical field as described above in the theory section. Nevertheless these results show that it is possible to evaluate the ac transit time form capacitance data as a function of the frequency.

5.5. Conclusion

The transit time of a single carrier in SCLC with field-dependent mobility has a lower value than in the constant mobility case, as one would expect, due to the increase of the drift velocity, and it depends strongly on the polarization. Furthermore the mobility dependence on the field tends to flatten the electrical field towards a constant value, which allows us to provide a simplified formula for the dc transit time that is in good agreement with the exact value. Experimental capacitance spectra of single carrier devices can be predicted numerically and describe well the capacitance step in the measured spectra, however the latter contain a strong contribution at low frequencies due to trapping and release of carriers and also frequency dispersion in the dielectric capacitance of the polymer.

5.6. References

[1] H. C. F. Martens, H. B. Brom and P. W. M. Blom, Phys. Rev. B **60**, R8489 (1999).

[2] S. Berleb and W. Brütting, Phys. Rev. Lett. **89**, 6601 (2002).

[3] J. Bisquert, G. Garcia-Belmonte, A. Pitarch, et al., Chem. Phys. Lett. **422**, 184 (2006).

[4] H. C. F. Martens, J. N. Huiberts and P. W. M. Blom, Appl. Phys. Lett. **77**, 1852 (2000).

[5] A. Pitarch, G. Garcia-Belmonte and J. Bisquert, J. Appl. Phys. **100**, 084502 (2006).

[6] J. Shao and G. T. Wright, Solid-St. Electron. **3**, 291 (1961).

[7] R. Kassing and E. Kähler, Solid State Commun. **15**, 673 (1974).

[8] D. Poplavskyy and F. So, J. Appl. Phys. **99**, 033707 (2006).

[9] D. M. Pai, J. Chem. Phys. **52**, 2285 (1970).

[10] H. Bässler, Phys. Status Solidi (b) **175**, 15 (1993).

[11] P. W. M. Blom, M. J. M. de Jong and M. G. van Munster, Phys. Rev. B **55**, R656 (1997).

[12] P. S. Davids, I. H. Campbell and D. L. Smith, J. Appl. Phys. **82**, 6319 (1997).

[13] B. K. Crone, P. S. Davids, I. H. Campbell, et al., J. Appl. Phys. **84**, 833 (1998).

[14] I. I. Fishchuk, A. Kadashchuk, H. Bässler, et al., Physical Review B **70**, 245212 (2004).

[15] B. Ramachandhran, H. G. A. Huizing and R. Coehoorn, Phys. Rev. B **73**, 233306 (2006).

[16] J. Bisquert, J. M. Montero, H. Bolink, et al., Phys. Status Solidi (a) **203**, 3762 (2006).

[17] R. H. Young, Philos. Mag. Let. **70**, 331 (1994).

[18] P. N. Murgatroyd, J. Phys. D: Appl. Phys. **3**, 151 (1970).

[19] A. Shumka and M.-A. Nicolet, Solid-St. Electron. **6**, 106 (1964).

[20] R. Kassing, Phys. Status Solidi (a) **28**, 107 (1975).

[21] A. Van der Ziel, "*Solid State Physical Electronics"* (Prentice-Hall, Englewood Cliffs, 1976).

[22] H. H. P. Gommans, M. Kemerink, G. G. Andersson, et al., Phys. Rev. B **69**, 155216 (2004).

6

Trap-limited Mobility in Space-charge-limited Current in Organic Layers

6.1. Introduction

The full description of the charge transport in organic layers by the space-charge limited current (SCLC) model usually requires to include field-[1-3] or density-dependent mobility[4] according to the percolation models.[5] Experimentally, the determination of transit times in single-carrier devices has been widely used to measure the mobility by time-of-flight (TOF)[6] and impedance spectroscopy techniques,[7,8] among others.[9] It has also been recognized that the role of energetic disorder is crucial for an adequate knowledge and control of the properties of organic transport layers. Transport in a single-carrier device has been often rationalized in terms of an extended state and a distribution of traps in the bandgap.[10-12] In this approach, the traps produce a decrease of the transport rate in the extended states.[13] However, in general the dynamics of traps is far more complex, since the traps relaxation intersects with the transport features throughout the layer.[14] While the trapping-diffusion dynamics can be solved completely in homogeneous situations,[15] the typical carrier distribution at high injection currents in an organic layer in the SCLC regime is highly inhomogeneous.[16]

The aim of this chapter is to go beyond a quasistatic approximation to the trap-limited mobility (in which free and trapped charge remain in local equilibrium)[10,17] and to treat rather generally an apparently simple problem, a two level system composed of a transport state and a single trap level. The advantage of this model is that we can fully classify the different dynamic regimes of the system by the interplay of the relevant kinetic constants. This gives us physical insight in the interpretation of more general systems with a distribution of localized levels (e.g., exponential or Gaussian) which can be calculated numerically, a method also applied to dual-carrier devices.[7,18,19] However, the latter systems are beyond the scope of this chapter.

The problem treated in this chapter has been already considered some decades ago by Dascalu[20,21] and Kassing,[22,23] for the particular case of a slow-

shallow trap (i.e., when the transit time is shorter than trapping time) and this case is also solved numerically in the present chapter. In addition, we consider the dynamic results in the frequency domain for fast traps, and also for deep traps. By formulating a general analytical model valid for a fast-shallow trap, we find a delay in the transit time (and thus, a mobility decrease) due to multiple trapping, as measured by means of impedance techniques.[24]

The chapter has the following structure. Firstly, a mathematical description is presented of the single-trap model, secondly, physical implications according to the applications of the model are discussed, and finally, we provide the main conclusions.

6.2. Single-trap Model

The SCLC for single-carrier transport (neglecting diffusion) of electrons in a transport level with density n_c that drift in the electric field *F*, a trap level of occupancy f_t and total density N_t, is described by: the continuity equation, the drift-current equation, Poisson equation and the trap dynamics equation, respectively[6,15]

$$\frac{dJ}{dx} = 0 \tag{6.1}$$

$$J = q\mu_0 n_c F + \varepsilon_r \varepsilon_0 \frac{\partial F}{\partial t} \tag{6.2}$$

$$\frac{dF}{dx} = \frac{q}{\varepsilon_r \varepsilon_0}\left(n_c + N_t f_t\right) \tag{6.3}$$

$$\frac{\partial f_t}{\partial t} = c n_c \left[1 - f_t\right] - e f_t \tag{6.4}$$

Here q is the elementary charge, μ_0 is the mobility, $\varepsilon_r \varepsilon_0$ the dielectric constant, and c and e are the coefficients for electron capture and release,

respectively. The potential can be calculated by integrating the electrical field along the thickness L

$$V = \int_0^L F dx \tag{6.5}$$

The population of the extended states at the energy level E_c, for a non degenerate semiconductor, relates to the Fermi level E_F as

$$n_c = N_c e^{(E_F - E_c)/k_B T} \tag{6.6}$$

where N_c is an effective density of states in the transport level (conduction band). Assuming that the trap level at energy E_t reaches equilibrium with the extended states (with the same Fermi level), the trap occupancy is given by

$$f_t = \frac{1}{1 + e^{(E_t - E_F)/k_B T}} \tag{6.7}$$

In steady state, Eq. (6.4) gives

$$f_t = \frac{1}{1 + e/(cn_c)} \tag{6.8}$$

Therefore, the detailed balance condition provides the following relationship for the trap emission and capture coefficients:

$$e = cN_c e^{(E_t - E_c)/k_B T} \tag{6.9}$$

Let us denote steady-state by $\bar{x}$ and small perturbation by $\hat{x}$ applied at a certain angular frequency ω. Therefore every electrical variable can be expressed as $x = \bar{x} + \hat{x}$ to linearize the whole system of equations up to the first order[25,26]. As shown in Ref.[14], by solving Eq. (6.4) for a small perturbation, we obtain

$$\hat{f}_t = \frac{1}{\bar{n}_c} \frac{\bar{f}_t (1 - \bar{f}_t)}{1 + i\omega/\omega_t} \hat{n}_c \tag{6.10}$$

This term gives the contribution to the spectra of the capacitance and conductance of the trap. The trap frequency is defined as

$$\omega_t = \frac{e}{1-\bar{f}_t} \tag{6.11}$$

This is the maximum frequency that the trap is acting as such, since at higher frequencies the trap cannot follow the ac perturbation, as will be described in Sec. 6.3. Inserting Eq. (6.9) in Eq. (6.11), we find the dependence of ω_t on the trap energy and the occupation, as

$$\omega_t = \frac{cN_c e^{(E_t-E_c)/k_BT}}{1-\bar{f}_t} \tag{6.12}$$

It should be remarked that in the SCLC regime, $\bar{f}_t$ is position-dependent along the organic layer. The impedance is defined as the quotient of potential to current density,

$$Z(\omega) = \frac{\hat{V}(\omega)}{\hat{J}(\omega)} \tag{6.13}$$

$\hat{V}(\omega)$ is determined by spatial integration of $\hat{F}(\omega)$ from the solution of the above described model. The boundary conditions at the injecting contact used to solve the electrical variables along the thickness in *dc* and *ac* conditions are:[27,28]

$$\bar{n}_c(x=0) = N_c \text{ and } \hat{F}(x=0) = 0 \tag{6.14}$$

Capacitance and conductance are defined as follows:

$$C'(\omega) = \mathrm{Re}\left[\frac{1}{i\omega Z(\omega)}\right] \tag{6.15}$$

$$g(\omega) = \mathrm{Re}\left[\frac{1}{Z(\omega)}\right] \tag{6.16}$$

6.3. Theoretical Results

In this section it is shown the results of the calculations of the capacitance and the conductance spectra for different trap properties and voltages, compared to the trap-free case. We first describe the latter case as a reference, and then discuss variations of energetics (E_t), by considering a shallow and a deep trap level, and the trap kinetics (c), for a fast and a slow trap. The different configurations are given in Table I.

6.3.1. Trap-free

The well-known trap free SCLC model with constant mobility is given by the analytical expression for stationary and impedance responses as[29]

$$J = \frac{9}{8}\varepsilon\mu_0\frac{V^2}{L^3} \tag{6.17}$$

$$Z(\omega) = \frac{6}{g_0(i\omega\tau_0)^3}\left[1 - i\omega\tau_0 + \frac{1}{2}(i\omega\tau_0)^2 - \exp(-i\omega\tau_0)\right] \tag{6.18}$$

where the transit time, the geometrical capacitance and the conductance are, respectively,

$$\tau_0 = \frac{4}{3}\frac{L^2}{\mu_0 V} \tag{6.19}$$

$$C_g = \frac{\varepsilon}{L} \tag{6.20}$$

$$g_0 = \frac{dJ}{dV} = \frac{3}{\tau_0}C_g \tag{6.21}$$

For low frequency, the admittance is

$$Y(\omega) = g_0 + i\omega\frac{3}{4}C_g \tag{6.22}$$

and for high frequency it is

$$Y(\omega) = \frac{2}{3} g_0 + i\omega C_g \tag{6.23}$$

It is well known that the capacitance spectrum makes a step from $3C_g/4$ to C_g at around the transit time frequency, i.e., when the small perturbation of charge carriers injected by the frequency perturbation voltage is able to arrive at the collecting contact. However, in experimental data, this ideal behaviour is usually distorted, mainly at low frequencies, by the trap contribution to capacitance.

6.3.2. Steady-state Characteristics of Organic Layers with Shallow and Deep Traps

Experimental measurements of *J-V* curves have been used to determine the transport properties in organic layers.[30,31] Simulations of the current-potential curves and the Fermi level distributions are displayed in Fig. 6.1 for two different trap energy levels configurations. These results are well understood and described in the literature.[32] For a shallow trap, the trap population is much less than the population of the transport level, hence the electric field distribution is not significantly altered, causing only a slight variation in the Mott-Gourney square law

$$J \approx \frac{9}{8} \varepsilon \theta \mu_0 \frac{V^2}{L^3} \tag{6.24}$$

where θ is a carrier-density dependent factor of trapped and free charge defined as[24]

$$\theta^{-1} = \left(1 + \frac{\langle \bar{n}_t \rangle}{\langle \bar{n}_c \rangle} \right) \tag{6.25}$$

with the brackets denoting an average over the thickness of the film. For a deep trap, the occupancy of the trap level increases and the trapped charges play a

crucial role in the current density-voltage curves. At low bias, most carriers are trapped, thus significantly altering the carrier and electric field distributions with respect to trap-free case, leading to an abrupt increase of the current slope, $J \propto V^m$ with $m \geq 2$. At high bias, the trapping sites are already filled and all the additional injected carriers are located in the transport level. This situation bends the curve from a higher voltage exponent than 2, towards a square law dependence.

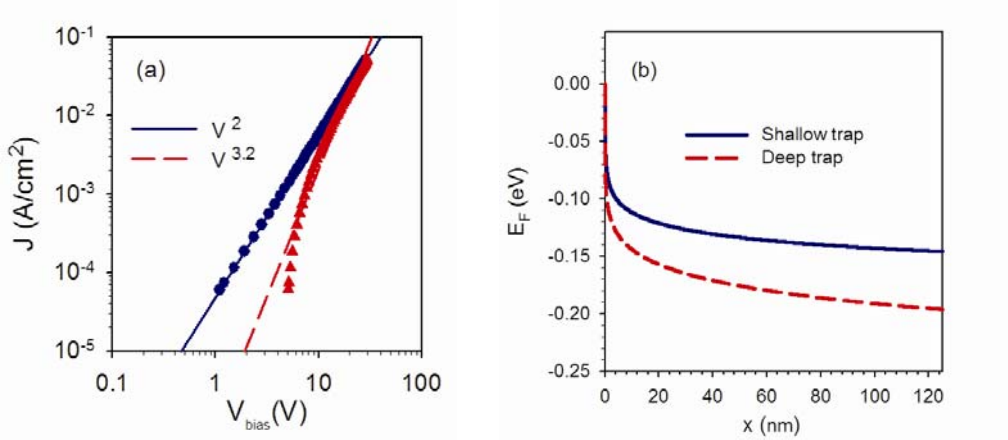

Fig. 6.1 Model simulations of shallow ($E_c - E_t = 0.1\,\mathrm{eV}$) and deep ($E_c - E_t = 0.5\,\mathrm{eV}$) trap configurations represented by blue solid lines and red dashed lines. **(a)** Current density voltage-characteristics for a shallow trap and a deep trap are plotted by blue dots and red triangles. Fittings provide the exponent of the voltage. **(b)** Fermi level representations at 6V along the thickness, for a shallow trap (blue solid line) and a deep level (red dashed line).

6.3.3. Dynamic Characterization of Shallow Traps

Let us now focus our attention on the dynamic properties of the electrical variables (capacitance and conductance) in the case of the shallow trap. A general outline of the simulation results is displayed in Fig. 6.2. To accurately determine the *ac* transit times τ_{ac}, it is worth to apply the representation of

negative differential susceptance $(-\Delta B(\omega) = \mathrm{Im}(Y(\omega)) = -\omega(C'(\omega) - C_g)$, that provides peaks at certain frequencies f_{max} such that[33]

$$\tau_{ac} \approx 0.72 \cdot f_{\max}^{-1} \tag{6.26}$$

Figure 6.2(a) shows the capacitance spectra (normalized to C_g) for the trap-free case, as a reference, and a shallow trap with two different trap kinetics, fast and slow (as specified below). At low-frequencies, the presence of a shallow trap in the organic layer implies (1) a deviation of the capacitance spectra for the slow case, and (2) of transit time for the fast one. At high frequencies, all the spectra converge to C_g with smooth and decaying oscillations as theoretically expected. In experiments, a slight decrease of the capacitance occurs due to the dielectric relaxation of the material.[34]

As for conductance, Fig. 6.2(b), the normalized low-frequency value decreases by a factor θ and the calculated *ac* transit time (normalized to τ_0) is increased by θ, although only for fast traps, thus in Fig. 2(b) we obtain for low frequencies $g = 0.71 g_0$ and for high frequencies, $g = 2\theta g_0 / 3$. All these behaviours will be modelled and explained in terms of a quasi-equilibrium between the two states (trapping and transport levels) in the forthcoming subsections.

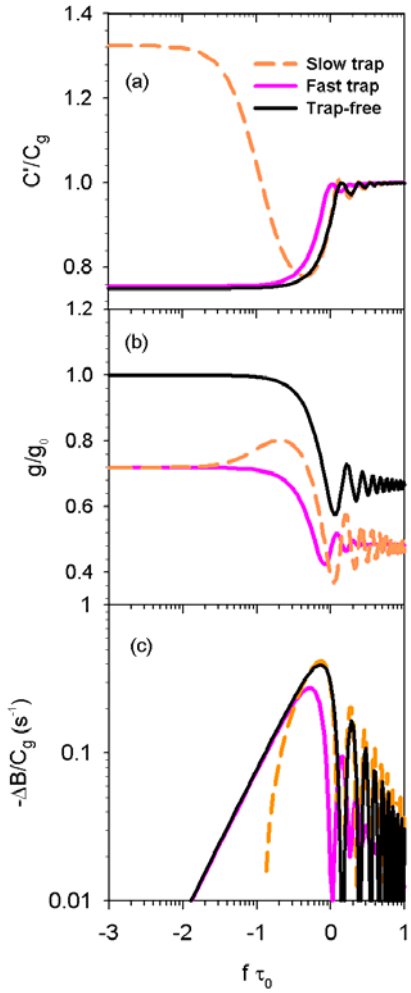

Fig. 6.2 Simulation spectra for shallow traps at 2V. Fast traps are plotted by pink lines, slow traps by orange dashed lines and trap free spectrum by black. **(a)** Capacitance spectra normalized to C_g for fast and slow traps. Low-frequency increase is displayed for slow traps whereas not for the fast ones. **(b)** Conductance spectra normalized to g_0 for fast and slow traps. **(c)** Negative differential susceptance $-\Delta B(\omega)$ normalized to C_g to extract transit times. In the case of fast trapping, ac transit time is $\tau_{ac} = 1.36\tau_0$ ($\tau_0 = 221.6\mu s$) with $\theta^{-1} \approx 1.40$, whereas for slow trapping no deviation from the trap free is observed.

6.3.4. Fast-shallow Traps

When the trap kinetics is fast, quasi-equilibrium prevails between carriers in the trap and transport levels. In this case we expect the standard formula of Rose[24] for trap limited transport to be valid

$$\mu = \theta\mu_0 \tag{6.27}$$

and therefore, the trap-limited transit time is

$$\tau = \theta^{-1}\tau_0 \tag{6.28}$$

In order to check Eq. (6.27), in Fig. 6.3 changes in the population of the traps were imposed by modifying N_t. The resulting capacitance spectra are well described by the trap-free case formulas by using the trap-limited values τ and g *instead* of τ_0 and g_0. In particular we obtain

$$g = \frac{dJ}{dV} = \frac{3}{\tau}C_g = \theta g_0 \tag{6.29}$$

The inset of Fig. 6.3 shows that Eq. (6.28) is indeed satisfied.

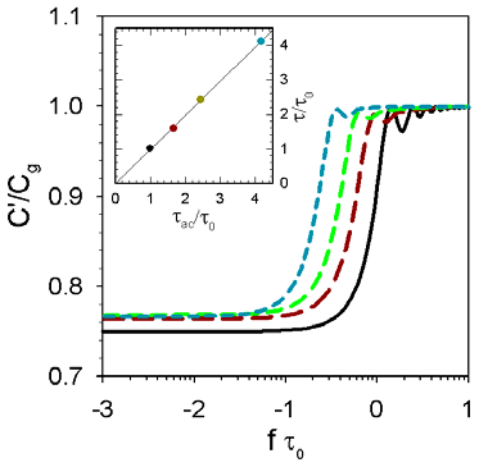

Fig. 6.3 Simulated capacitance spectra steps for fast shallow traps at 6V *(τ_0=73.8μs)* by varying trap densities, from left to right: N_t=$8\cdot10^{17}$, N_t=$8\cdot10^{17}$, $4\cdot10^{17}$, $2\cdot10^{17}$, 0 cm^{-3}. Inset shows an identification of transit times between the model discussed in the text, and the ac conductance calculation.

The physical interpretation of this situation is given in terms of the interplay between trapping-detrapping and the carrier transit time. If fast-shallow traps are present in an organic layer, a delay in the transit time is expected and thereby, a mobility decrease. An experimental method to corroborate whether this kind of energetic disorder exists, consists on the evaluation of the *ac* transit time from admittance spectroscopy, Eq. (6.26), and the *dc* transit time, Eq. (6.19). The possible deviation should be attributed to the presence of fast-shallow traps.

6.3.5. Slow-shallow Traps

If the trapped charge is not able to achieve the quasiequilibrium with the carrier concentration in the transport levels, the spectra present a large low-frequency capacitance that increases above the $3C_g/4$ value, Fig. 6.4. When exceeding the trap frequency ω_t of Eq. (6.11), capacitance rapidly decreases as trapping action ceases for the rest of the frequency range. In contrast to the previous case, here carriers are able to cross the organic layer and reach the collecting contact before being trapped, avoiding any delay and following the trap-free transit time τ_0. Dascalu and Kassing have given the analytical expression for the impedance in this situation[20-23]

$$Z(\omega)=\frac{6\alpha}{g_0}\sum_{k=0}^{\infty}\frac{\Gamma(\theta\alpha+1)}{\Gamma(\theta\alpha+k+2)}\frac{(-i\omega\tau_0)^k}{k+3} \tag{6.30}$$

with α being

$$\alpha(\omega)=1+\frac{\omega_c}{\omega_e}\frac{1}{1+i\omega/\omega_e} \tag{6.31}$$

Here $\omega_c = c\left(N_t - \langle \bar{n}_t \rangle\right)$ and $\omega_e = c\left(\langle \bar{n}_c \rangle + N_c e^{(E_t - E_c)/k_B T}\right)$ are the reciprocal lifetimes for electrons in the conduction band and in the trap level, respectively. For low-frequency with $N_t >> \langle \bar{n}_t \rangle$, we have the approximation[23]

$$Y(\omega) = g + i\omega \frac{C_g}{\omega_e \tau_0} \tag{6.32}$$

being $g = \theta g_0$ and for high-frequency:

$$Y(\omega) = \frac{2}{3} g + i\omega C_g \tag{6.33}$$

The low-frequency capacitance increase is usually found in experiments for single-carrier devices[7,8,35] and, according to our model, due to the slow-shallow trap contribution. The model also predicts a coincidence in transit times by *ac* and *dc* techniques unlike the previous case.

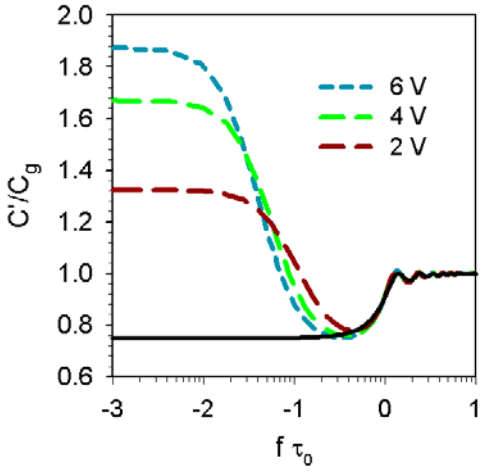

Fig. 6.4 Model representations of the capacitance spectra for slow shallow traps at voltages 6, 4 and 2 V, from top to bottom. The trap free spectrum is pictured in black.

In Fig. 6.5, it is shown that the low-frequency capacitance dependence with the voltage exhibits a peak when quasi-Fermi level crosses the trap energy level (E_t) corresponding to a maximum in the trap contribution to the capacitance,

Eq. (6.10). The low-frequency conductance is similar to the trap-free value at high voltages since free charges dominate the injected carrier concentration.

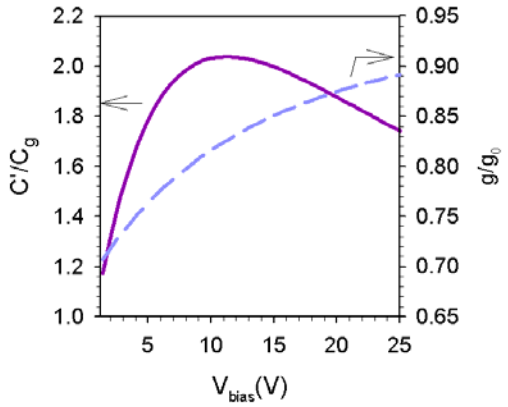

Fig. 6.5 Calculations of the low-frequency capacitance (violet solid line) and conductance (cyan dashed line) versus voltage at 1Hz.

6.3.6. Limit between Fast- and Slow-shallow Traps

In the previous subsection, we have shown two extreme behaviours dominated either by transit or trapping time. It is interesting to establish the conditions that determine which regime prevails. Let us define the trap and transit time frequencies as:

$$< \omega_t > \approx \frac{\beta N_c e^{(E_t - E_c)/k_B T}}{1 - < \bar{f}_t >} \tag{6.34}$$

$$\omega_{tt} = 2\pi / \tau_0 \tag{6.35}$$

If the trap frequency is larger than the reciprocal transit time, the fast trap regime with the multiple trapping transit time $\tau = \theta^{-1}\tau_0$ is present. In the opposite situation, the slow trap regime occurs with the trap-free transit time τ_0 value. Inserting Eqs. (6.34) and (6.35) in $< \omega_{tr} > \approx \omega_{tt}$, it is possible to quantify a

critical capture coefficient c_c as:

$$c_c \approx \frac{2\pi}{\tau_0} \frac{1 - < \bar{f}_t >}{N_c e^{(E_t - E_c)/k_B T}} \tag{6.36}$$

According to the parameters of Table I, this quantity is estimated as $c_c \approx 10^{-13} cm^3/s$. If a trap capture coefficient is lower than this critical value the trap is slow, whereas if it is higher, the trap is fast. In Fig. 6.6, normalized transit times are plotted versus normalized trap frequency and both transit time regimes are depicted showing a narrow transition from the trap-free formula to the multiple trapping one.

As pointed out at the end of subsection 2.2.1., to experimentally determine if shallow traps of an organic layer are slow or fast, the technique consists in comparing the transit times from ac (Eq. (6.26)) and dc (Eq. (6.19)). A coincidence would give us the slow result whereas a deviation indicates the presence of fast traps.

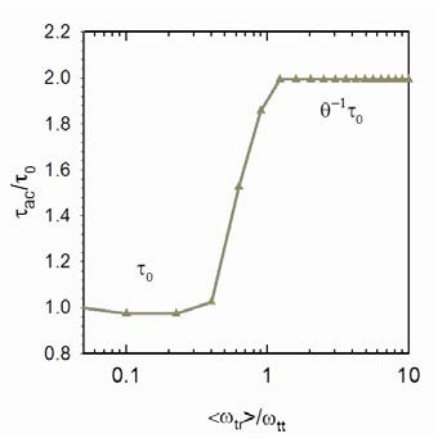

Fig. 6.6 Simulations of normalized transit times calculated from the ac conductance method versus normalized trap frequency at 6V and $N_t=3\cdot10^{17}cm^{-3}$, describing a step up from the classical transit time $\tau_0 = 73.8\mu s$ to the multiple trapping one, $\tau_{ac} = \theta^{-1}\tau_0$ with $\theta^{-1} \approx 2$. Classical transit time occurs for normalized trap frequency ($\omega_{tt} = 85\text{kHz}$) $\langle \omega_t \rangle / \omega_{tt} < \theta$ and multiple trapping for $\langle \omega_t \rangle / \omega_{tt} > 1$ according to dotted vertical marks.

6.3.7. Comparison between Dynamic and Static Capacitance

Dynamic capacitance, obtained from admittance spectroscopy at low frequencies, is frequently compared to the well-known static one.[10] In SCLC, the low-frequency capacitance has a value of $3C_g/4$,[29,36] whereas the static capacitance is set at $3C_g/2$.[10] This reduced factor of $1/2$ in the dynamic capacitance is attributed to the three contributions to the *ac* current (velocity modulation, density modulation and displacement term).[23] In a two level system with a shallow trap, the static capacitance is calculated by integrating the charge stored in the device per voltage unit as[10]

$$C_{st} = \frac{e}{V}\left(\int_0^L \overline{n}_c(x)dx + \int_0^L \overline{n}_t(x)dx\right) \tag{6.37}$$

where V is the bias applied along the organic layer. In Fig. 6.7, the static capacitance is plotted versus bias-voltage. It is observed that the value remains at $3C_g/2$ as in the trap-free case. At low voltages, the capacitance contribution essentially comes from the majority of the charge stored in the shallow trapping sites whereas at high voltages the capacitance is mainly due to free charge.

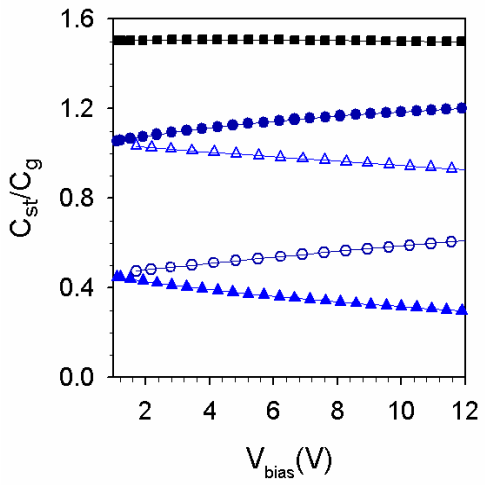

Fig. 6.7 Model calculations of the static capacitance versus voltage for a shallow trap (black squares). Free carrier contribution (solid and empty triangles) and trap carrier contribution (solid and empty circles) to static capacitance. Solid and empty symbols are for $N_t=1\cdot10^{17}$, $N_t=5\cdot10^{17}$, respectively.

6.3.8. Dynamic Characterization of Deep Traps

In contrast to the shallow trap energy level, where occupation is quite low, in the case of a deep trap, the opposite situation occurs as occupation is approaching the unity. This deviation strongly determines the contribution to the impedance from the trap dynamics Eq. (6.4). The trap levels are so heavily occupied that the temporal variation of $\bar{f}_t$ is governed by the emitting rather than the trapping term. The numerical solution for the capacitance and the conductance is shown in Fig. 6.8(a) and (b) displaying distinct features with respect to the trap-free spectrum: a low-frequency capacitance below $3C_g/4$, a conductance spectrum significantly lower, and increased oscillation in the transition from low to high frequencies. These results are independent of the traps kinetics, which is another particularity in comparison to the shallow-trap results.

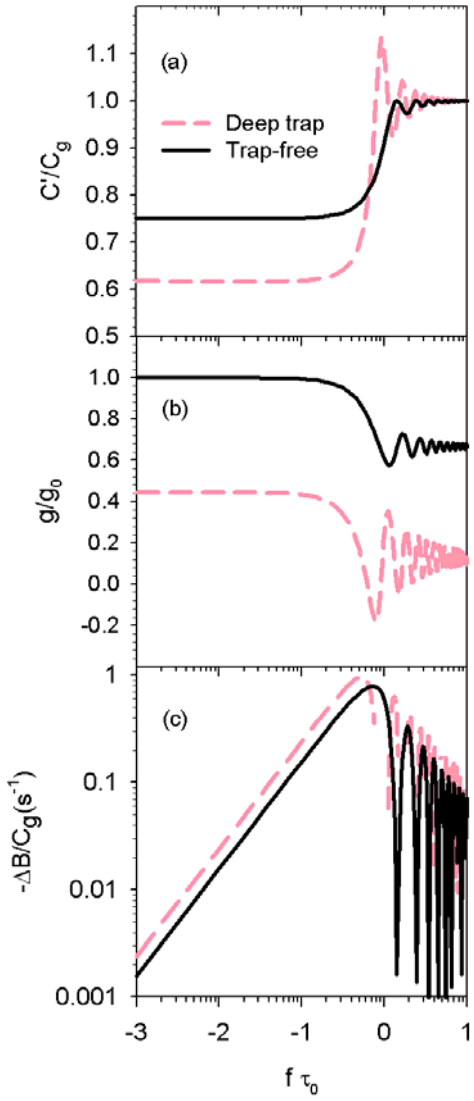

Fig. 6.8 Model solution of impedance spectra for deep trap at 6V. Traps are plotted by maroon dashed lines and trap-free spectrum in black as a reference. **(a)** Capacitance spectra normalized to C_g. **(b)** Conductance spectra normalized to g_0. **(c)** Negative differential susceptance $-\Delta B(\omega)$ normalized to C_g.

L (nm)	N_c (cm^{-3})	μ_0 ($cm^2/(Vs)$)	E_t (eV)	N_t (cm^{-3})	c (cm^3/s)
125	10^{19}	$4.7 \cdot 10^{-7}$		10^{17}	
Trap properties		Shallow	-0.1	Fast	10^{-12}
		Deep	-0.5	Slow	10^{-14}

Table I. Material parameters used in the simulation of transport in an organic layer

6.4. Conclusion

The single-trap model has been described and numerically solved for SCLC for impedance studies in order to determine the dynamical properties of carrier transport and storage depending on energy (shallow and deep) and kinetics (fast and slow) of the trap. For a fast-shallow trap, an analytical model is provided and validated by means of the multiple trapping formula for mobility $\mu = \theta\mu_0$, where θ depends on the steady-state solution (trapped and free charge). For a slow-shallow trap, the available analytical model has been revised. Both regimes, fast and slow, have been characterized depending on the dominance of either trapping or transit processes and an experimental method has been also provided by comparing *dc* and *ac* transit times. A deep trap results in a decrease in the low-frequency capacitance (with respect to the trap-free case) and also in a delay in the transit times.

6.5. References

[1] H. Bässler, Phys. Status Solidi (b) **175**, 15 (1993).

[2] P. N. Murgatroyd, J. Phys. D: Appl. Phys. **3**, 151 (1970).

[3] P. S. Davids, I. H. Campbell and D. L. Smith, J. Appl. Phys. **82**, 6319 (1997).

[4] C. Tanase, P. W. M. Blom, D. M. de Leeuw, et al., Phys. Status Solidi (a) **201**, 1236 (2004).

[5] M. C. J. M. Vissenberg and M. Matters, Physical Review B **57**, 12964 (1998).

[6] P. W. M. Blom and M. C. J. M. Vissenberg, Mater. Sci. Eng. **27**, 53 (2000).

[7] D. Poplavskyy and F. So, J. Appl. Phys. **99**, 033707 (2006).

[8] Gommans, Kemerink, Andersson, et al., Phys. Rev. B **69**, 155216 (2004).

[9] S. Shirota and H. Kageyama, Chem. Rev. **107**, 953 (2007).

[10] B. Ramachandhran, H. G. A. Huizing and R. Coehoorn, Phys. Rev. B **73**, 233306 (2006).

[11] M. M. Mandoc, B. de Boer and P. W. M. Blom, Phys. Rev. B **73**, 155205 (2006).

[12] V. I. Arkhipov, E. V. Emelianova and G. J. Adriaenssens, Phys. Rev. B **64**, 125125 (2001).

[13] A. L. Alvarez, B. Arredondo, B. Romero, et al., IEEE Trans. Electron Devices **55**, 674 (2008).

[14] J. Bisquert, Phys. Rev. B **77**, 235203 (2008).

[15] J. Bisquert and V. S. Vikhrenko, Electrochim. Acta **47**, 3977 (2002).

[16] G. T. Wright, Solid-St. Electron. **2**, 165 (1961).

[17] J. Bisquert, Phys. Chem. Chem. Phys. **10**, 3175 (2008).

[18] N. D. Nguyen and M. Schmeits, Phys. Rev. B **75**, 075307 (2007).

[19] M. Schmeits, J. Appl. Phys. **101**, 084508 (2007).

[20] D. Dascalu, Int. J. Electron. **21**, 183 (1966).

[21] D. Dascalu, Solid-St. Electron. **11**, 491 (1968).

[22] R. Kassing and E. Kähler, Solid State Commun. **15**, 673 (1974).

[23] R. Kassing, Phys. Status Solidi (a) **28**, 107 (1975).

[24] A. Rose, "*Concepts in Photoconductivity and Allied Problems"* (John Wiley & Sons, New York, 1963).

[25] A. Van der Ziel, "*Solid State Physical Electronics"* (Prentice-Hall, Englewood Cliffs, 1976).

[26] W. Brütting and S. Berleb, Phys. Rev. Lett. **89**, 286601 (2002).

[27] P. W. M. Blom, M. J. M. de Jong and M. G. van Munster, Phys. Rev. B **55**, R656 (1997).

[28] N. F. Mott and R. W. Gurney, "*Electronic processes in ionic crystals"* (Oxford University Press, London, 1940).

[29] J. Shao and G. T. Wright, Solid-St. Electron. **3**, 291 (1961).

[30] A. J. Campbell, M. S. Weaver, D. G. Lidzey, et al., J. Appl. Phys. **84**, 6737 (1998).

[31] F. So, B. Krummacher, D. Poplavskyy, et al., J. Appl. Phys. **102**, 091101 (2007).

[32] M. A. Lampert and P. Mark, "*Current Injection in Solids"* (Academic Press, Inc., New York, 1970).

[33] H. C. F. Martens, J. N. Huiberts and P. W. M. Blom, Appl. Phys. Lett. **77**, 1852 (2000).

[34] H. C. F. Martens, H. B. Brom and P. W. M. Blom, Phys. Rev. B **60**, R8489 (1999).

[35] J. M. Montero, "*Injection and Transport in Organic Light-Emitting Diodes (OLEDs)"* (Universitat Jaume I, MSc Thesis, Castellón, 2007).

[36] D. Dascalu, Solid-St. Electron. **12**, 444 (1969).

7

Trap Origin of Field-dependent Mobility of the Carrier Transport in Organic Layers

7. Trap Origin of Field-dependent Mobility of the Carrier Transport in Organic Layers

7.1. Introduction

Charge transport in organic semiconductors has been widely studied by using current density-potential (*J*-*V*) curves and time- or frequency-resolved measurements (e.g., time of flight, impedance spectroscopy (IS), etc.).[1] In experimental measurements of SCLC transport it is often observed that carrier mobility depends on bias voltage. However, the well-known Mott-Gourney square law $J \propto V^2$, for trap-free materials with constant mobility μ, was not generally found whereas a stronger *J*-*V* dependence actually was.[2,3]

Typically, two continuous models have been applied in the literature to understand this current-density deviation and, thereby, to model the experimental data.[4] In the first approach, *J*-*V* characteristics behave as $J \propto V^2 \exp(0.89\gamma\sqrt{V/L})$ under the assumption of field-dependent mobility $\mu \propto \exp(\gamma\sqrt{F})$ that explains the extra-current required along the voltage range.[5,6] Experimental determination of mobility by different techniques such as IS supported this assumption.[7] However, the second interpretation is based on the framework of SCLC with constant mobility and a transport level, under the influence of an exponential distribution of traps in the band-gap that capture and release charge carriers, Fig. 7.1. Current-density-voltage characteristics display the law $J \propto V^m$ with m>2.[8]

A similar behaviour is explained by means of a carrier density-dependent mobility model that stems from hopping conductivity in an exponential density of states.[9-11] Following Tanase et al.,[4] the carrier-density dependence of the mobility has been further developed[12-14] and these authors find out that the current-voltage characteristics of organic devices can be adequately modelled. However, in point of fact many groups modelling transport in organic layers continue to use the field-dependence of the mobility.[15-19] It seems therefore, very important to establish the connection between the two approaches and this is the topic of the present chapter. We show here that the apparent field-dependence of the mobility can be explained in terms of a multiple trapping

scheme involving a broad distribution of localized states. This last model lies behind the carrier-dependence of the mobility.[20]

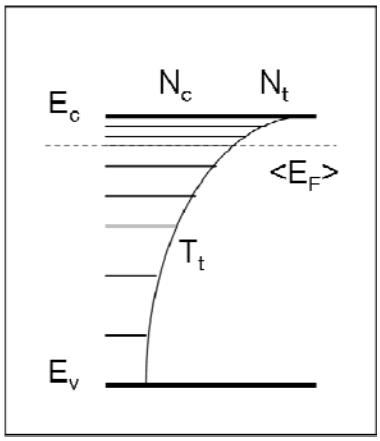

Fig. 7.1. Schematic energy diagram of the multiple-trapping transport picture. The horizontal scale indicates the density of traps in the band-gap. Representative model quantities are indicated: effective density of transport states N_c, band-gap energy E_c-E_v, effective density of trap states N_t, characteristic trap temperature T_t (determining the shape of the exponential tail) and the average Fermi level $<E_F>$.

In the previous chapter, we implemented numerically the multiple-trapping model with only a single-trap.[21] We showed that the shape of capacitance spectra (obtained from IS) is critically modified by trapping properties (i.e., kinetic constants and energetic position). Particularly, fast trapping accounts for a transport limitation since carriers may be harshly hindered. The case of a slow-shallow trap provides a low-frequency capacitance increase, whereas for a fast-shallow trap, the step-up of the capacitance exhibits a deviation that directly affects the determination of mobility. In addition, the density of states in organic semiconductors has been conventionally treated as a gaussian function, however, an exponential distribution was found to be a good approximation of the effective distribution of the tail states.[4] Here we extend the previous analysis, from a single-trap to an exponential density, in order to discuss the measurements of mobility by means of IS at different voltages. The results of our calculation indicate that field-dependent mobility, commonly

found in experimental measurements, may be understood in terms of the multiple-trapping picture.

7.2. Mobility Measurements by IS

The IS technique is based on the measurement of impedance or equivalently, admittance, Y ($Y(\omega) = G(\omega) + iB(\omega)$), obtained from the application of a small voltage harmonic modulation of angular frequency ω. $G(\omega)$ and $B(\omega)(=\omega C(\omega))$ are the conductance and susceptance, respectively, as a function of the radian frequency. Capacitance spectra can be extracted as $C(\omega) = \mathrm{Im}(Y/\omega)$.[1]

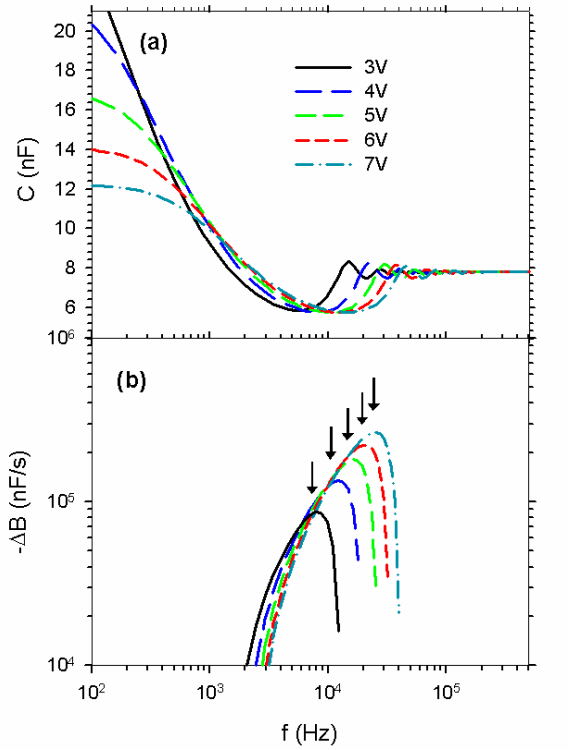

Fig. 7.2 Model representations at voltages ranging from 3V to 7V. (a) capacitance spectra and (b) negative differential susceptance extracted from the upper pannel.

Model representations have been carried out by an extension of the model of Ref.[21] to an exponential distribution of traps. Figure 7.2 (a) shows capacitance spectra at different steady state voltages applied on a thin film at room temperature. Input parameters concerning the device geometry, charge transport and carrier trapping values are displayed in Table II. In contrast to the single-trap model, two different behaviors are obtained in the frequency ranges of low and intermediate frequencies. This is due to the fact that the exponential distribution comprises a wide span of localized-states according to energetic position and trap dynamics. First, at low frequencies, capacitance undergoes an increase which is more appreciable the less voltage is applied due to the lower occupation of the exponential density of traps. Second, by lowering the Fermi level, more slow-shallow traps within the distribution are emptied causing the low-frequency contribution to capacitance.

To determine the mobility by means of the IS technique, we use the representation of the negative differential susceptance ($-\Delta B(\omega) = -\omega(C(\omega) - C_g)$), where C_g is the geometrical capacitance. Figure 7.2 (b) displays peaks at intermediate frequencies f_{max} (arrows) that provide the mobility by the expression:[22]

$$\mu = \frac{4}{3}\frac{L^2 f_{\max}}{0.72 \cdot (V_{bias} - V_{th})} \tag{7.1}$$

where $(V_{bias} - V_{th})$ is the voltage drop in the bulk layer in SCLC.

Calculations of mobility are carried out for different carrier capture coefficients as a function of the square root of the electric field $F^{1/2}$, which is approximated by $(V/L)^{1/2}$, see Fig. 7.3. Remarkably, the fitting to the field-dependent expression

$$\mu = \mu_0 \exp(\gamma\sqrt{F}) \tag{7.2}$$

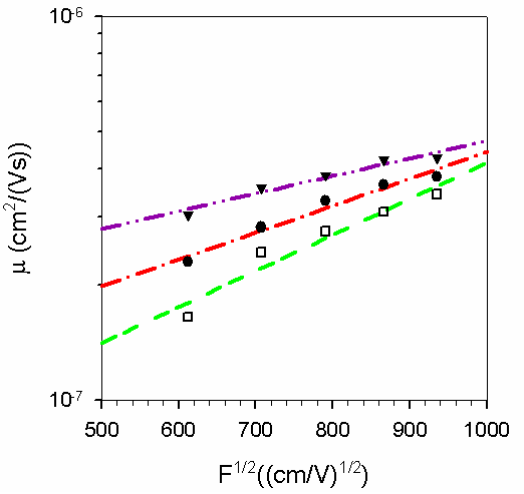

Fig. 7.3 Model representation of mobility versus $F^{1/2}$ by the IS technique for different capture coefficients $c = 7\cdot10^{-13}$, $4\cdot10^{-12}$, $9\cdot10^{-12} cm^3/s$, from top to bottom. Mobility fittings are ranged as: $1.6\cdot10^{-7} cm^2/(Vs) > \mu_0 > 4.8\cdot10^{-8} cm^2/(Vs)$ and $1.1\cdot10^{-3}(cm/V)^{1/2} < \gamma < 2.2\cdot10^{-3}(cm/V)^{1/2}$.

provides common mobility values obtained in organic materials. Mobility parameters μ_0 and γ are the zero-field mobility and the field activation factor, respectively. While the values of μ_0 are expected (the trap-free mobility was appropriately selected for simulation), the most interesting feature corresponds to the exponential factor γ governing the voltage-variation of the mobility. The values $1.1\cdot10^{-3}(\mathrm{cm/V})^{1/2} < \gamma < 2.2\cdot10^{-3}(\mathrm{cm/V})^{1/2}$ derived from the simulation are in the suitable order of magnitude for organic layers as reported in the literature.[23,24] According to the multiple-trapping picture, trap-limitation of mobility stems from the fast-shallow traps within the exponential distribution of localized states. By the application of more voltage, Fermi level covers more trapping states resulting in a less trap-limited transport that enhances the device performance.

Parameter	**Value**
Thickness L	80 *nm*
Device area A	0.235 cm^2
Transport effective density of states N_c	10^{19} cm^{-3}
Relative dielectric constant ε_r	3
Trap-free mobility μ_{0n}	$5 \cdot 10^{-7}$ $cm^2/(Vs)$
Temperature T	300 *K*
Band-gap E_c- E_v	3.1 *eV*
Trap effective density of states N_t	$5 \cdot 10^{17}$ cm^{-3}
Characteristic trap temperature T_t	1500 *K*
Trapping capture coefficient c	$7 \cdot 10^{-14}$ cm^3/s

Table II. Parameters of the numerical simulation

7.3. Conclusion

In summary, we have demonstrated that the apparent mobility dependence on the electric field $\mu \propto \exp(\gamma\sqrt{F})$, usually found by experimental techniques such as IS, may be explained in terms of a multiple-trapping picture. Computational results of our model (SCLC with constant mobility and a transport level under the trapping-detrapping dynamics of an exponential density of traps) yielded a mobility enhancement with the electric field in IS simulations. The main reason is that the trap-limitation of mobility (due to the exponential distribution of localized-states) is reduced as more voltage is applied.

7.4. References

[1] F. So, B. Krummacher, D. Poplavskyy, et al., J. Appl. Phys. **102**, 091101 (2007).

[2] P. W. M. Blom, M. J. M. de Jong and M. G. van Munster, Phys. Rev. B **55**, R656 (1997).

[3] A. J. Campbell, D. D. C. Bradley and D. G. Lidzey, J. Appl. Phys. **82**, 6326 (1997).

[4] C. Tanase, E. J. Meijer, P. W. M. Blom, et al., Phys. Rev. Lett. **91**, 216601 (2003).

[5] H. Bässler, Phys. Status Solidi (b) **175**, 15 (1993).

[6] P. N. Murgatroyd, J. Phys. D: Appl. Phys. **3**, 151 (1970).

[7] S. W. Tsang, S. K. So and J. B. Xu, J. Appl. Phys. **99**, 013706 (2006).

[8] P. Mark and W. Helfrich, J. Appl. Phys. **33**, 205 (1962).

[9] B. Ramachandhran, H. G. A. Huizing and R. Coehoorn, Phys. Rev. B **73**, 233306 (2006).

[10] M. C. J. M. Vissenberg and M. Matters, Phys. Rev. B **57**, 12964 (1998).

[11] M. M. Mandoc, B. de Boer, G. Paasch, et al., Phys. Rev. B **75**, 193202 (2007).

[12] R. Coehoorn, W. F. Pasveer, P. A. Bobbert, et al., Phys. Rev. B **72**, 155206 (2005).

[13] W. F. Pasveer, J. Cottar, C. Tanase, et al., Phys. Rev. Lett. **94**, 206601 (2005).

[14] P. W. M. Blom, C. Tanase, D. M. de Leeuw, et al., Appl. Phys. Lett. **86**, 092105 (2005).

[15] Y. Z. Wu, C. R. Zhang and D. J. Zhang, Appl. Phys. Lett. **95**, 033508 (2009).

[16] M. Giulianini, E. R. Waclawik, J. M. Bell, et al., Appl. Phys. Lett. **94**, 083302 (2009).

[17] N. S. Christ, S. W. Kettlitz, S. Valouch, et al., J. Appl. Phys. **105**, 104513 (2009).

[18] I. Hwang, C. R. McNeill and N. C. Greenham, J. Appl. Phys. **106**, 094506 (2009).

[19] J. Brückner, N. Christ, O. Bauder, et al., Appl. Phys. Lett. **96**, 041107 (2010).

[20] J. Bisquert, Phys. Chem. Chem. Phys. **10**, 3175 (2008).

[21] J. M. Montero, J. Bisquert, G. Garcia-Belmonte, et al., Org. Electron. **10**, 305 (2009).

[22] J. M. Montero, J. Bisquert, G. Garcia-Belmonte, et al., Phys. Status Solidi (a) **204**, 2402 (2007).

[23] M. M. Mandoc, B. de Boer and P. W. M. Blom, Phys. Rev. B **73**, 155205 (2006).

[24] I. H. Campbell, D. L. Smith, C. J. Neef, et al., Appl. Phys. Lett. **74**, 2809 (1999).

Interpretation of Trap-limited Mobility in Space-charge-limited Current in Organic Layers with an Exponential Density of Traps

8.1. Introduction

Charge carrier mobility is the crucial parameter governing the transport and recombination in the bulk of organic materials. The description of charge transport in organic layers by space-charge limited current requires an interpretation of mobility by different semi-empirical models with field- or density-dependence. The interconnection between both frameworks was given in the previous chapter.

In the 90s, field-dependent mobility models were proposed by Bässler, as the result of assuming hopping transport in a Gaussian density of states (DOS).[1] Field-dependent mobility in organic layers, such as in sandwiched films composed of either poly(p-phenylene vinylene) (PPV) derivatives or aluminium hydroxyquinoline (Alq3), became widely accepted. However, the trend changed with the advent of the new century due to breakthrough studies on charge transport in field-effect transistors. Tanase et al. pioneered comparison of mobility values for two solution-processed organic polymers: poly(2-methoxy-5-(3',7'-dimethyloctyloxy)-p-phenylene vinylene) (OC_1C_{10}-PPV) and poly(3-hexyl thiophene) (P3HT), performed in two different configurations, i.e., field-effect transistors and hole-only diodes.[2] The first structure displayed mobility results up to three orders of magnitude higher than the latter configuration. This experimental fact endorsed the density-dependent mobility model, proposed by Vissenberg and Matters in amorphous organic transistors, that stems from hopping percolation in an exponential DOS.[3] As demonstrated by Arkhipov et al., hopping transport in disordered materials can be reduced to a trap-controlled transport composed of an effective transport level and a broad distribution of localized states (traps) that only retain mobile charges.[4] Currently, several authors are considering this framework, transport via an extended state under the influence of an exponential density of traps.[5-7] In the present chapter we implement this assumption in SCLC to analyze its implications to charge carrier mobility.

From an experimental point of view, determination of mobility is commonly given throughout the study of transit times (i.e., time needed for carriers to cross the sample electrode-to-electrode) in the wide range of the methods available in the literature: time-of-flight, transient electroluminescence, dark injection and impedance spectroscopy (IS), among others.[8,9] The IS technique will focus our computational calculations to provide physical insight on experimental measurements of capacitance spectra. As demonstrated in the theoretical work of a single-carrier device in SCLC with only a single trap of chapter six, there is a strong correlation between the shape of capacitance spectra and the nature of traps lying in the band-gap. Particularly, a classification of them was established attending its energy depth and its dynamic activity to capture and release charge carriers (i.e., shallow: fast and slow, and deep traps).[10] Meanwhile fast-shallow traps were responsible for the delay of transit times (i.e., shifted capacitance step-ups), slow-shallow traps were for low-frequency capacitance increases. The aim of this chapter is extending these ideas to a wider set of traps, from a single to an exponential density in the band-gap, in order to further test the theoretical framework with experimental capacitance data: a single-carrier device composed of N,N'-diphenyl-N,N'-bis(1-naphtylphenyl)-1,1'-biphenyl-4,4'-diamine (α-NPD).

The forthcoming pages follow the subsequent structure: firstly, the exponential-density-trap model, secondly, the results and discussion section and, finally, the conclusions.

8.2. The Exponential-density-trap Model

The SCLC regime for electron transport in disordered organic semiconductors comprises two classes of energy states: one transport level with density n_c where carriers drift in the electric field F, and an exponential distribution of localized states with density n_t, that corresponds to immobilized trapped charge. The mathematical description is well-known in the literature

and entails: the continuity equation, the drift current equation and Poisson equation, respectively.[11]

$$\frac{dJ}{dx} = 0 \tag{8.1}$$

$$J = q\mu_{0n} n_c F + \varepsilon_r \varepsilon_0 \frac{\partial F}{\partial t} \tag{8.2}$$

$$\frac{dF}{dx} = \frac{q}{\varepsilon_r \varepsilon_0}\left(n_c + n_t\right) \tag{8.3}$$

Furthermore, the trap dynamics equation is considered for every energy level E_t in the exponential distribution of traps with occupancy $f_t(E_t)$ along the band-gap as[12]

$$\frac{\partial f_t}{\partial t} = c n_c \left[1 - f_t\right] - e f_t \tag{8.4}$$

Here q is the elementary charge, μ_{0n} is the trap-free mobility, $\varepsilon_r \varepsilon_0$ the dielectric constant, and c and e are the coefficients for electron capture and release, respectively. The potential can be calculated by integrating the electric field along the thickness *L*:

$$V = \int_0^L F dx \tag{8.5}$$

In fact, the same system of equations stands for the hole transport just by changing the spatial and energy scales origins at once. The population of the extended states at the energy level E_c, for a non-degenerate semiconductor, relates to the Fermi level E_F as

$$n_c(E_F) = N_c e^{(E_F - E_c)/k_B T} \tag{8.6}$$

where N_c is an effective density of states in the transport level.

The trapped population is the overall density of charge carriers located by the exponentially distributed traps along the band-gap,

$$n_t(E_F) = \int_{E_V}^{E_c} g_t(E_t) f_t(E_t, E_F) dE_t \tag{8.7}$$

$$g_t(E_t) = \frac{N_t}{k_B T_t} e^{\frac{E_t - Ec}{k_B T_t}} \tag{8.8}$$

where N_t is an effective density of traps and T_t the characteristic trap temperature. Assuming that every trap energy level, E_t, reaches equilibrium with the extended state (with the same Fermi level), the trap occupancy is given by

$$f_t(E_t, E_F) = \frac{1}{1 + e^{(E_t - E_F)/k_B T}} \tag{8.9}$$

In steady state, Eq. (8.4) gives

$$f_t = \frac{1}{1 + e/(cn_c)} \tag{8.10}$$

Therefore, the detailed balance condition provides the following relationship for the trap emission and capture coefficients:

$$e = cN_c e^{(E_t - E_c)/k_B T} \tag{8.11}$$

Let us denote steady-state by $\bar{x}$ and small perturbation by $\hat{x}$ applied at a certain angular frequency ω. Hence every electrical variable can be expressed as $x = \bar{x} + \hat{x}$ to linearize the whole system of equations up to the first order.[13] As shown in Ref.[14], by solving Eq. (8.4) for a small perturbation, we obtain:

$$\hat{f}_t(E_t) = \frac{1}{\bar{n}_c} \frac{\bar{f}_t(1 - \bar{f}_t)}{1 + i\omega/\omega_t} \hat{n}_c \tag{8.12}$$

This term gives the contribution to the spectra of the capacitance and conductance of every trap level. Every trap frequency is defined as,

$$\omega_t(E_t) = \frac{e}{1-\bar{f}_t} \tag{8.13}$$

This is the maximum frequency that the trap is acting as such, since at higher frequencies the trap cannot follow the *ac* perturbation.[15] Inserting Eq. (8.11) in Eq. (8.13), we find the dependence of ω_t on trap energy and occupation, as

$$\omega_t = \frac{cN_c e^{(E_t-E_c)/k_BT}}{1-\bar{f}_t} \tag{8.14}$$

It should be remarked that in the SCLC regime, $\bar{f}_t$ is position-dependent along the organic layer. The impedance is defined as the quotient of potential to current density,

$$Z(\omega) = \frac{\hat{V}(\omega)}{\hat{J}(\omega)} \tag{8.15}$$

$\hat{V}(\omega)$ is determined by spatial integration of $\hat{F}(\omega)$ from the solution of the above described model. The boundary conditions at the injecting contact used to solve the electrical variables along the thickness in *dc* and *ac* conditions are[15,16]

$$\bar{n}_c(x=0) = N_c \text{ and } \hat{F}(x=0) = 0 \tag{8.16}$$

Capacitance and conductance are defined as follows:

$$C(\omega) = \mathrm{Re}\left[\frac{1}{i\omega Z(\omega)}\right] \tag{8.17}$$

$$g(\omega) = \mathrm{Re}\left[\frac{1}{Z(\omega)}\right] \tag{8.18}$$

8.3. Theoretical framework

8.3.1. Steady-state Characteristics of Organic Layers with an Exponential Density of Traps

Experimental measurements of *J-V* curves are usually analyzed to interpret the performance behaviour and charge transport of a wide range of electronic devices, such as OLEDs,[17] transitors[2] and solar cells.[18] In our case, single-carrier organic layers, we calculate the steady-state solution from the above model: Eqs.(8.1)-(8.3) and Eqs.(8.5)-(8.9); and the results are displayed in Fig. 8.1. Input data are shown in Table III.

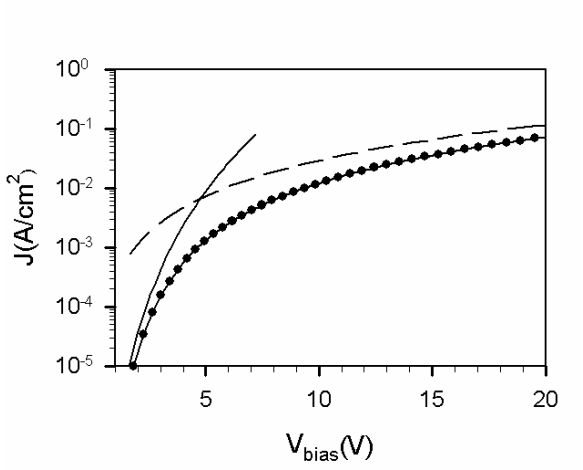

Fig. 8.1 Simulations of current-density-voltage characteristics (line and scatter plot) pictured together with the analytical formulae: Eq. (8.19) (solid line) and Child's law, Eq. (8.20) with $\theta = 1$, (dashed line).

At low voltages, most of the ohmically injected charges are trapped ($n_t >> n$, in Poisson equation) and the representation approaches the formula:[19,20]

$$J = e\mu_{0n} N_c \left(\frac{\varepsilon}{eN_t}\right)^l \left(\frac{l}{l+1}\right)^l \left(\frac{2l+1}{l+1}\right)^{l+1} \frac{V^{l+1}}{L^{2l+1}} \tag{8.19}$$

whereas at high voltages, $n_t << n$, the Mott-Gourney square law modified by shallow traps is followed,

$$J = \frac{9}{8}\varepsilon\theta\mu_{0n}\frac{V^2}{L^3} \tag{8.20}$$

where $\theta^{-1}(=1+<n_t>/<n_c>)$ is a carrier-density dependent factor of trapped and free charge located by the shallow traps.[19] It should be remarked that trap dynamics, Eq. (8.4), have not been included in the present calculations and the mobility parameter is thereby defined as μ_{0n}, independent of voltage.

8.3.2. Impedance Response of Organic Layers with an Exponential Density of Traps

Experimental measurements of capacitance spectra extracted from impedance response, Eq. (8.17), are usually a powerful tool to determine charge transport parameters such as carrier mobility, for holes and electrons.[8,20,21]

The model described in section 8.2 was already analytically solved by Dascalu with the approximation of $J \propto V^2$ and two suggested trapping coefficients independent of occupation (δ and Ψ) which would be in contradiction of the voltage dependence of mobility if extended to any voltage range.[22-24] However, our computational results of capacitance with the exponential density of traps have no restrictions and cover the whole model previously exposed. Fig. 8.2 (a) shows capacitance calculations with material parameters of Table III and no series resistance R_s considered. Deviation from the well-known trap-free spectrum is displayed as a reference. Low-frequency capacitance exhibits an increase value far over the traditional $0.75C_g$ and this behaviour is attributed to the slow-shallow traps within the distribution that cannot achieve the quasi-equilibrium with the transport level. At higher frequencies approaching the transit time, fast-shallow traps trapping-detrapping dynamics intersect with the transit of charge carries from the injecting to the collecting contacts causing a time delay, as shown by peaks (arrows) in Fig. 8.2

(b). Trap-limited mobility is interpreted in terms of this trap-controlled transport. Both roles of shallow traps (slow and fast) now occur at once with the exponential density of traps unlike our previous work of a single-trap.[10] Deep traps contribution is also slightly observed in the first peak of the capacitance step-up. As a minor comment, other capacitance simulations with a slower capture trap rate yielded slight lower values than $0.75C_g$ in the vicinity of the transit time frequency.

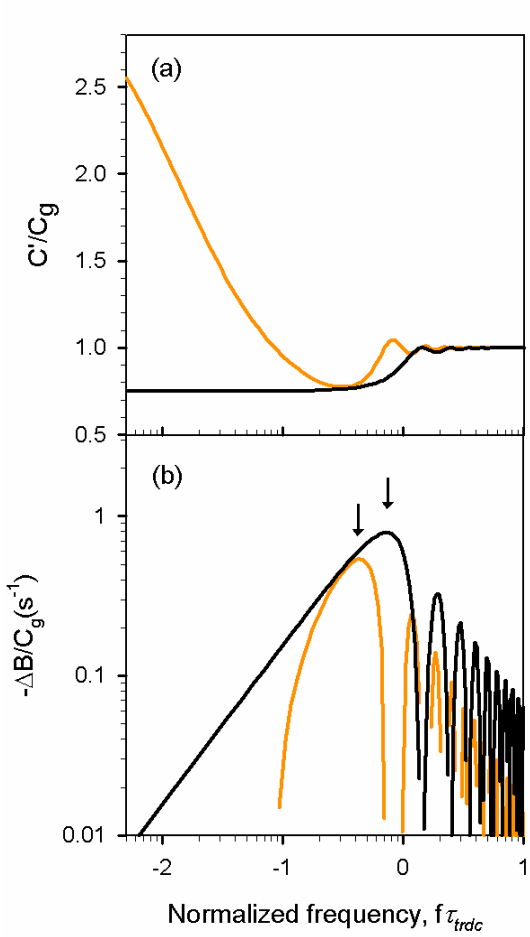

Fig. 8.2 Model simulations at 3V of **(a)** capacitance and **(b)** and differential susceptance spectra, Eq. (8.24), with an exponential density of traps (orange dashed line) in comparison to the trap-free spectrum (black solid line). Frequencies are normalized to transit time τ_{trdc}, Eq. (8.26).

Since we are dealing with an inhomogeneous system, Fermi level and occupation vary along the thickness, Fig. 8.3 (a), especially abruptly close to the injection region and with a smoother functional dependence in the wide range of the sample thickness. Therefore, an average Fermi level $<E_F>$ can be given as an appropriate approximation to simplify the theoretical analysis.

Thus the average occupancy becomes:

$$\left\langle \bar{f}(E_t, E_F) \right\rangle \approx \bar{f}(E_t, \left\langle E_F \right\rangle) \tag{8.21}$$

and Fig. 8.3 (b) shows the average occupied density of traps as well as the empty ones under the above approach. Presumably, the most shallow and empty traps will behave as fast whereas the less shallow and full ones will be slow (see Eq. (8.14)).

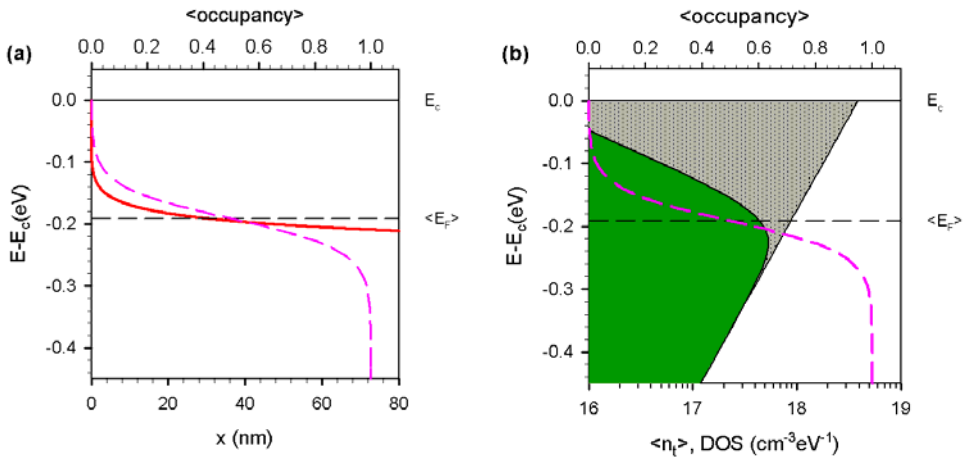

Fig. 8.3 (a) Simulations at 3V of the Fermi level along the thickness (solid line) and average occupancy (dashed line) that stems from the average Fermi level $<E_F>$. **(b)** Coloured area is displayed for the average occupied trap density of states (DOS) whereas shadowed area corresponds to the empty trapping density of states. Average occupancy is also printed (pink dashed line) together with average Fermi level $<E_F>$ and transport energy level E_c as references.

Nevertheless, further approach to the trapping rates along the energy distribution in the band-gap is of prime importance to disentangle the different roles of every trap energy state in the contribution to the capacitance spectra,

Fig. 8.4. Capture rate c is defined as energy independent with a higher value than the normalized emission rate e/N_c, Eq. (8.11). However, the definitive discriminating parameters to classify whether the shallow energy states are purely fast or not, are: the capture rate c and the critical capture coefficient c_c defined as:

$$c_c(E_t) \approx \frac{3\pi\mu_{0n}V}{2L^2}\frac{1-\bar{f}_t(E_t,\langle E_F\rangle)}{N_c e^{(E_t-E_c)/k_BT}} \tag{8.22}$$

and its discussion was also established in Ref.[10]. If c is larger than c_c along a certain energy interval in the band-gap, these shallow energetic levels behave as fast-shallow traps resulting in a larger transit time and thereby, in trap-limited mobility. This energy region below the transport level $(E_c \geq E_t \geq E_L)$ can be calculated as $c_c(E_L) \cong c$, where E_L is interpreted as the lowest energy level acting as purely fast,

$$E_L = k_B T\, Ln\left[\left(\frac{3\pi\mu_0 V}{cN_c L^2}\right)\exp\left[\frac{(E_c-\langle E_F\rangle)}{k_B T}\right]-1\right]+\langle E_F\rangle \tag{8.23}$$

which is dependent on: the voltage V dropped along the organic layer in space-charge, the Fermi level $<E_F>$ and device specifications. For shallow levels below E_L, $(E_L > E_t > \langle E_F\rangle)$, trap dynamics start to gradually change from fast to slow as far as deeper states we are dealing with. That makes difficult to quantify the reduced factor θ that commonly relates the trap-limited mobility to the trap-free one.[19]

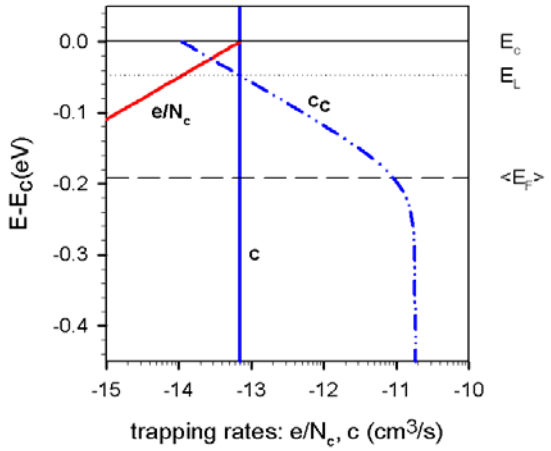

Fig. 8.4 Trapping coefficients are displayed for the 3V model simulation: normalized emission rate (e/N_c) and trapping rate (c) are represented by coloured solid lines. Critical capture coefficient is also given by a dash-dotted line. Reference energy levels are: transport E_c, limit E_L and average Fermi $<E_F>$ levels.

In order to experimentally test the multiple-trapping interpretation,[25] model capacitance spectra are generated at different voltages in figure 8.5.. By increasing the voltage dropped in the space-charge, Fermi level moves up towards the transport level, covering more trapping states in the band-gap. As a consequence, the range of the energy distribution acting as purely fast $(E_c \geq E_t \geq E_L)$ becomes narrow since E_L (Eq.(8.23)) moves up as well. This means that there are less unoccupied trapping sites that can trap and release charges quickly whilst they drift electrode-to-electrode by the local electric field. In other words, trap-limited mobility becomes lower controlled by traps the more voltage is applied since less fast-shallow traps are acting as such. As regards the low-frequency behaviour with the voltage, the same reasoning can be given since the energy region, $(E_L > E_t > \langle E_F \rangle)$, containing the slow-shallow traps, becomes more reduced as well. Thus less low-frequency increase is expected the more voltage is applied. The high frequency domain is characterized by a certain plateau at C_g followed by a capacitance decrease due

to the inclusion of a series resistance R_s in the simulation. In real devices this resistance mainly stems from its metallic contacts.

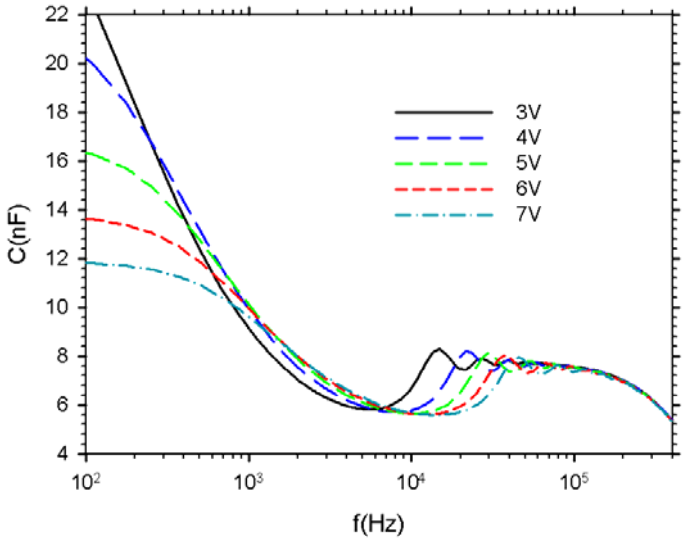

Fig. 8.5 Model representation of capacitance spectra at voltages ranging from 3V to 7V. Simulation parameters are shown in Table III.

8.4. Experimental Analysis

Let us now apply the model and theoretical framework to interpret the capacitance spectra of the hole-only device based on N,N'-diphenyl-N,N'-bis(1-naphtylphenyl)-1,1'-biphenyl-4,4'-diamine (α-NPD) of Nguyen *et al.*[26]. In the publication, the authors model the data by considering: drift-diffusion transport with a Gaussian density of traps and field-dependent mobility, however, the low-frequency capacitance exhibits a rather sharp behaviour in contrast to the experiments. This feature may be better described by an exponential distribution of traps that would result in a smoother capacitance variation at low-frequency.

We show the experimental capacitance spectra at different voltages of a thick hole-only device retrieved from Ref.[26], Fig. 8.6.

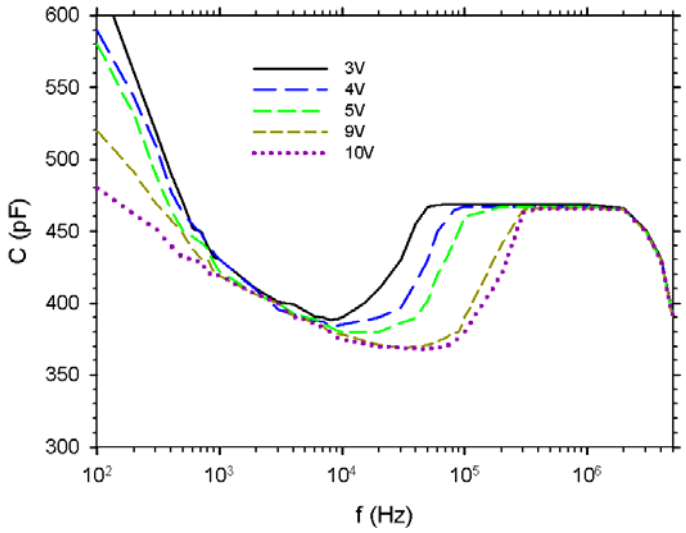

Fig. 8.6 Experimental capacitance spectra of a hole-only α-NPD device at different voltages. Representation obtained from data of Ref.[26]

The capacitance behaviour in general agrees well with our model at every frequency range. The low-frequency capacitance part (LF) displays an increase which is directly modulated by the trapping distribution, concretely by the slow-shallow traps. The LF capacitance increase is more noticeable the less voltage is applied, i.e., for the lower set of voltages (3V-5V) more than for the higher ones (9V-10V), as expected. The intermediate frequency (IF) is characterized by the presence of a minimum value of the capacitance spectra and its position shifts depending on the voltage. Our model predicts all the minima achieving the value of 0.75 of the geometrical capacitance C_g of the organic layer, however, the experimental data lies more over this limit the less voltage is applied. This feature seems to be better described by Nguyen's model. In the IF region the average transit time of the carriers τ_{tr} can be

extracted by means of the IS technique throughout the representation of the susceptance (=Im(*Y*)), concretely, the negative differential susceptance:

$$-\Delta B(\omega) = -\omega(C(\omega) - C_g) \tag{8.24}$$

The position of the maxima define peaks corresponding to *ac* transit times at different voltages thereby[27]

$$\tau_{trac} \approx 0.72 \cdot f_{\max}^{-1} \tag{8.25}$$

and mobility values can be extracted by using the *dc* transit time expression,

$$\tau_{trdc} = \frac{4}{3} \frac{L^2}{\mu\ (V_{bias} - V_{th})} \tag{8.26}$$

Inserting Eq. (8.25) in Eq. (8.26), it holds:

$$\mu = \frac{4}{3} \frac{L^2 f_{\max}}{0.72 \cdot (V_{bias} - V_{bi})} \tag{8.27}$$

Calculations of mobility yielded mobility enhancement the more voltage is applied in the bulk. Particularly, the fitting to the classical field-dependent mobility expression (with the electric field *F* approximated by $(V/L)^{1/2}$),

$$\mu = \mu_0 \exp\left(\gamma\sqrt{F}\right) \tag{8.28}$$

provided experimental mobility values of $\mu_0 = 2.9 \cdot 10^{-4}\, cm^2/(Vs)$ and $\gamma = 2.6 \cdot 10^{-3} (cm/V)^{1/2}$. This mobility dependence on voltage, measured by means of IS, is interpreted in the present paper as a trap-limited mobility governed by the dynamics of the fast-shallow traps in the band-gap. The field-dependent mobility is induced by the reduction of the trapping action as far as more voltage covers more trapping sites in the exponential distribution of localized-states. As regards the high frequency range (HF), it is composed of two different parts: a relatively wide plateau lying at the capacitance value of C_g and a sharp decrease from a frequency cutoff onwards. The latter behaviour

of the HF is dominated by the series resistance of the whole device structure causing the capacitance drop.

In summary, the shape of capacitance spectra with an exponential density of traps is strongly determined by the bias-voltage, providing: (1) a deviation of transit times translated into a field-dependent mobility and also (2) a low-frequency capacitance increase over the traditional $0.75C_g$ for trap-free materials.

Parameter	**Value**
Thickness $\boldsymbol{L}$	80 *nm*
Device area $\boldsymbol{A}$	0.235 cm^2
Series resistance $\boldsymbol{R_s}$	34 Ω
Transport effective density of states $\boldsymbol{N_c}$	10^{19} cm^{-3}
Relative dielectric constant $\boldsymbol{\varepsilon_r}$	3
Trap-free mobility $\boldsymbol{\mu_{0n}}$	$5 \cdot 10^{-7}$ $cm^2/(Vs)$
Temperature $\boldsymbol{T}$	300 *K*
Band-gap $\boldsymbol{E_c - E_v}$	2.4 *eV*
Trap effective density of states $\boldsymbol{N_t}$	$5 \cdot 10^{17}$ cm^{-3}
Characteristic trap temperature $\boldsymbol{T_t}$	1500 *K*
Trapping capture coefficient $\boldsymbol{c}$	$7 \cdot 10^{-14}$ cm^3/s

Table III. Material parameters implemented for simulations.

8.5. Conclusion

It has been corroborated the theoretical framework of the multiple-trapping picture in organic layers that comprises an exponential density of trapping states under SCLC. Interpretation of the voltage dependence of: the trap-limited mobility and the low-frequency capacitance behaviour, is provided by the analysis of capacitance spectra. The presence of pure fast-shallow traps determines the limitation of the charge transport mobility whereas slow-shallow traps causes the low-frequency capacitance increase. Both features are modulated by two respective voltage-dependent energy regions in the band-gap, i.e., for the first one, the energy interval is $E_c \geq E_t \geq E_L$, and for the latter one, it is $E_L > E_t > \langle E_F \rangle$.

8.6. References

[1] H. Bässler, Phys. Status Solidi (b) **175**, 15 (1993).

[2] C. Tanase, E. J. Meijer, P. W. M. Blom, et al., Phys. Rev. Lett. **91**, 216601 (2003).

[3] M. C. J. M. Vissenberg and M. Matters, Phys. Rev. B **57**, 12964 (1998).

[4] V. I. Arkhipov, E. V. Emelianova and G. J. Adriaenssens, Phys. Rev. B **64**, 125125 (2001).

[5] B. Ramachandhran, H. G. A. Huizing and R. Coehoorn, Phys. Rev. B **73**, 233306 (2006).

[6] M. M. Mandoc, B. de Boer and P. W. M. Blom, Phys. Rev. B **73**, 155205 (2006).

[7] M. M. Mandoc, B. de Boer, G. Paasch, et al., Phys. Rev. B **75**, 193202 (2007).

[8] F. So, B. Krummacher, D. Poplavskyy, et al., J. Appl. Phys. **102**, 091101 (2007).

[9] S. Shirota and H. Kageyama, Chem. Rev. **107**, 953 (2007).

[10] J. M. Montero, J. Bisquert, G. Garcia-Belmonte, et al., Org. Electron. **10**, 305 (2009).

[11] A. Van der Ziel, "*Solid State Physical Electronics*" (Prentice-Hall, Englewood Cliffs, 1976).

[12] J. Bisquert and V. S. Vikhrenko, Electrochim. Acta **47**, 3977 (2002).

[13] W. Brütting and S. Berleb, Phys. Rev. Lett. **89**, 286601 (2002).

[14] J. Bisquert, Phys. Rev. B **77**, 235203 (2008).

[15] P. W. M. Blom, M. J. M. de Jong and M. G. van Munster, Phys. Rev. B **55**, R656 (1997).

[16] M. A. Lampert and P. Mark, "*Current Injection in Solids*" (Academic Press, Inc., New York, 1970).

[17] G. Garcia-Belmonte, J. M. Montero, Y. Ayyad-Limonge, et al., Curr. Appl. Phys. **9**, 414 (2009).

[18] I. Mora-Seró, S. Giménez, T. Moehl, et al., Nanotechnology **19**, 424007 (7pp) (2008).

[19] A. Rose, "*Concepts in photoconductivity and allied problems"* (John Wiley & Sons, New York, 1963).

[20] H. C. F. Martens, J. N. Huiberts and P. W. M. Blom, Appl. Phys. Lett. **77**, 1852 (2000).

[21] M. Schmeits, J. Appl. Phys. **101**, 084508 (2007).

[22] D. Dascalu, Int. J. Electron. **21**, 183 (1966).

[23] D. Dascalu, Solid-St. Electron. **9**, 1020 (1966).

[24] T. Okachi, T. Nagase, T. Kobayashi, et al., Appl. Phys. Lett. **94**, 043301 (2009).

[25] J. Bisquert, Phys. Chem. Chem. Phys. **10**, 3175 (2008).

[26] N. D. Nguyen and M. Schmeits, Phys. Rev. B **75**, 075307 (2007).

[27] J. M. Montero, J. Bisquert, G. Garcia-Belmonte, et al., Phys. Status Solidi (a) **204**, 2402 (2007).

List of Conclusions

The present study on charge transport in organic layers aimed to provide physical understanding of the carrier mobility in disordered semiconducting materials which is under scientific research in the main specialized journals. The traditional view of a constant value in inorganic semiconductors does not apply for the organic ones and this feature plays a crucial role in the performance of organic-based electronic devices.

The major conclusions drawn from the thesis are as follows:

1) A universal scaling test in organic layers is given to verify the carrier mobility model governing the charge transport. The general scaling relationship for field-dependent mobility occurs in terms of the variables *JL* and *V/L* whereas for the density dependence the thickness scaling occurs in terms of different variables, $J^{1/\beta}L$ and *V/L*.

2) In the case of field-dependent mobility, experimental data of SY-copolymer (*J-V* curves and capacitance spectra) can be accordingly modelled, particularly, as regards the transit times.

3) Since the multiple-trapping picture lies on the density-dependent mobility model, different roles that a single trap can play and their implications to mobility were explained by means of IS. Fast-shallow traps are responsible for the trap-limited mobility and slow-shallow traps are for the low-frequency capacitance increase.

4) The interconnection between both mobility models (i.e., dependent on either the local electric field or charge density) is interpreted in terms of multiple-trapping transport with an exponential density of traps by means of IS.

5) The full detailed multiple-trapping picture explains experimental capacitance spectra measurements collected from a layer of Alq_3. Fast-shallow traps lies in the range of $E_c \geq E_t \geq E_L$ where the energy level E_L depends on the voltage dropped in the bulk. This level discriminates the localized-states that purely behave as fast-shallow

traps and that region diminishes the more voltage is applied. The same occurs for the slow-shallow traps reigning in the energy interval of $E_L > E_t > \langle E_F \rangle$. As a consequence, low-frequency capacitance increase and trap limitation of mobility, both features obtained from IS, become more reduced the more voltage is applied.